EFFECTS OF HYDRODYNAMIC STRESS ON GROWING *SACCHAROMYCES CEREVISIAE* IN A SLURRY REACTOR.

Valérie Lamaignère
Diplôme d'Ingénieur en Génie Chimique (ENSIGC, Toulouse, France)

Half dissertation submitted in fulfilment of the requirement for the degree of
MASTER OF SCIENCE IN ENGINEERING

Department of Chemical Engineering
University of Cape Town
Cape Town, South Africa.

Supervisor: PROF. S.T.L. HARRISON

June 2003

Acknowledgements

I would like to express my sincere thanks to the following people for their help and support throughout the duration of research project:

- Prof. Sue Harrison, my supervisor, for her guidance and encouragement through the undertaking and completion of this thesis.
- Dr Andrew Robinson and fellow postgraduate students in the Bioprocess Engineering group for their advice and helpful participation in my experimental work.
- Mohammed Jaffer of the Electron Microscopy Unit, for the long time he spent doing TEM analysis.
- For his help with statistical analysis of experimental results, Prof Tim Napier-Munn.
- The staff and students of the Department of Chemical Engineering for making my stay at UCT enjoyable and successful.
- My parents and family, for their unconditional support and encouragement, even so far from home.

Synopsis

Recent studies have shown that damage to microbial cells can lead to changes in the cells's integrity, viability, metabolic rate, metabolic pathway and morphology (Logan and Dettmer, 1990; Smith *et al.*, 1990; Toma *et al.*, 1991; Illing and Harrison, 1999). Growth of the micro-organisms in the presence of solid particles, such as minerals bioprocessing (Bailey and Hansford, 1993), soil bioremediation (Kleijntjens *et al.*, 1992, as cited by Scholtz-Brown, 1998), immobilised biocatalyst systems (Croughan *et al.*,1988), can further increase the damage to the cells. Since this negatively impacts on the productivity of industrial processes, it is important to quantify and model the metabolic and structural responses of microbes to hydrodynamic stress.

Using a non-growing system of yeast and silica sand, Scholtz-Brown and Harrison (2002 a) report that the dominant mechanism of cell damage in a slurry reactor is interaction between particles and cells, as opposed to cell interactions with turbulent fluid eddies. Nemati and Harrison (1999, 2000) present the following responses of *Sulfolobus metallicus* to hydrodynamic stress, when the microbes are grown in the presence of pyrite:

- Over the range 42.5 – 202 microns (mean diameter), the particle size has no influence on the growth and activity of the cells. Constant values for both the specific growth rate and yield factor are obtained.
- The lag phase is more pronounced at higher pulp densities and in the presence of larger particles.
- Below a critical particle size and above a critical solid loading, cell disruption and impaired metabolic activity are observed.

The objectives of this research thesis were to understand and quantify biological responses to hydrodynamic stress by investigating the activity of the yeast *Saccharomyces cerevisiae*, cultivated in the presence of a range of solid loadings, solid sizes and agitation rates. The influence of inoculum size, inoculum age and type of agitator were also investigated. This study was carried out with the intention of identifying biological responses to hydrodynamic stress and modelling observed effects on microbial activity. Both metabolic and structural responses were investigated. Analytical techniques for the identification and quantification of a loss of viability, loss of integrity, changes in morphology and changes in the metabolic rate were selected and validated.

All the hydrodynamic parameters investigated: solids loading, solid size, inoculum age, inoculum size, agitation rate and agitator type, played a determinant role on the growth of yeast in a slurry reactor. There existed optimum conditions for the growth of *Saccharomyces cerevisiae* in the presence of solid particulates in a slurry reactor. Over the conditions tested, the following values were selected: 0.5% (v/v) or less solids loading, particle size in the range 600 – 850 μm, 10% inoculum size, agitation performed by a Rushton turbine at 565 rpm. As only two inoculum ages were tested, no optimum could be determined. However, a 24 hour inoculum was more readily damaged (with reference to yeast performance).

Critical values below which or above which a negative influence on yeast performance was observed could be identified. The critical solids loading range was from 0.5% to 1% (v/v), depending on assay used. At 5% solids loading, no cell growth, substrate

consumption or product formation were observed, indicating a loss of metabolic activity. Little difference was noticed between 2 and 10% inoculum sizes in the extent of yeast growth, glucose consumption and ethanol production. Thereafter the critical value below which the yeast activity changed was set at 2% (v/v) inoculum size. Below an impeller speed of 565 rpm, rate and extent of growth decreased, even though cell viability remained in the reported class for unstressed systems. Above 600 rpm, decrease in both viability and activity was noticed.

General trends on the influence of hydrodynamic parameters were observed. When increasing solids loading from 0 to 2% by volume, a decrease in the apparent specific growth rate occurred. This suggested an increase in the specific death rate constant, supported by a decreased fraction of viable cells. On increase of the particle size fraction to 850 to 1130 μm, a decrease in stationary phase biomass concentration, cell viability, specific growth rate, magnitude of negative cell surface charge and biomass yield were noted. Performances of the smaller size fraction (465 to 600 μm) were similar to the optimal fraction in terms of growth rate, biomass yield and total cell number. However reduction in viability with time occurred. When the inoculum size was decreased, the specific growth rate and the biomass yield decreased. When increasing inoculum age from 14 hour to 24 hour, little difference was observed in total cell concentration. However, loss of viability, lower budding index and change in substrate consumption and ethanol production were observed. At high agitation rate (850 rpm and 1% by volume solid loading), cell damage was observed. Paradoxically, rate and extent of growth also decreased below 565 rpm. In that case, another stress mechanism was suspected to occur in the bioreactor. Using a pitched-blade turbine, the presence of the solid particles had no influence on the growth of *Saccharomyces cerevisiae* at 565 rpm and 1% (v/v) solids loading. However, when comparing the two agitators, reduced rate and extent of growth, and lower budding index were observed with a pitched-blade turbine.

When a decrease in the apparent specific growth rate was combined to a decrease in viable cell fraction, the concept of increase in specific death rate was outlined. Specific death rate k_d was considered to be a function of the various hydrodynamic parameters. The death rate constant was modelled as a power law function of solids loading. A good fit was found between experimental and calculated points. Above 565 rpm, the death rate constant was also expressed as a power law function of the agitation rate N. Correlation with experimental data was not as good as in the previous case. When using a 24 hour inoculum age rather than a 14 hour inoculum, the decrease in viable cell concentration in stationary phase and in budding index suggested that death rate was not negligible in the absence of extreme hydrodynamic stress. Investigating the effect of inoculum size on the growth of *Saccharomyces cerevisiae*, yeast viability remained quite high for all experiments (above 92%). In this case, it was concluded that a decrease in inoculum size did not cause an increase in the death rate but a reduction in yeast activity.

When exposed to hydrodynamic stress, yeast develop mechanisms to adapt and resist the stress. Increasing the lag phase, i.e. increasing the period of acclimatisation, is one of these strategies. Thus when solids loading is increased from 0 to 2% (v/v), the lag phase is doubled. Similarly, the lag phase increased when the inoculum size was decreased. Another resistance mechanism lies in morphological changes. TEM analysis on samples at 0% and 1% solids loading revealed that the presence of solid particulates strongly affects the cell wall structure. While no influence on the cell size could be outlined, an increase in the cell wall thickness was observed with increased level of stress. Moreover the cell wall was very irregular at 1% solids loading, suggesting a repair occurred where

the cell has been injured. These results are confirmed by TEM observations at 1% solids loading and 850 rpm.

Under adverse conditions, yeast switch from growth to maintenance. Thus, increasing solids loading, the decrease in cell growth rate with unchanged substrate consumption, illustrated by a decrease in $Y_{X/S}$, suggested that additional substrate was diverted from cell growth to provide extra energy for cell maintenance. Similarly, below 2% (v/v) inoculum size and at 24 hour inoculum age, rapid glucose uptake and decrease in growth rate confirmed a shift in metabolic activity.

Investigating the influence of agitation on the growth of yeast, paradoxical results were obtained. Below 565 rpm (i.e. at a low level of hydrodynamic stress) and using a pitched-blade impeller, which produces lower turbulence intensity, reduced rate and extent of growth were observed. Here, a different stress was postulated to occur in the bioreactor. Low agitation rate and lower mixing (generated by the pitched-blade turbine) could result in oxygen limitation, which would restrict the cell growth.

From the data collected in this study, it was possible to determine the response of yeast *Saccharomyces cerevisiae* to some hydrodynamic stresses. Responses have been quantified in terms of viability, metabolic rate (growth rate, glucose utilisation rate and ethanol production rate), morphology (cell wall thickness and structure), and integrity. However, no investigation has been performed on changes in metabolic pathway. Studies on the release of stress indicators such as HSP's, trehalose or glygogen, under conditions of physical stress, are recommended. While no literature can be found about the influence of the inoculum on the growth, this work points out the importance of the inoculum state. Nevertheless, our study was limited, especially for inoculum age, where only two ages could be compared. Further work should be conducted to determine optimum inoculum age and size for growth. From this study, it has been shown that the cell wall plays a determinant role in adapting to hydrodynamic stress. Transmission Electron Microscopy allowed study of the cell wall morphology. However, further work should be carried out to investigate changes in the cell wall composition. Some authors mention the phenomenon of cross-protection, where one stress effector leads to an increased tolerance to a number of different stresses. In industrial processes, micro-organisms usually experience several stresses at the same time. It is therefore valuable to investigate the effects of different stresses combined to hydrodynamic stress, for a better understanding of cross-protection mechanisms (Lee, 2000; Sharma, 1997).

GLOSSARY

Budding Cell	A cell in which cell division is occurring and a "bud" is being formed by the process of asexual reproduction. These cells are identified by microscope cell counting, the bud being one-third the size of the mother cell.
Budding Index	The fraction of the total cell number which are budding.
Cavitation	Formation of vapour cavities in a fluid, due to a significant reduction in pressure, which oscillate through collapse and rebound cycles until they are destroyed by pressure recovery.
Cell Activity	The extent of cell growth.
Cell Damage	Refers to the altered response of cells on exposure to stresses. This may be manifest as a change in the cells'morphology, ability to grow and reproduce, metabolic rate and/or metabolic pathway.
Cell Death Rate	The rate at which cells die due to viability loss and disruption.
Dead Cell	A cell which has stained blue from the methylblue staining technique, determined from the microscope analysis. These cells correspond to a loss in viability.
Disrupted Cell	A cell in which hydrodynamic stress has caused a break in the cell wall, causing a leakage of intracellular product into the growth medum.
Fermentation	The anaerobic process by which yeast cells inoculated into a polysaccharide rich medium (wort) convert sugars to carbon dioxide, ethanol, glycerol and biomass.
Exponential Phase	The period of significant growth after the lag phase.
Hydrodynamic Stress	Physical stresses exerted on the cell wall due to the mechanical process of agitation in the presence of solids.
Integrity of the cell envelope	The intactness of the cell envelope.
Lag Phase	A period of insignificant overall cell growth while cells acclimatise to a changed environment.
Lag Time	The time period of the lag phase.
Microcarrier	A non-biological particle onto which microbial cells are attached.
Mother Cell	The cell providing the platform for further cell growth through

	the production of buds.
Transmission Electron Microscopy	Microscopy technique used to determine the cell wall thickness. Owing to the short wavelengths obtained by accelerating electrons, details of biological matter can be visualized on a submicron scale.
Saccharomyces cerevisiae	A unicellular *eukaryotic* cell belonging to the yeast family.
Slurry Reactor	Stirred tank reactor where solid particles are agitated in the presence of a liquid.
Stationary Phase	The period of negligible cell growth, due to nutrient deficiency, following the exponential phase.
Viable Cell	A living cell that has the ability to bud (i.e. to reproduce).
Viability	A term to describe the ability of cells to grow and reproduce; losses of viability may occur via loss of structural integrity, cell death or replicative deactivation
Zeta Potential	The charge of a particle at the surface of shear. An indication of cell surface charge.

ABBREVIATIONS

ANOVA	Analysis of variance
ATP	Adenosine triphosphate
CS	Collision Severity
HSP	Heat Shock Proteins
ICS	Impeller collision severity
ISF	Integrated Shear factor
PBT	6-bladed Pitch-bladed turbine
ROS	Reactive oxygen species
RT	6-bladed Rushton turbine
TCA	Tricarboxylic acid cycle
TCS	Turbulent Collision Severity
TEM	Transmission Electron Microscopy
TOC	Total organic carbon

NOMENCLATURE

Symbol	Description	Units
B	Baffle width	m
C	Distance of impeller blade from tank bottom (Appendix B)	m
C	Constant (Equation 2.33)	
C	Cell concentration	cells/mL
C_0	Initial cell concentration	cells/mL
C_1	Cell concentration at t_1	cells/mL
C_i	Bead concentration	g/L
C_m	Microcarrier concentration	g/L
C_V	Volumetric solid concentration	
CS_S	Collision severity based on shear model	$J.s^{-1}$
CS_T	Collision severity based on eddy velocity	cm
d_p	Particle diameter	m
D	Impeller blade diameter (Appendix B)	m
D	Reactor diameter	m
D_i	Impeller diameter	m
D_t	Vessel diameter	m
E	Energy input per unit volume	$W.s.m^{-3}$
G	Glucose concentration	$g.L^{-1}$
H	Liquid height	m
H_u	Impeller disk diameter	m
k	First order disruption rate constant	s^{-1}
k_d	Death rate constant	h^{-1}
K_S	Saturation constant in Monod equation.	$g.L^{-1}$
L	Impeller paddle width	m
l_C	Kolmogorov microscale length	m
P	Impeller power input	W
P_V	Pressure at any point of maximum fluid velocity	Pa
P_∞	Pressure upstream of an orifice	Pa
n	Impeller speed	rps
n_b	Number of impeller blades	
N	Impeller speed	rpm
N_C	Frequency of cell-cell collisions	Hz
N_P	Power number	
q	Specific death rate	h^{-1}
q_1	Specific death rate due to fluid-cell interactions	h^{-1}
q_2	Specific death rate due to microcarrier-microcarrier interactions and microcarrier-bead interactions	h^{-1}
q_P	Specific ethanol production rate	$g.L^{-1}.\ h^{-1}.Cells^{-1}.$ mL
q_s	Specific glucose uptake rate	$g.L^{-1}.\ h^{-1}.Cells^{-1}.$ mL
R	Soluble protein released at time t	mg protein/mg cells
R_i	Maximum soluble protein released under the specified operating conditions.	mg protein/mg cells

R_g	Specific glucose uptake	h^{-1}
S	Substrate concentration	$g.L^{-1}$
t	Time	h
t_C	Average circulation time	h
t_1	Time at which stationary phase is reached	h
T	Tank diameter	m
v	Kinematic viscosity of the medium (Equation 2.9)	$m.s^{-1}$
v	Relative cell velocity (Equation 2.12)	$m.s^{-1}$
v_∞	Velocity upstream of an orifice	$m.^{s-1}$
V	Reactor volume	m^3
V_{susp}	Flow rate of the cell suspension	$m^3.s^{-1}$
X	Biomass concentration	million $cells.mL^{-1}$
W	Impeller paddle height	m
$Y_{X/S}$	Biomass yield on consumed substrate	$cells.mL^{-1}.g^{-1}.L$
$Y_{P/S}$	Product yield on consumed substrate	$g_{ethanol}.g_{glucose}^{-1}$
$Y_{P/X}$	Product yield on produced biomass	$g.L^{-1}.\ cells^{-1}.mL$

Greek letters	**Description**	**Units**
α	Microcarrier volume fraction (Equation 2.26)	
α	Volume fraction of cells (Equation 2.12)	
μ	Specific growth rate	h^{-1}
μ_{max}	Maximum specific growth rate	h^{-1}
μ_{max}^*	Upper limit of the maximum specific growth rate	h^{-1}
τ	Shear stress	
γ	Shear rate	
μ_L	Viscosity of the fluid	
ε	Energy dissipation rate	$m^2.s^{-3}$
σ	Cavitation number	
σ_i	Critical cavitation number	
θ	Average circulation time	s
ϕ	Volume fraction of solid particles	
ρ_b	Microcarrier bead density	$kg.m^{-3}$
ρ_P	Particle/cell density	$kg.m^{-3}$

Subscripts

L	Liquid
P	Particle
0	Initial

TABLE OF CONTENTS

LIST OF FIGURES

LIST OF TABLES

Chapter 1: Introduction

1.1 BACKGROUND AND OBJECTIVES OF STUDY

Microbial growth in the presence of solid particles has a number of important applications in industry, including mineral bioprocessing (Bailey and Hansford, 1993), where micro-organisms are used to leach finely divided sulphide minerals, soil bioremediation (Kleijntjens *et al.*, 1992, as cited by Scholtz-Brown, 1998; Ryan *et al.*, 1991; Stegmann *et al.*, 1994), immobilised biocatalyst systems (Croughan *et al.*,1988). These systems generally involve the growth of micro-organisms in aerated and agitated bioreactors. High agitation intensities and gas flow rates promote good mass transfer of nutrients to the cells (Toma *et al.*, 1991) and high cell concentrations in the bioreactors (Croughan *et al.*, 1988). However extreme hydrodynamic conditions caused by high levels of agitation and aeration have also been reported to cause cell damage (Toma *et al.*, 1991; Illing and Harrison, 1999). The presence of solid particles under hydrodynamic stress may aggravate damage to the cells. Responses to hydrodynamic stress may be quantified in terms of change in integrity, viability, metabolic rate, metabolic pathway and morphology (Logan and Dettmer, 1990; Smith *et al.*, 1990; Toma *et al.*, 1991; Illing, 1996).

Focussed on generating improved understanding of the influence of particulates in the slurry bioreactor, baker's yeast *Saccharomyces cerevisiae* grown in the presence of silica sand has been chosen as the model organism for this study. *S.cerevisiae* is recognised as one of the micro-organisms most resistant to mechanical disruption (Keleman and Sharpe, 1979). Scholtz-Brown (1998) investigated the effect of particulates (inert silica sand) on stationary phase *Saccharomyces cerevisiae* in slurry bioreactors, with a particular reference to cell disruption in a stirred tank reactor. The effect of incompletely and completely suspended solids on cell disruption was studied and models describing cell disruption as a function of the operating parameters presented. Here dependence on power input per unit volume as well as solids loading was shown. Further cell disruption was shown to occur primarily from solid-cell-solid collisions. This project is an extension of Scholtz-Brown's work and focuses on the growth of yeast in the presence of silica sand in a slurry bioreactor. Further it supports concomitant studies of the influence of particulates on microbial activity and leach rates in thermophilic bioleaching of sulphide minerals (Nemati and Harrison, 2000; Sissing, 2002).

The objectives of this research thesis are to understand and quantify responses to hydrodynamic stress by investigating the activity of yeast, cultivated in the presence of various solid loading, solid sizes and agitation rates. The influence of inoculum size, inoculum age and type of agitator are also investigated. This study is carried out with the intention of identifying biological responses to hydrodynamic stress and modelling observed effects on microbial activity. Both metabolic and structural responses are investigated.

1.2 STRUCTURE OF THE THESIS

An overview of slurry systems involving the growth of micro-organisms with solid particulates is presented in Chapter 2, together with a literature survey on yeast characteristics. Reported responses to different stresses are presented and models developed to describe cell damage are reviewed.

Chapter 3 deals with the experimental materials and procedure used in this study and presents methods selected for the identification, characterisation and quantification of any cell damage throughout the growth.

Reproducibility of the experimental results were investigated and findings are presented in Chapter 4. Statistical methods are described and results obtained for each analytical method reported. Thereafter, experiments conducted at 0% and 1% solid loading are compared statistically. Conclusions are drawn on the reproducibility of the results.

In Chapter 5, results obtained from the experiments to assert the influence of the solid particles in terms of solids loading on the growth are presented and discussed. A model for the death rate constant as a function of solids loading is proposed.

The influence of the inoculum state on yeast growth in the slurry bioreactor is reported and discussed in Chapter 6, while the influence of the agitator in terms of impeller type and agitation rate are presented in Chapter 7. Based on those findings, conclusions are drawn and recommendations put forward in Chapter 8.

There are seven appendices to the text. Appendix A provides the composition of the media used for all experiments: pre-inoculum growth medium, inoculum and reactor growth media. In Appendix B, a schematic representation and geometry of the cell-culture experimental rig are presented. Detailed assay methods employed in the study are described in Appendix C. Data used for the investigation of the reproducibility at 0% and 1% by volume solid loadings are tabulated in Appendix D, while results for analysis of variance are summarised in Appendix E. Appendix F presents experimental data obtained for the different parameters investigated: solids loading, solid size, inoculum age, inoculum size, agitation rate and agitation type. Finally, calculations used to estimate growth parameters (yield factors, specific growth rate, substrate utilisation rate, ethanol production rate, lag duration) are outlined in Appendix G.

Chapter 2: Literature review

2.1 INTRODUCTION

Microbial growth in the presence of solid particles has a number of industrial applications, including bioleaching of minerals, soil bioremediation, immobilised biocatalyst systems and bead mills (Scholtz-Brown, 1998).
Most of these systems are aerobic bioreactors. High agitation rates and gas flow rate promote good mass transfer of oxygen and nutrients to the cells. However, the presence of solid particles under these hydrodynamic conditions may aggravate damage to yeast. This is supported by the use of bead mills for cell disruption for intracellular product release. Biological response to hydrodynamic stress may be quantified in terms of change in integrity, viability, metabolic rate, metabolic pathway and morphology (Logan and Dettmer, 1990; Smith *et al.*, 1990; Toma *et al.*, 1991; Illing and Harrison, 1999).
To understand how yeast respond to hydrodynamic stress, it is necessary to consider the structure of the microorganisms, in particular the cell wall as it is the first barrier of defence against physical stress (Walker, 1998). This is reviewed in Section 2.3.
The reported responses to different stresses (nutrient deprivation, heat shock, osmotic shock, oxidative stress, hydrodynamic stress) are presented in Section 2.4, in order to define yeast strategies to overcome stress.
Finally, as this study is carried out with the intention of modelling observed effects of microbial activity, models developed to describe cell damage are reviewed (Section 2.5).

2.2 INDUSTRIAL RELEVANCE: REVIEW OF SLURRY SYSTEMS

Mineral bioprocessing, soil remediation, immobilised cell systems and bead mills are industrial processes that use micro-organisms in the presence of solid particles.

2.2.1 Mineral bioprocessing

An example of mineral bioprocessing uses a mixed culture of chemolithotrophic bacteria to oxidise iron and sulphur containing ores. The oxidation process breaks down the ore matrix, allowing the dissolution of metals ions and making precious metal more amenable to further treatment.
Bioleaching is a well-established technology for the pre-treatment of refractory gold concentrates, with seven processes operating world-wide at commercial scale. At present, there is growing interest in the bioleaching of base metal concentrates (e.g. Cu, Ni), with high temperature archae providing an improved rate and an extent of leaching in these systems. Stirred tank and air lift reactors are favoured for the process as they allow

operating conditions (pH, temperature) to be controlled. High agitation is required in order to ensure that the high oxygen demand is met. High rates of agitation are also necessary to ensure complete solids loading. In addition, high agitation rates are favoured in order to ensure complete mixing (Nemati *et al.*, 2000; Scholtz-Brown, 1998).
However, high agitation rates and the presence of solid particulates could result in cell damage.

2.2.2 Soil bioremediation

Soil bioremediation involves the controlled use of micro-organisms to break down hazardous organic chemicals in soil. The pollutants are degraded to biomass and chemicals such as water, carbon dioxide (aerobic degradation) or methane (anaerobic degradation). Soil bioremediation is regarded as a relatively inexpensive and efficient treatment method. In addition the soil ecosystem is not destroyed.
In our study, the situation of particular interest is the *ex-situ* treatment of soils. The contaminated soil is excavated and treated with micro-organisms. The main advantage of *ex-situ* treatment of soil as compared to *in-situ* is that better control over the operating parameters is possible. Stirred tank reactors have been used (Ryan *et al*, 1991; Stegmann *et al.*, 1994) to treat this soil. A better understanding of this type of system will allow for the design of more efficient treatment facilities (Scholtz-Brown, 1998).

2.2.3 Immobilised cell systems

Cell immobilisation involves the attachment of cells to solid particles. Some of the advantages are an increased number of cells per reactor volume (Tyagi *et al.*, 1992), faster continuous production of secondary metabolites, easier downstream removal of micro-organisms and better oxygen transfer (Rosvear *et al.*, 1987; Webb *et al.*, 1996) and stabilisation of genetically engineered cells (Shu *et al.*, 1996).
Cell immobilisation can be achieved by active or passive immobilisation. Active immobilisation involves the attachment of the cells to the solid particles by chemical or physical means. The chemical bonding of *Saccharomyces cerevisiae* cells to solid support for the production of ethanol is an example of active immobilisation (Bandyopadhyay *et al.*, 1982). Passive immobilisation occurs when films or flocs of cells form naturally on, around or within solids surfaces or particles. Wastewater treatment (Bayley *et al.*, 1986), the growth of micro-organisms on biomass support particles (Atkinson *et al*, 1981) and the growth of animal cell culture on microcarrier (Croughan *et al.*, 1987; Cherry and Papoutsakis, 1988) are examples of passive immobilisation. The immobilisation of *Saccharomyces cerevisiae* for the production of recombinant proteins (Heslot *et al.*, 1991) is another illustration of this phenomenon. In this case, immobilisation was found to improve plasmid stability and productivity (Kanayama *et al.*, 1988).

2.2.4 Bead Mill

Bead mills are used to disrupt microbial cells in order to recover intracellular components. In this case, the cells are agitated at high impeller tip speeds, in the presence of a high fraction of inert particles (44-47% by volume). Glass beads are a popular grinding element although zirconium oxide and ceramic beads are also used. The cells are disrupted as a result of collisions and grinding between stream layers of solids at different

velocities (Engler, 1985). Disruption is influenced by process variables such as bead diameter, density and loading, cell concentration in feed, flow rate of feed, agitation speed and configuration, geometry of the grinding chamber and temperature (Harrison, 1991). Smaller bead sizes are generally more effective. For yeast cells, beads in the range 0.2 to 2.3 mm are used, with an optimum size of 0.25 – 0.5 mm. Schutte *et al.* (1983) determined that 80% solid loading was optimum for disruption of bakers' yeast. Increasing agitation speed is reported to generally increase disruption. However a levelling off of disruption is obtained at higher speeds (Schutte *et al.*, 1983).
The bead mill is an example of extreme conditions within a slurry reactor where high agitation rates and solids loading are desired, to result in cell disruption.

The other processes represent the opposite extreme, where it is desirable to have the highest possible growth rate with the highest possible solids loading in order to get the maximum possible rate of production. *S. cerevisiae* is used as a model organism and hence understanding is generated around it.

2.3 YEAST CHARACTERISTICS

2.3.1 Cell morphology

Saccharomyces cerevisiae is a unicellular eukaryote. Tschopp *et al.* (1987) (as cited in Walker, 1998) found that *S. cerevisiae* cells are generally ellipsoidal, with a large diameter ranging from 5 to10 μm and a small diameter of 3 to 7 μm. The mean cell volumes are respectively 29 and 55 μm^3 for a haploid and a diploid cell.
S. cerevisiae are small cells and are reported to be resistant to hydrodynamic forces, as opposed to larger animal cells, which lack a cell wall. Table 2.1 gives an indication of the relative strength of bacterial and yeast cells. It reports the applied pressures necessary to disrupt half the population in each culture, in a cell disrupter apparatus.

Table 2.1 Applied pressures necessary to disrupt half the population of a given culture.

Micro-organism	Characteristics	Pressure (Pa)
E. coli	Gram-negative rods	1.5×10^7
B. subtilis	Gram-positive rods	2.4×10^7
L. casei	Pleomorphic Gram-positive rods	3.1×10^7
S. faecalis	Gram-positive ovoid cocci	1.5×10^8
S. aureus	Gram-positive cocci	1.9×10^8
S. cerevisiae	Oval yeast cells	1.5×10^8

Adapted from Kelemen and Sharpe, 1979.

This project concerns the nature of the response of *S. cerevisiae* to hydrodynamic stress, so only the cell envelope characteristics will be discussed here, as the first barrier of defence against external stress.

2.3.1.1 Cell envelope

The arrangement of the cell envelope is shown in Figure 2.1. It consists of a rigid cell wall separated from the plasma membrane by a periplasmic space.

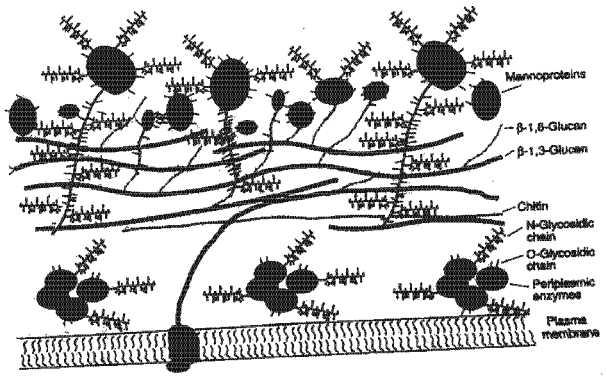

Figure 2.1 Schematic of the yeast cell wall (Walker, 1998)

2.3.1.2 Plasma membrane

The plasma membrane is a bilayer composed mostly of phospholipids and sterols. The membrane contains various structural and enzymic proteins which facilitate communication between the cell interior and the environment (Prokop *et al.*, 1992). Intrinsic proteins are inserted in the bilayer, while extrinsic protein molecules cover part of the lipid bilayer where they interact with membrane lipids and proteins by polar binding. The plasma membrane forms a diffusion barrier between the cytoplasm and the culture medium (Walker, 1998).

2.3.1.3 Yeast cell wall

The cell wall of yeast cells is relatively thick, generally 70-200 nm. Cell wall thickness reported in the literature is presented in Table 2.2. The cell wall represents 15-25% of the total dry mass of the cell. It is a prominent and distinguishing feature of all yeast (Walker, 1998).

Table 2.2 Yeast cell wall thickness, as reported in the literature

	Wall thickness (nm)	
Moor and Muhlehaler (1963)*	70 ± 10	
Srinorakutara *et al.* (1995)*	70 - 100	
Srinorakutara *et al.* (1998)	70 ± 15	
Walker (1998)	100 - 200	
Gaskova *et al.* (1998)*	175 ± 15 260 ± 42	(depending on glucose concentration in the growth media)
Smith *et al.* (2000a)	90	

* *as cited by Smith et al. (2000a)*

Fleet (1991) emphasises that the cell wall is not simply a static exoskeleton whose only role is to protect the protoplast. The yeast cell wall is a multifunctional organelle involved in cell protection, shape maintenance, cellular interactions, reception, attachment and specialised enzymatic activities.

The cell wall is regarded as an assemblage of mostly polysaccharide polymers, the rigidity of which imparts form and strength to the cell. The properties and functions of the cell wall change constantly during the life cycle of the cell (Klis *et al.*, 2002).

The yeast cell wall consists predominantly of 3 macromolecular components: lipids, proteins and polysaccharides (mannan, glucan and chitin). Polysaccharides are the most abundant constituents in the wall, accounting for 80 – 90% of the wall by mass. Glucan and mannan are the predominant polysaccharides with only a small amount of chitin present.

Glucan is a polymer of glucose, accounting for approximately 60 wt% of the cell wall. Different types of glucan have been classified by Manners *et al.* (1973) and Fleet and Manners (1975), according to the relative abundance of β(1,3) and β(1,6) linkages between the glucose residues. The alkali insoluble/acid insoluble fraction has a fibrillar appearance and confers rigidity to the wall. The predominantly β(1,6) fraction is thought to be the anchorage point for chitin while the alkali soluble portion is amorphous and confers flexibility to the wall. Glucan is also an anchorage point for mannan and provides an extracellular metabolic store of glucose.

In the yeast cell wall, mannan is always found to be covalently linked to protein, hence mannoprotein is a better representation for this macromolecule. The mannoproteins represent 25-50% of the cell wall of *S. cerevisiae* (Jayatissa and Rose, 1976) with the protein content amounting to 5-10%. Mannoproteins linked to each other by sulphur bonds, form the outer cell wall layer while the inner layer is formed by covalent mannoprotein-glucan bonds. Although apparently rigid in structure, it participates in a number of morphological changes, including budding, mating and sporulation.

Chitin is an unbranched and highly rigid polymer of N-acetyl-D-glucosamine, joined through β(1,4) linkages. Less than 10% of the cell wall consists of glucosamine polymers. Most of the chitin is found in the bud scar zone of mother cells. This suggests that chitin has a specific involvement with cell division, but its precise role remains unclear (Kapteyn *et al.*, 1998). Because of the rigidity of the chitin molecules, older yeast cells with more bud scars are more rigid and inelastic, which may cause them to respond differently to hydrodynamic stress.

The cell wall is the main obstacle to cell lysis. Wall thickness is reported to increases with age, but the presence of bud scars, consisting of chitin, in older cells interrupts the rigid glucan layer, making these cells more susceptible to mechanical damage. As the cell increases in age, the physiological state of the cell wall must deteriorate due to an increase in the number of bud scars and the cell must die after having given rise to a certain number of buds (Vrana *et al.*, 1982). The cell wall rupture may be achieved mechanically or by enzymatic digestion of its constituents. Extreme treatment is required to disrupt the cells by mechanical means resulting in damaged organelles and membrane fragments. The maximum shear stress tolerable by *S. cerevisiae* is in the order of 8×10^7 N/m^2 (Mersmann *et al*, 1990), making it one of the most resistant cells to rupture and over 10^5 fold more resistant than animals cell (Augenstein *et al.*, 1971). Kelemen and Sharpe

(1979) suggested that the structure of the outer membranes of the cells might be determinant in cell resistance to shear stress. They compared the forces required to disrupt different micro-organisms and observed that the ease of disruption was related to the shape of the micro-organism and the chemical composition of the cell wall.

Some changes in the cell wall structure are expected under conditions of hydrodynamic stress. These structural changes will occur in order to increase mechanical strength and thus limit the amount of cell damage that may occur.

2.3.2 The surface properties of *Saccharomyces cerevisiae*

Since it is the cell wall of *S cerevisiae* that contacts its environment, it is the cell wall properties, most notably the surface charge and hydrophobicity of this surface, which determine its interaction with the environment.

Many authors have confirmed that yeast cells bear a net negative charge at the pH values of growth (Eddy *et al.*, 1958; Beavan *et al.*, 1979). This negative charge has been attributed to the phosphate groups of the outer cell wall phosphomannan. The other cell wall constituent influencing the net charge is protein. Protein is a source of negatively charged carboxyl groups and positively charged amino-groups. Chitin is uncharged. Jayastissa and Rose (1976) treated yeast cells with 60% hydrofluoric acid and observed that carboxyl groups were removed or phosphate groups were esterified. It is unclear whether these effects are to be expected under less vigorous treatments. The equilibria of phosphate, carboxyl and amino groups may be represented as (Bowen *et al.*, 1992):

$$H_3PO_4 \Leftrightarrow H_2PO_4^- + H^+ \qquad pK=2.12 \qquad \text{Equation 2.1}$$

$$H_2PO_4^- \Leftrightarrow HPO_4^{2-} + H^+ \qquad pK=7.21 \qquad \text{Equation 2.2}$$

$$HPO_4^{2-} \Leftrightarrow PO_4^{3-} + H^+ \qquad pK=12.32 \qquad \text{Equation 2.3}$$

$$COOH \Leftrightarrow COO^- + H^+ \qquad pK=4.1 \qquad \text{Equation 2.4}$$

$$NH_3^+ \Leftrightarrow NH_2 + H^+ \qquad pK=10.5 \qquad \text{Equation 2.5}$$

Assuming that these ionisation potentials remain the same for ions in the yeast cell wall, the degree of ionisation of each group may be determined at a particular pH level. The pH level is varied by suspending the cells in buffer solutions of various pH levels. The groups contributing to the overall cell surface charge as pH is varied are summarised as follows:

Table 2.3 Effect of pH on yeast cell wall constituents ionisation.

pH	Nature of Yeast Cell Wall Group		
2.0	H_3PO_4	COOH	NH_3^+
4.0	$H_2PO_4^-$	COOH	NH_3^+
7.0	$H_2PO_4^-$	COO^-	NH_3^+

Bowen *et al.* (1992) showed that the average ratio of positively charged groups to negatively charged groups at low pHs is 1:0.57. Eddy *et al.* (1958) and Beavan *et al.* (1979), have worked with the premise that the charge attributable to phosphate groups was proportional to the electrokinetic mobility of the cells at pH 4.0, while that attributed to carboxylic groups was proportional to the difference in mobility between pH 7.0 and pH 4.0. They also reported that the charge attributable to carboxyl groups increased as cultures progressed from the exponential to the stationary phase, while that caused by the phosphate groups tended to decline. Bowen *et al.* (1988) used this method in their analysis of yeast quality in brewing. Their experiments showed a reduction in the number of negatively charged groups in the outer cell wall layer after 24 hours of fermentation and upon successive fermentation cycles. It is to be noted that pH dropped from 5.1 to 3.7 during fermentation. They also found that zeta potential decreased from -26.5 to -38.0 mV as pH was increased from 3.5 to 5.5.

Brewing yeast has been shown to exhibit modified surface charge when exposed to physiological stresses such as dehydration and rehydration (Rapoport *et al*, 1985). Smart *et al.*, (1995) starved brewing yeast for 24 hours in sterile water at pH 4.0 and noticed modified surface topography. Non-starved yeast had rough surface topography and a mean diameter of 4.51 μm. Starved yeast were significantly smaller (1.57 μm) and displayed a smoother surface. The authors noticed that colonies derived from starved cells produced cells of similar morphology to the starved parent cells, even though they were propagated in the absence of physiological stress. It was suggested that starved parental cell wall fragments were included in daughter cells during budding, enabling the retention of starved wall characteristics. Thus starvation may modify cell wall protein templates, resulting in the inheritance of the starved cell wall characteristics. Starvation also resulted in a significant increase of zeta potential from -42.6 to -32.5 mV at pH 4.0. Robinson *et al.* (2001) investigated the effect of aeration on surface properties of brewers' yeast. They observed that strains exhibited a lower zeta potential when grown aerobically, compared to anaerobic conditions.

Differences have been reported between hydrophobicity of top and bottom fermenting yeast strains. The hydrophobicity of top fermenting strains is greater than that of bottom fermenting strains (Amory and Rouxhet, 1988) and is correlated to the nitrogen to phosphate ratio measured by XPS. Dengis *et al.* (1995) confirm that top fermenting strains are generally more hydrophobic. Robinson *et al.* (2001) compared four strains of *Saccharomyces cerevisiae*, grown anaerobically or aerobically. They found that the hydrophobicity of the cells increased during the exponential phase under anaerobic conditions, while hydrophobicity remained low throughout propagation for the aerobically grown yeast. Once stationary phase was reached, no further change in hydrophobicity was observed.

Rhymes and Smart (1996) observed the preferential attachment of hydrophobic latex beads to the polar regions of individual cells. In budding cells, there was a distinct lack of attachment to the mother/daughter region. This indicates that the mature regions of the cells, particularly old bud scars may be more hydrophobic than younger cell wall material. Chitin is the major component of bud scars, hence it is probable that chitin contents of cells is a major determinant in its level of hydrophobicity.

2.3.3 Cell growth

2.3.3.1 Cell growth cycles

Figure 2.2 shows a schematic representation of the cell growth cycle. The G0 phase occurs when one or more nutrients are depleted. This is an off-cycle quiescent state. During the G1 stage, the mother cell will continue growing until a critical cell size is reached. Once this critical cell size is reached, the cell traverses to the Start or S phase of growth. The Start in G1 has two phases, Start A is the nutrient and growth check point. Start B is the replication and proliferation check point. If the requirements are met then a bud starts forming. The bud starts to grow during the G2 phase and mother and daughter cells separate in the M phase.

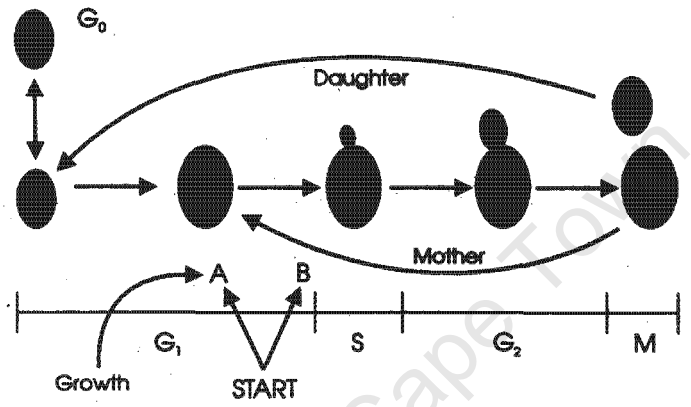

Figure 2.2 Cell growth cycle (Walker, 1998)

2.3.3.2 Growth kinetics

When growing yeast cells in a batch reactor, the following phases are observed (Shuler and Kargi, 1992):

- Lag phase
- Logarithmic phase
- Deceleration phase
- Stationary phase
- Death phase

The lag phase is the time required (after inoculation) for the cells to adapt to the surrounding environment. Molecular reorganisation takes place in order to accommodate any differences in the media.

The logarithmic phase occurs after the cells have adapted to the new environment and start to reproduce. In the logarithmic phase, there is a high nutrient concentration and cell growth is independent of nutrient concentration.

Entry into the stationary phase is governed by the nature of the limiting nutrient. Depletion of a carbon source will result in entry into the stationary phase. However, a depletion of nitrogen results in meiosis.

The last phase in the growth curve is the death phase. It is very difficult to distinguish between the stationary and the death phase. This is due to the fact that the lysed cell release nutrients into the media, which are taken up by the active cells. Death occurs as a result of nutrient depletion or an excess of toxic by-products.

The acceleration and deceleration phases represent the transition between lag and exponential growth phase, and exponential growth phase and stationary phase respectively.

In general (with the exception of the lag phase), the growth rate of yeast is given by:

$$\frac{dX}{dt} = \mu X \qquad \text{Equation 2.6}$$

where X is the yeast biomass concentration ($g.L^{-1}$)
t is the time (h)
μ is the specific growth rate (h^{-1}).

For the case of exponential growth, μ is given by μ_{max}, the maximum specific growth rate. In general, μ can be given by a modified Monod equation accounting for both nutrient limitation and cell death through Equation 2.7.

$$\mu = \frac{\mu_{max} S}{K_S + S} - k_d \qquad \text{Equation 2.7}$$

Where μ_{max} is the maximum specific growth rate (h^{-1})
S is the substrate concentration ($g.L^{-1}$)
k_d is the death rate (h^{-1})
K_S is the saturation constant equal to nutrient concentration which limits growth to half its maximum rate ($g.L^{-1}$).

This may be further modified to account for presence of inhibitors, temperature effects, etc.

2.3.3.3 Growth requirements

Most yeast grow best in a temperature range of 20 to 30°C. The maximum growth temperature for *S. cerevisiae* is 35 to 43°C. Yeast generally prefer a pH of 4.5 to 6.5 but they can grow in the range of pH 3 to 8 (Walker, 1998). Water is necessary in high concentrations for growth and metabolism, as substrates and enzymes are all in aqueous solution or colloidal suspension.

A range of elemental compositions of *S. cerevisiae*, reported in Bailey and Ollis (1986) and by Krzystek *et al.* (1998) are summarised in Table 2.4.

Table 2.4 Elemental composition of *Saccharomyces cerevisiae*.

Composition	Authors
$CH_{1.66}N_{0.13}O_{0.4}$	Bailey and Ollis (1986)
$CH_{1.75}N_{0.15}O_{0.50}$	Bailey and Ollis (1986)
$CH_{1.64}N_{0.16}O_{0.52}P_{0.01}S_{0.005}$	Bailey and Ollis (1986)
$CH_{1.61}N_{0.15}O_{0.52}$ + 8% Ash	Krzystek and Ledakowicz (1998)

These formulas vary depending on the yeast strain and growth conditions. However, they give an indication of the macronutrients required by the yeast in order to grow.

Yeast are chemoorganotrophic organisms, which means they get carbon and energy from compounds in fixed, organic linkage. Sugars are the most common carbon sources, glucose being the most widely utilised by yeast. Carbohydrates also provide elemental hydrogen. Oxygen is an essential growth factor. Yeast cannot grow in the complete absence of oxygen. As a matter of fact, oxygen provides a substrate for respiratory enzymes during aerobic growth. But it is also required for certain growth-maintaining hydroxylations such as those involving the biosynthesis of sterols and unsaturated fatty acids (Walker, 1998). Hence *S. cerevisiae* yeast are auxotrophic for oleic acid and ergostrerol under anaerobic conditions. The competition between fermentation and respiration is controlled by the availability of both glucose and oxygen (Bailey and Ollis, 1986). At suitable values of glucose and dissolved oxygen concentrations, glucose is utilised for respiration, provided maximal cell yields per unit amount of glucose consumed. If glucose concentration increases above a certain level, metabolism switches to fermentation, even in the presence of oxygen. Yeast have a nitrogen content of around 10% of their dry weight. Inorganic nitrogen sources, such as ammonium salts, are largely utilised to grow yeast. Ammonium sulphate is commonly used, as it also provides a source of assimilable sulphur, essential for the bio-synthesis of sulphur-containing amino-acid (Walker, 1998). Phosphorus is present in nucleic acids and in phospholipids, and therefore needs to be provided to the yeast. Orthophosphate and condensed inorganic phosphate are common sources of phosphorus in yeast growth media.
Yeast also require some minerals. Potassium and magnesium are necessary to establish the metallic cationic environment in the yeast cell. Other minerals, referred to as trace elements, are required in the micromolar or nanomolar range and include Mn, Ca, Fe, Zn, Cu, Ni, Co and Mo. Some of the other growth factors required by *S. cerevisiae* are vitamins, such as biotin, pantothenic acid and thiamine.

2.4 BIOLOGICAL RESPONSE TO STRESS

2.4.1 Responses to physicochemical stress

In microbial processes, microbes are subjected to a range of stresses through the train from inoculum development through the bioreactor to cell harvesting. Stresses such as nutrient deprivation, heat shock, osmotic shock, and oxidative stress have been well studied compared to hydrodynamic stress and influence cell growth, product formation, ease of solid-liquid separation, to name a few. General stress responses occur for a wide number of different stress types. Thus where a stress response is general it is possible that it may be observed in other stress conditions that have not been fully investigated (Ruiss, 1997). Therefore it is important to review biological responses to physicochemical stresses to understand those of hydrodynamic stress.

2.4.1.1 Nutrient deprivation

The nature of the biological response to nutrient depletion is dependent on the limiting nutrient, for example oxygen, nitrogen, carbon, sulphur, etc (de Winde *et al.*, 1997).
In *S. cerevisiae*, nutrient availability is verified during the G1 phase of cell division. Budding will only occur if there is sufficient nutrient. Yeast can metabolise a wide variety of carbon sources, in the order of their ease of metabolism. After depletion of a specific carbon source, a period of minimal growth occurs during which enzymes required to metabolise the next carbon source are induced and synthesised. When all the carbon sources are consumed, the yeast enters the stationary phase. Nitrogen is required for the synthesis of nucleotides and amino-acids, building blocks for nucleic acids and proteins. These compounds are essential for regulating metabolic activity within the cell. Thus their synthesis is tightly regulated with respect to the availability of nitrogen sources. Nitrogen is also a major building block in the various energy storage compounds. A combination of oxygen availability and glucose availability control the yeasts' selection of the respirative or fermentation metabolism, yielding biomass or ethanol respectively.

In some cases of nutrient deprivation, it has been observed that yeast cells undergo morphological changes. The change from yeast-like growth by the formation of buds to pseudohyphal growth by cell fission type growth was originally observed in response to nitrogen deprivation. Recently this has been observed as a response to limitation of other nutrients. Pseudohyphal growth assists the yeast in foraging for its limited nutrients (de Winde *et al.*, 1997). Further Slaughter and Nomura (1992b) report an increased extracellular protease activity on nitrogen limitation. This again assists the yeast in foraying for its limiting nutrient.

Starvation is also reported to affect cell wall surface charge. *S. cerevisiae* cells exhibit negatively charged surfaces due to the presence of phosphate groups in the outer cell wall mannoprotein layers (Amory *et al.*, 1988). Smart *et al.* (1995) measured the zeta potential of starved and non-starved yeast. They observed that starvation resulted in a significant reduction in zeta potential (increase of the negative charge). Robinson and Harrison (2001) report a dependence of surface charge and hydrophobicity on the availability of oxygen during yeast growth.

Glycogen forms a readily available carbon and energy storage compound in yeast which can account for up to 40 % of cell dry mass (Oliver, 1991, as cited in Nkosi, 2001). Quain *et al.* (1981) report that the accumulation of glycogen in brewing yeast shows 3 distinct phases: rapid depletion during the initial hours of pitching, accumulation during the bulk of the fermentation and gradual depletion towards the end of fermentation. Decline in glycogen concentration at the end of fermentation is attributed to the provision of maintenance energy under conditions of starvation (Quain, 1988). Metabolism of glycogen results in generation of ATP and the synthesis of sterols and fatty acids. These compounds are critical in maintaining the structure and function of the cell membrane and determining the extent of cell multiplication. Reduced glycogen levels on pitching correlate with a reduced rate of attenuation and yeast growth (Murray *et al.*, 1984, as cited in Nkosi, 2001). Contrary to glycogen which accumulates under conditions of "plenty", trehalose is found to accumulate under starvation (be it carbon, nitrogen or phosphate) conditions (Quain, 1991). Trehalose accumulation appears to be a general response to stress. For example, heat shock, cold shock, exposure to toxic chemicals (e.g. ethanol), and dessication all promote trehalose synthesis (Wiemken, 1990; Quain, 1991). Plourde-Owobi *et al.* (2000) points out the remarkable contribution of trehalose in stress tolerance, as the higher the trehalose content, the longer the cell survival to a severe heat shock and to glucose starvation. It is hypothesized that trehalose acts as a protecting agent which stabilizes membrane structure (Iwahashi *et al.*, 1995).
Lee (1999) also reports that severe nutrient limitation leads to induction of heat shock proteins. Thus HSP26 is induced by carbon source limitation, HSP118 by sulphur limitation (Lee, 1999). In summary, Berry (1989) observed that while the nutritional requirements of yeast are not very demanding, they should be controlled precisely to ensure maximum growth rate and optimum yields.

2.4.1.2 Temperature shock

Temperature shock is the only stress type against which yeast does not have any barrier. Yeast has no means of controlling temperature. As a consequence, the cells have to adapt to the given temperature conditions. Temperature shock affects numerous different aspects of yeast physiological functions. These include cell viability, general cell morphology, cell division and growth, plasma membrane structure and function, cytoskeletal integrity, mitochondrial structure and function, intermediary metabolism, protein synthesis and chromosomal structure and function (Walker, 1998).

Heat shock leads to disruption of cellular processes, increased protein unfolding and aggregation, and conformational and structural changes in the membranes. Under conditions of stress induced by temperature, yeast evoke an active response which results in the shutting down of the majority of normal cellular functions and increase of the expression of a number of specific stress-response genes (Birch and Walker, 2000). These so-called heat shock genes form an essential part of the response mechanism to stress. The primary function of heat shock proteins is to accumulate rapidly following a stressful event, not only to protect cells against these damaging effects of stress, but also to confer an increased tolerance to subsequent stresses (Lee, 1999). In addition, other metabolic changes occur in stressed cells, such as the accumulation of the protectant storage carbohydrate trehalose. Trehalose is known to be one of the most effective substances for *in vitro* preservation of membranous structures and enzyme activities during desiccation, freezing or heating (Piper, 1997).

The protection of stress response compounds in exposure to further stress is the early probe of investigation. Tamura *et al.* (1998), cited by Lee (1999) showed that a pressure shock pre-treatment increased the resistance of yeast to subsequent heat shock at 51°C, pressure shock at 150MPa, and ethanol shock at 14% v/v. They correlated this with the increased expression of HSP 104p, present at 3.4 times the normal level following a pressure shock of 75 MPa. This phenomenon of one stress effector leading to an increased tolerance to a number of different stresses is known as cross protection (Lee, 1999).

2.4.1.3 Osmotic shock

Water is essential for microbial cells, as a solvent for membranes, a reactive agent for biochemical reactions or as a key factor in cell morphology. Therefore microbes have developed mechanisms to control osmolarity (the relative water content) (Hohmann, 1997). Osmotic shock can result from changes in salt concentration or sugar concentration for example. Generally, a change in salt concentration results in an inflow or outflow of water from the yeast cell. A mechanism of adaptation to the stress is the accumulation or release of glycerol in order to restore the osmotic balance. Moreover, due to the inflow or outflow of water, osmotic shock results in drastic changes to cell volume (Hohmann, 1997). Thus the addition of salt or sugar to the growth medium is reported to cause cell shrinkage. As a result, cell membrane and cytoskeleton can be damaged, leading to the release of wall compounds and changes in the cells' budding pattern. In the context of high gravity brewing, the negative effects of high osmotic pressures on yeast activity have been considered. High sugar concentrations result in slower rates of fermentation and cell growth, thus reducing fermentation productivity. The expression of heat shock proteins is also reported to be a response to osmotic shock (Lee, 1999). Sharma (1997) also reports an increased status of trehalose in cells grown under hypersaline conditions. He suggests that this increase in trehalose content may be contributing to the survival of cells grown under hypersaline conditions as well as to their ability to withstand toxic concentration of alcohol. The phenomenon of cross protection was also pointed out, as cells grown under increased NaCl concentrations were more ethanol tolerant than controls (Sharma, 1997).

2.4.1.4 Oxidative stress

Oxidative stress occurs when cells come into contact with reactive oxygen species (ROSs). These ROSs tend to attack macromolecules within the cell. Copper and iron are metals essential for life due to their involvement as enzyme cofactors in a wide variety of biological reactions. However these metals are also involved in reactions which generate ROSs. Thus cells need to have finely tuned mechanisms which allow for the accumulation of sufficient quantities of these metals, without excessive accumulation (Saunter and Thieve, 1997). The change from anaerobic to aerobic fermentation conditions has been demonstrated to evoke an oxidative stress response in brewing yeast. Sudden transition from anaerobiosis to aerobiosis led to a drop in cellular viability of 5-7% (Lee, 1999).

2.4.2 Quantification of stress response

Five categories of biogical response to stress have been identified: change in viability, metabolic rate, metabolic pathway, morphology and integrity (Basson, 1996; Illing and Harrison, 1999).

Viability
Viability is defined as the ability of a cell to divide or its ability to exclude viability stains. The methods used to determine the cell's viability are based on either regrowth studies such as plate or slide counts, or vital stain techniques. Staining techniques are based on sustained metabolic activity such that the dye is either excluded or reduced (Smart *et al.*, 1999; Basson, 1996; Robinson, 2001).

Metabolic rate
Changes in metabolic rate have been observed as decreased growth rate, substrate utilisation rate, oxygen utilisation rate and metabolite production rate (Illing, 1996). Toma *et al.* (1991) describes decreased ATP generation, decreased specific growth rate and lower O_2 uptake under excess turbulence. During fermentation, the metabolic rate varies according to oxygen and other nutrient availability, product inhibition and physiological status. In order to use metabolic rate as a measure of physiological status, careful control of the remaining nutrients is required (Nkosi, 2001). To predict overall metabolic activity of yeast, oxygen utilisation rates can be used (Basson, 1996).

Metabolic pathway
A shift in the product spectrum or metabolic flux, a change in the metabolism from the TCA cycle to the glycolytic pathway (Toma *et al.*, 1991) and the release of stress indicators such as HSPs and trehalose have been reported as metabolic pathway changes (Walker, 1998; Potgieter, 2002).

Morphology
Morphological changes with regard to size and shape have been described. Wase and Patel (1988) showed that the mean cell volumes of *Bacillus cereus*, *Staphylococcus epidermis*, *Saccharomyces cerevisiae* and *Escherichia coli* were directly proportional to the agitation rate of the fermenter. Break-up of cell aggregates (*Corynebacterium glutamium*) under different levels of agitation and aeration is also reported as an example of morphological change (Illing and Harrison, 1999).

Integrity
The loss of cell integrity occurs when either the cell membrane or cell wall or both are ruptured (Dunlop *et al.*, 1994). The extent of cell disruption can be measured in terms of total cell count (Cherry and Papoutsakis, 1987; Dunlop *et al.*, 1994; Zhang *et al.*, 1995), protein release (Lowry, 1951; Pearce, 1993; Scholtz-Brown, 1998), or nucleic acid release (Croughan and Wang, 1989). Release of invertase can also be used to detect cell wall damage (Goldstein, 1975, as cited in Pearce (1993)). Loss of integrity represents the most extreme form of yeast cell damage.

2.5 HYDRODYNAMIC STRESS

2.5.1 Physical sources of stress

2.5.1.1 Shear

Depending on its intensity, a shear field may be stimulatory, inhibitory or destructive. Yeast are generally quite robust and not easily damaged under typical submerged culture processing conditions; however, even the most robust cells are broken when subjected to suitable combinations of high stress and exposure time (Chisti, 1999; Illing, 1996).

The magnitude of the fluid mechanical forces is often expressed as shear stress, τ or shear rate, γ. These quantities are related; thus in laminar newtonian flow,

$$\tau = \gamma^* \mu_L \qquad \text{Equation 2.8}$$

where μ_L is the viscosity of the fluid.

Shear rate is a measure of spatial variation in local velocities in a fluid. Cell damage in a moving fluid is sometimes associated with the magnitude of the prevailing shear rate or the associated shear stress, but these quantities are never easily defined in the relatively turbulent environment of most reactors (Chisti, 1999; Kelemen *et al.*, 1979).

Influences of shear stresses are reflected in the industrially important aspects of production rate, productivity and product spectrum. Responses to shear has been characterised using various indices, including growth rate, cell viability, regrowth potential, release of intracellular material, changes in oxygen uptake rate, ATP, productivity of metabolites, biochemical composition of the cells, and alterations in the morphology of cells and cell aggregates (Chisti, 1999; Robinson, 2001).
The French press is an example of application of shear stress used to disrupt microbial cells. Brookman (1975) studied the influence of the apparatus characteristics on disruption (measured in terms of soluble protein release). While disruption increased exponentially with increasing pressure, complete disruption was achieved at 50,000 psi. The release of soluble protein was independent of the velocity of the yeast suspension passing through the needle valve, but increased exponentially with decreasing needle length. At a constant pressure peak, the shorter the time of the pressure change, the greater the cell disruption. The evidence of shear effects as the major mechanism of cell damage was outlined, the rate of change of pressure being the key parameter for cell disruption. Lange *et al.* (2001) also investigated the effect of high shear stress on *S. cerevisiae* viability. Cell suspensions were submitted to shear stress by flowing through a narrow capillary. They found that shear stress did not affect total cell number, nor yeast cells were disrupted, even at the highest shear stress value (2770 Pa). However when submitted to shear stress of 2770 Pa, viability decreased rapidly as the duration of exposure to shear stress increased. They concluded that an intensity threshold exists above which the stress generated affects the viability of the yeast. This was already suggested by Kelemen and Sharpe (1979). They used a disrupter to subject different micro-organisms (including *S.cerevisiae*) to extremely high shear forces, causing disruption. They observed that little or no disruption occurred until a certain level of applied

pressure was reached. Thereafter the proportion of disrupted cells increased rapidly with increasing disrupter pressure, until almost all the cells were disrupted.

2.5.1.2 Interaction with turbulent eddies

The interaction of cells with turbulent eddies is a second mechanism causing hydrodynamic trauma. In the turbulent region where energy dissipation occurs by eddy interaction, the scale of the energy transfer between eddies and between eddies and cells becomes significant. Energy dissipation occurs by the breakdown of large eddies into progressively smaller ones until the smallest eddies disintegrate by viscous action. For isotropic turbulence, the size of these smallest eddies, known as the Kolmogorov microscale length, is calculated by Equation 2.9, with the eddy velocity given in Equation 2.10 (Kolmogorov, 1941, cited by Robinson, 2001; Cherry and Papoutsakis, 1988).

$$l_c = \left(\frac{\nu^3}{\varepsilon}\right)^{\frac{1}{4}} \qquad \text{Equation 2.9}$$

$$v = (\varepsilon\nu)^{\frac{1}{4}} \qquad \text{Equation 2.10}$$

where l_c = Kolmogorov microscale length (m)
v = kinematic viscosity of the medium ($m.s^{-1}$)
ε = Specific energy dissipation rate ($m^2.s^{-3}$)

The specific energy dissipation rate (ε) can be estimated by determining the volume in which the energy is dissipated and the time scale of the event. The extent to which turbulent kinetic energy is transferred to micro-organisms depends on the relative size of the Kolmogorov eddies and the cell. Eddies larger than the microbial particle will not dissipate energy at the cell surface and the cell is described to be entrained by the eddy. Eddies much smaller than the particle have insufficient energy to cause significant cell break-up. Eddies whose size approaches the particle diameter impart the maximum hydrodynamic force. A number of researchers have investigated the microscale length on cell viability in stirred and bubble column bioreactors on plant cell, animal cells and microcarrier systems (Dunlop *et al.*, 1994, Cherry and Papoutsakis, 1988, Croughan *et al.*, 1987, Illing and Harrison, 1999). Significant shear damage to cells in a turbulent environment was only observed when the cells, aggregates or microcarriers were of the same size or larger than the Kolmogorov eddies. Cherry and Papoutsakis (1988) investigated the negative effects of excessive agitation on tissue cells in microcarrier culture. They observed that a decreasing smallest turbulence size between 100 and 200 μm (compared to 180 μm typical microcarrier size) caused reduced cell growth (measured in terms of apparent cell growth, net effect of actual growth minus any cell death). Investigating the fluid-mechanical sensitivity of plant cells in a stirred bioreactor, Dunlop *et al.* (1994) established a hierarchy of responses, ranging from biological inhibitory effect on regrowth ability to loss of membrane integrity, loss of mitochondrial activity, aggregate breakup, and finally lysis. The turbulence in stirred tanks is highly inhomogeneous and the most negative cell-eddy interactions are assumed to occur in the impeller zone, where maximum fluid velocities are found (Illing and Harrison, 1999). Illing (1996) found that cell lysis, viability and metabolism were not affected by turbulent forces in stirred-tank reactors. However, break-up of cell aggregates was observed at an impeller tip speed of 6.7 m/s and a superficial gas velocity of 0.005 m/s in the absence of mass transfer limitation. As the impeller tip speed was increased from 1.68 to 6.7 m/s at

a constant superficial gas velocity of 0.005 m/s, Illing and Harrison (1999) observed a decrease in the mean aggregate diameter from 3.3 μm to 1.75 μm. The predominant mechanism of aggregate disruption was the erosion of primary cells from the aggregate surface.

2.5.1.3 Cavitation

In regions of low pressure within the flow, cavities of vapour can form spontaneously. These then collapse in regions of higher pressure in a process called cavitation. This oscillating behaviour and rapid collapse of the cavities exert large forces on particles suspended in the fluid (Save *et al.*, 1994, 1997). The cavitation number (σ), defined in Equation 2.11 determines the likelihood of cavitation occurring.

$$\sigma = \frac{P_\infty - P_v}{\left(\rho \times v_\infty^2\right)/2} \qquad \text{Equation 2.11}$$

where P_∞ = pressure upstream of an orifice (Pa)
P_v = pressure at any point of maximum fluid velocity (Pa)
v_∞ = velocity upstream of the orifice ($m.s^{-1}$)

It represents the ratio of forces collapsing cavities to those causing their formation. Cavitation will occur at cavitation numbers below a critical cavitation number σ_c. Hydrodynamic cavitation is intentionally used to cause yeast disruption and protein release and is reported to be one of the most energy efficient disruption techniques.

2.5.1.4 Cell-cell and cell-obstacle interactions

Physical cell-cell or cell-obstacle collision is another mechanism of cell damage.
The level of damage depends on both the frequency and intensity of collisions (Illing, 1996). A collision of a cell requires the force driving the microorganisms together to exceed the force required to remove the liquid layer between them (Illing, 1996).

The frequency of cell-cell collisions where the Kolmogorov microscale is of a similar size to the cells can be estimated by Equation 2.12 derived by Cherry and Papoutsakis (1988):

$$N_c = \left(\frac{v\alpha^2}{d_p^4}\right)\left(\frac{\pi d_p^3}{6\alpha}\right) \qquad \text{Equation 2.12}$$

where α = volume fraction of cells
v = relative cell velocity ($m.s^{-1}$)
N_c = frequency of cell-cell collisions (Hz)
d_p = particle diameter (m).

The collision severity, CS, is then defined as the product of the frequency and kinetic energy of collisions per cell (Equation 2.13). Alternatively, the relative velocity can be based on a shear model which leads to a shear based collision severity expression given in Equation 2.14.

$$CS_T = \frac{(\varepsilon v)^{\frac{3}{4}} \pi^2 \rho_p \alpha d_p^2}{72} \qquad \text{Equation 2.13}$$

$$CS_s = \frac{(\varepsilon/\nu)^{\frac{3}{2}} \pi^2 \rho_p a d_p^{\frac{3}{2}}}{72}$$ Equation 2.14

where ρ_p = particle/cell density (kg.m^{-3})
CS_f = collision severity based on eddy velocity (cm)
CS_s = collision severity based on shear model (J.s^{-1})

Scholtz-Brown *et al.* (2002) demonstrated that the major source of stress in a slurry bioreactor is solid-cell-solid collisions and not cell-cell collisions.

2.5.2 Responses to hydrodynamic stress

2.5.2.1 Non-growing systems

Studies on the effect of particulates on freely suspended micro-organisms in slurry bioreactors, using a yeast – silica model system, have been conducted by Harrison *et al.* (2002). These workers investigated the effect of particulate parameters, including loading (5% to 40% (v/v)), diameter (25 to 1800 μm), density (1600 to 4500 kg.m^{-3}) and shape (smooth or jagged), on the disruption of stationary phase *Saccharomyces cerevisiae* in a completely suspended system. While the maximum extent of disruption was independent of the solid parameters, the disruption rate constant increased as a power law function of volume fraction of solids. Increased particle density and smoothness resulted in a marginal increase in rate constant. The critical particle size of 300 μm was determined below which the rate of cell disruption was greatly reduced. Monitoring both invertase release and the release of cytoplasmic proteins, cell envelope damage was observed to occur more rapidly than cell disruption, under mild conditions. Scholtz-Brown and Harrison (2002 a and b) used the same system to investigate the effect of completely and incompletely suspended solids. Significant cell disruption occurred for solids volume fractions in the range 0.05-0.40, while negligible disruption occurred in the absence of solid particles. This suggested that the dominant mechanism of cell disruption was interaction between particles and cells as opposed to cell interactions with turbulent fluid eddies. Disruption approached a quadratic dependence on the solid volume fraction at loading fractions of 10 and 20%, indicating the importance of solid-cell-solid interactions. Models, describing cell disruption as a function of the operating parameters, were proposed. They are further detailed in Section 2.6.1. In accordance with Harrison *et al.* (2002), the disruption rate of *Saccharomyces cerevisiae* at an agitation intensity of 750 rpm (impeller tip speed of 2.91 m.s^{-1}) was found to increase in a power law fashion from 7.08 × 10^{-5} s^{-1} at 5% (v/v) inert solids to 4.05 × 10^{-3} s^{-1} at 40% inert solids. At speeds above the critical impeller speed for complete suspension, the k values increased linearly with impeller speed.

2.5.2.2 Growing systems

Literature of the effect of agitation on growth is frequently contradictory. Toma *et al.* (1991) considered *Brevibacterium flavum*, *S. cerevisiae* and *Trichoderma reesei*. They discovered there is an optimum impeller speed above which cell growth, and activity decrease due to hydrodynamic stresses. The extent of growth was expressed in terms of specific growth

rate, calculated from biomass concentration of *B. flavum*, determined turbidimetrically at 650 nm. Activity was expressed in terms of oxygen uptake rate, RNA, DNA and ATP content and aconitase activity. Wase and Patel (1985) observed that agitation speed had no effect on cell growth or dry biomass concentration in their study on *Bacillus cereus*, *Staphylococcus epidermidis*, *Saccharomyces cerevisiae* and *Escherichia coli* in a chemostat. However, they found that mean cell volume was directly proportional to the agitation rate. The increased cell volume was due to an increase in the water content of the cells. The impeller speed was varied in the range 1.6 to 5.3 m/s.
Ruis (1997) argues that *S. cerevisiae* growth proceeds more slowly under conditions of mild stress and may be suspended completely under conditions of severe stress. Slower growth may provide time and allow diversion of energy to respond to the stress. However, no indication about how cells respond to stress is given. Cells may develop resistance to the stress, enabling the cells to survive until the stress is reduced or eliminated. The mechanism of such a resistance was not explained. They report that only stress which results from the exhaustion of nutrients will cause the cells to enter into the stationary phase. Other stresses result in a slower growth of yeast cultures or in extreme cases cell death. That is contrary to Nemati and Harrison (2000) who found that physiological stress and low environment pH caused *Sulfolobus metallicus* to enter stationary phase.

Not only agitation rate, but also the nature of the flow has to be considered. Chisti (1999) reported on the effects of different types of impellers. Agitation-associated damage can be reduced substantially by replacing the Rushton turbines with axial flow hydrofoil impellers. These findings confirm that different types of impellers generate very different shear fields at identical tip speed. Scholtz-Brown (1998) used both Rushton turbine and pitched-blade turbine to disrupt yeast cells in a slurry reactor. She observed the same maximum extent of cell disruption, irrespective of the flow pattern. However the rate of cell disruption was less for the pitched-blade turbine. Pearce (1993) also found with a mineral bio-oxidation system that neither the Rushton nor the axial impeller at an impeller speed of 350 rpm inhibited the growth of *thiobacilli*. At 630 rpm, no activity appeared in the tank agitated by a Rushton turbine while the growth rate started to increase after a lag phase of 14 days with the pitched-blade turbine. These findings are in agreement with Hackl *et al.* (1989), which reports that pitched-blade turbine has a higher pumping capacity than Rushton turbine and, for a given impeller speed, requires less power. As a consequence, it produces lower turbulence intensity.

The yeast cell wall is a key factor in the response of micro-organisms to hydrodynamic stress. Toma *et al* (1991) theorise that the inhibition of microbial growth and productivity, in the absence of cell death, is due to limited mass transfer in stagnant eddies of microscales of turbulence and shear forces damaging cell membranes. They use the term *turbohyphobiosis* to describe this effect. Chisti (1999) reports that the composition of the growth medium and the specific growth rate used for the culture influence the robustness of the cell. Cells grown in fully defined media that lacked one or more components essential to synthesis of a normal cell wall are often less robust. Growth at a higher specific rate will often produce weaker cells. Cells experiencing physiological stress (e.g. starvation) are more susceptible to shear-stress-related damage. These findings are consistent with the resistance of microbes to mechanical cell breakage as a function of growth condition (Harrison, 1991; Gray *et al.*, 1972; Bayer *et al.*, 1967; Felix, 1982; Golovina et al., 1973; Fish and Lilly, 1984). Smith *et al* (2000) developed a micromanipulation technique to measure the force required to burst single cells and established a mathematical model to extract the mechanical properties of *Saccharomyces*

cerevisiae cell wall. They determined that yeast cell populations strengthen as they enter stationary phase by increasing wall thickness, without altering the average elastic properties of the cell-wall material. They considered the biochemical composition of cell walls. Cell walls of *S. cerevisiae* consist predominantly of glucan with (1,3)-β and (1,6)-β linkages, and mannan covalently linked to protein (mannoprotein). They proposed that mechanical properties are only a function of the β-glucans, whereas the role of mannoproteins is to control porosity.

There is limited literature on the effect of non-biological particles in a slurry bioreactor on microbial performance. Solid particulates in suspension increase hydrodynamic stress, by increasing shear forces exerted on the cell. Thermophilic bioleaching of mineral ores, conducted above 65°C, is mediated by thermophilic archae of the genus *Sulfolobus*. Owing to their unique cell wall structure, these cells are postulated to exhibit greater sensitivity to mechanical handling. Reduced performance in the presence of intense agitation and high solids loading in a slurry reactor has been cited in bioleaching studies using *Sulfolobus* (Escobar *et al.*, 1993; Norris and Barr, 1988). Recent studies have been carried out by Nemati and Harrison (1999, 2000) to investigate how the bioleaching microbe in growing phase respond to the presence of non-biological particles.

Particle size effects have been investigated by Nemati and Harrison (1999). They considered the bioleaching of pyrite by acidophilic thermophile *Sulfolobus metallicus*. The size of the mineral ranging over a mean diameter of 42.5 – 202 micron did not influence the growth and the activity of the cells and relatively constant values for both the specific growth rate (μ) and yield factor (Y) were achieved. Effect of pulp density (solids loading) has also been considered. Still considering the rate of bioleaching of *Sulfolobus metallicus*, Nemati and Harrison (2000) found that in the experiment with 3% pyrite, the increase in biomass concentration continued until the complete oxidation of pyrite. The exhaustion of pyrite led to a sharp decrease in biomass concentration. With mineral pulp densities of 6 and 9% (v/v), a plateau region in biomass concentration curves was observed, indicating the stationary phase of microbial growth. It must be noted that the oxidation of pyrite was accompanied by a decrease in pH. The shift to microbial growth from exponential phase to stationary phase occurred when the pH decreased to a value between 0.9 to 1.0. So the reduced performance at solids loading in the range of 12 – 15% (v/v) may result from the physiological stress imposed by the low environmental pH or from a combination of the high mineral concentration and the low environmental pH. The presence of solid particulates strongly affects the lag phase. Nemati and Harrison (1999) determined that the lag phase was more pronounced in the presence of larger particles. They also found that lag phase in microbial growth was longer at higher pulp densities.

Critical levels of hydrodynamic stress have been identified. Nemati and Harrison (1999) found that in the presence of pyrite with a mean diameter of 6.4 micron (size fraction < 25 micron), no biological activity was observed. The number of cells, as well as their size, decreased dramatically over a short period. Apparently the attrition, due to the presence of small particles, disrupted the structure of the cells. This implies that the reduction of particle size below a critical level could increase the extent of the particle-particle collision and impose severe attrition on the cells. Applying a mineral pulp density of 18% (v/v), the complete suspension of pyrite led to a dramatic decrease in concentration of biomass and inactivity of the cells. Both cell disruption and impaired metabolic activity result when a critical pulp density is exceeded. The system used allowed the negative

influence of high solids loading to be characterised. However the maximum critical concentration of mineral tolerated is system specific.

2.5.2.3 Quantification of hydrodynamic stress response

The effects of hydrodynamic stress have been summarised in a work by Basson (1996) displayed in Figure 2.3 below.

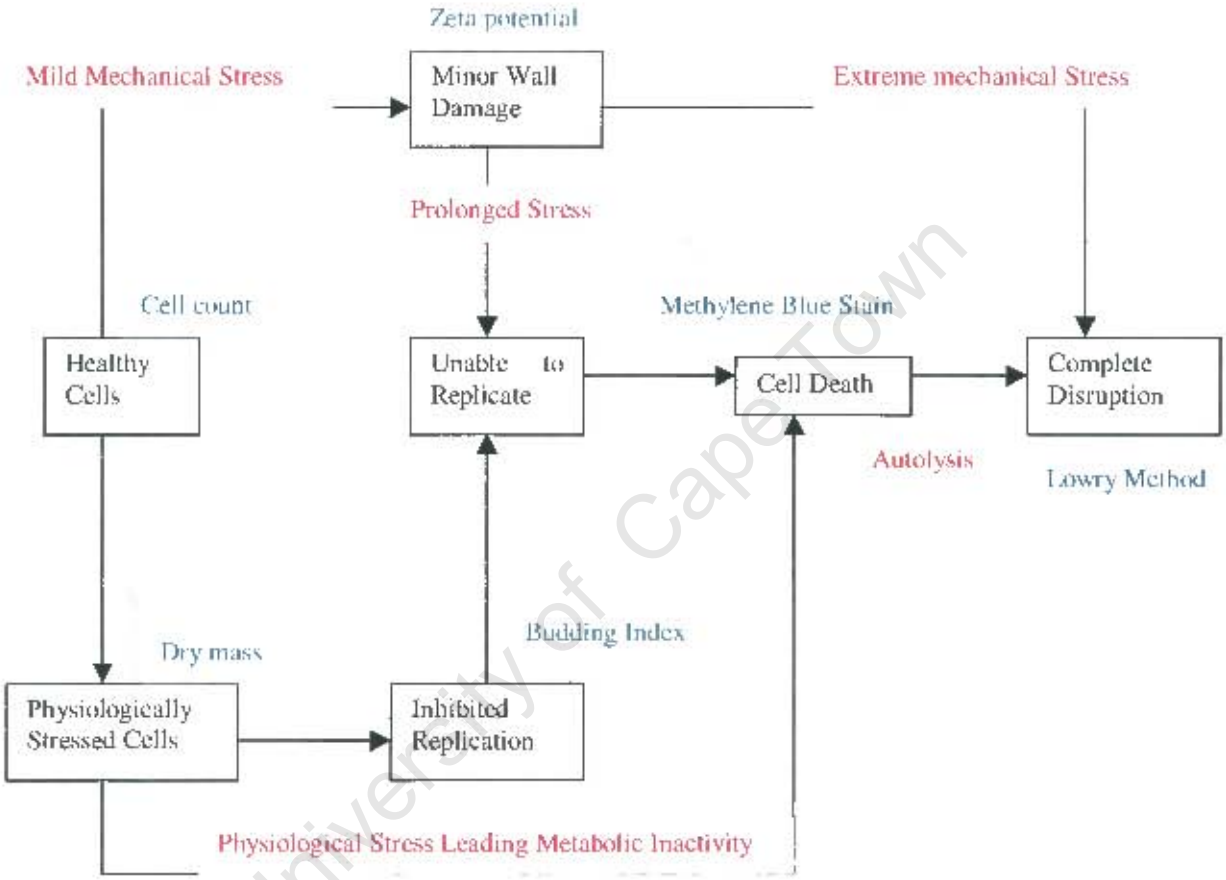

Figure 2.3 The effects of hydrodynamic stress on cells and the suggested analyses by which to quantify these effects (Basson, 1996).

2.6 MODELLING OF HYDRODYNAMIC DAMAGE

Modelling cell damage and disruption in biological processes enables its prediction under particular operating conditions. A model will facilitate the design of large-scale bioreactors, so that, in processes where cells are in contact with a solid particle phase, the cell damage and disruption can be minimised or maximised, depending on the application.

2.6.1 Non-growing systems

Scholtz-Brown *et al.* (2002) disrupted freely suspended *S. cerevisiae* in a slurry reactor using silica particles as the solid phase. Their work showed protein was released from disrupted cells according to first order kinetics of the form:

$$R = R_i (1-\exp(-kt)) \qquad \text{Equation 2.15}$$

where R is the soluble protein released at time t (mg protein/mg cells).
R_i is the maximum protein released under the specified operating conditions (mg protein/mg cells).
k is the first order disruption rate constant (s^{-1}).

The first order disruption rate (k) exhibited a power law dependency on the solids volume fraction. Although the degree of solids suspension had no effect on the maximum extent of cell breakage, it had a significant effect on k. At speeds below the critical impeller speed at a constant solids loading, k exhibited a power law dependence on the impeller speed corresponding to an increase in the volume fraction of suspended solids with impeller speed. Above the critical impeller speed at a constant solids loading, they observed a linear relationship between k and impeller speed.

Models for the disruption of stationary phase *S.* cerevisiae :

Three models have been developed for describing the effects of solids concentration and agitation rate on cell disruption, above the critical impeller speed.
The first model incorporates solids loading and agitation rate into an expression for the disruption rate constant which is analogous to an oxygen mass transfer model (Scholtz-Brown *et al.*, 2002).

$$k = 7.11 \times 10^{-5} (P/V)^{0.56} \phi^{1.64} \qquad \text{Equation 2.16}$$

where P is the impeller power input (W)
V is the reactor volume (m^3)
ϕ is the volume fraction of solid particles.

This model describes the rate of protein release from cells into the supernatant upon cell disruption. The cell concentration is not explicitly shown in Equation 2.16 since it was maintained at a constant average value in the experimental study. Moreover, the model accounts only for cell-solid interactions as the mechanism of cell disruption.

The maximum energy dissipation rate per a unit fluid mass in a stirred tank occurs in the impeller discharge zone, so the majority of cell damage and disruption occurs in this region (Illing, 1999). The second model only considered the impeller zone in correlating the first order disruption constant with the energy input per pass through the impeller zone per unit volume of the vessel (Pt_c/V). t_c is the average circulation time of the liquid and may be estimated for a 6-bladed Rushton turbine in a fully baffled cylindrical vessel using equation 2.17 (Reed *et al.*, 1977, as cited in Scholtz-Brown *et al.* (2002)):

$$t_c = \frac{4V}{3ND^3} \qquad \text{Equation 2.17}$$

where D is the reactor diameter (m)
N is the impeller speed (rps)

The energy input per pass through the impeller zone per unit of vessel may then be incorporated in a mass transfer-type model in order to predict the disruption rate constant (Scholtz-Brown *et al.*, 2002):

$$k = 4.76 \times 10^{-6} (P t_c / V)^{0.90} \phi^{1.61} \quad \text{Equation 2.18}$$

A mechanistic model based on cell-eddy interactions, solid-cell-solid collisions, solid-cell collisions and solid-cell-reactor collisions has been suggested in the form of equation 2.19 (Scholtz-Brown *et al.*, 2002):

$$k = A (\varepsilon/\nu^3)^{3/4} + B c\phi^2 N^n + D c\phi N^n \quad \text{Equation 2.19}$$

where A, B, D and n are constants.
ε is the turbulent power dissipation rate per mass of liquid (kg^{-1}).
ν is the liquid kinematic viscosity (m^2/s).
$c\phi$ represents the solid-cell and the solid-cell-reactor wall collision mechanisms.
c is the biomass concentration (kg/m^3).
N is the impeller speed (rpm).

The first term represents cell-eddy interactions and is negligible in this study. The remaining terms account for the interaction between particles and the cells.

Final result was:

$$k = 2.27 \times 10^{-7} \phi^2 N^{1.68} + 1.05 \times 10^{-8} \phi N^{1.68} \quad \text{Equation 2.20}$$

Solid-cell-solid collisions were identified as being the primary cause of cell disruption, as opposed to solid-cell or solid-cell-reactor collisions.

These models have all been derived for constant biomass concentrations and therefore make no allowance for biomass growth.

2.6.2 Growing systems

2.6.2.1 Hydrodynamic Effects on Animal Cells grown in Microcarrier

Cells on microcarriers are susceptible to damage from fluid mechanical forces owing to microcarrier size being similar to Kolmogorov eddy size in submerged culture.
Croughan *et al.* (1986) grew FS-4 cells on microcarriers in 250 mL spinner flasks. For cultures containing 3g/L microcarriers, they found a decrease in the rate of cell growth with increasing agitation rate from 60 to 220 rpm. They modelled their results according to specific growth and death rates given in Equations 2.21 and 2.22:

$$\ln\left(\frac{C}{C_0}\right) = (\mu - q)(t - t_0) \quad \text{for } t < t_1 \quad \text{Equation 2.21}$$

$$\text{and } \ln\left(\frac{C}{C_1}\right) = -q(t - t_1) \qquad \text{for } t > t_1 \qquad \text{Equation 2.22}$$

where C_0 is the initial cell concentration at time t_0 (cells/mL)
C is the cell concentration at time t
C_1 is the cell concentration at time t_1
t_1 is the time at which stationary phase is reached (h)
μ is the specific growth rate (h^{-1})
q is the specific death rate (h^{-1})

Croughan *et al.* (1986) used these models to calculate specific growth and death rates for various impeller speeds. The death rate ranged from 0 to 0.027 L/h as agitation rate was increased from 60 to 220 rpm. The specific growth rate was constant at 0.016 L/h.

Hu (1983) correlated the growth on microcarrier cultures with an integrated shear factor, shown by Equation 2.23.

$$ISF = \frac{2\pi N D_i}{D_t - D_i} \qquad \text{Equation 2.23}$$

where D_i is the impeller diameter (m)
D_t is the vessel diameter (m)

They plotted the relative extent of growth of FS-4 cells on microcarriers as a function of integrated shear factor and found that maximum relative growth occurred for ISF in the range 7 to 18 L/s, decreased growth between ISF 18-30 L/s and no growth beyond 30 L/s. They determined that maximum cell growth and zero cell growth can be observed at the same impeller tip speed, depending on vessel size and geometry. Although this means of analysis is useful, an integrated shear factor is not readily incorporated into a mechanistic model of hydrodynamic effects on cells.

Papoutsakis and O'Connor (1992) found that increased agitation slowed the rate of increase in viable CHO cells attached to microcarrier beads. Croughan and Wang (1988) investigated whether cell growth was inhibited, unchanged or enhanced by hydrodynamic forces in microcarrier cultures. They noted two effects by which high agitation levels may inhibit cell growth: decrease of biosynthetic ability required for cell growth, or non-replication of the cells. The authors' experiments showed that at high agitation rates, cells were either removed from microcarriers, inhibited from growing at their maximum rate or both. Cell fragments were observed from cell cultures agitated from growing at their maximum rate. For cell cultures agitated at 60 rpm in spinner flasks, complete whole cell lysis occurred over a period of 1-2 days. It is unclear whether fragments were generated through lysis of free or attached cells. It was noted that all cells removed from the microcarrier became non-viable upon removal. Results showed that freely suspended animal cells were not affected by moderate increases in agitation or exposure to moderate shear stresses. Secondary growth was previously postulated to occur when cells that were exposed to high agitation rates were once again grown at favourable agitation rates. However data strongly indicated that there was a situation of growth and death with no secondary growth. No growth inhibition was observed, even during conditions of extensive cell disruption and death. Croughan and Wang (1988) concluded that a cell's decision to replicate depends on genetic programming which is uninterrupted by adverse hydrodynamic conditions.

Hu (1983) found no decrease in growth rate of mammalian cells when the microcarrier concentration with attached cultures was increased from 5 to 15 g/L. Croughan *et al.* (1988) also increased solids loading in microcarrier systems by adding beads which did not support cell attachment or growth. They noted that at high bead concentrations, cell systems showed very long lag phases, decreased growth rates and decreased multiplication ratios (final cell concentration over initial cell concentration). They found that the maximum growth rate occurred at approximately 0.2 g/L microcarriers or an initial cell concentration of 1.5 x 10^4 cells/mL. They concluded that the existence of the maximum implied that there were at least two competing factors influencing growth rate. Initial cell concentration is increased with increased microcarrier concentration, favouring growth. Increased solids loading with increased microcarrier concentrations, results in decreased growth rate due to increased particle-cell collision frequency. The authors also found that below 35 rpm, increased microcarrier loading had negligible effect on cell activity or disruption. 35 rpm was probably very below the critical impeller speed required to suspend all microcarriers resulting in the true microcarrier density being well below the claimed value. They extended their previous model (Equations 2-8 and 2-9) to include the effects of microcarrier-microcarrier interaction and microcarrier-bead interaction. The new model is given by Equation 2.24:

$$\frac{dC}{dt} = \mu C - q_1 C - q_2 C_m C - \frac{q_2}{2} C_i C \qquad \text{Equation 2.24}$$

where q_1 is the specific death rate due to fluid-cell interactions (h^{-1})
q_2 is the specific death rate due to microcarrier-microcarrier interaction and microcarrier-bead interactions (h^{-1})
C_m is the microcarrier concentration (g/L)
C_i is the bead concentration (g/L)
C is the biomass concentration (cells/mL)

They found that Equation 2.24 correlated well with experimental data at 150 rpm in 250 mL spinner flasks. It was also found that at approximately 5.5 g/L microcarrier concentration, the specific death rate equalled the specific growth rate, with no net growth being observed.

Cherry and Papoutsakis (1987) investigated the effect of microcarrier concentration on the apparent growth rate of bovine embryonic kidney cells. They attributed the reduced apparent growth rate to collisions of microcarriers. These interactions were postulated to be the only interaction capable of producing enough energy to damage the model microorganism. This was confirmed by the bead to eddy size ratio showing little effect on the growth rate, thus implying microcarrier-fluid interaction resulted in negligible cell damage. The effect of these bead-bead collisions was characterised in terms of turbulence collision severity (TCS), defined as the product of collision kinetic energy and frequency.

$$TCS = (kinetic\cdot energy)\left(\frac{collisions}{(volume)(time)}\right)\left(\frac{beads}{volume}\right)^{-1} \qquad \text{Equation 2.25}$$

The effect of the microcarrier volume fraction may then be calculated from Equation 2.26:

$$TCS = \left(\frac{N_p N^3 D_i^5 \nu}{V}\right)\left(\frac{\pi^2 \rho_b \alpha d^2}{72}\right) \qquad \text{Equation 2.26}$$

where N_p is the power number $\left(\frac{P}{N^3 D_i^5 \rho_L}\right)$

P is the power input (W)

D_i is the impeller diameter (m)
ρ_b is the microcarrier bead density (kg/m^3)
α is the microcarrier volume fraction.

Collisions of the beads against the impeller or other reactor internals have a similar effect to bead-bead collisions, however the kinetic energy of collisions is much higher. Cherry and Papoutsakis (1987) defined an impeller collision severity (ICS) analogous to turbulence collision severity.

$$ICS = \frac{(kinetic \cdot energy)}{\left[\frac{reactor \cdot volume}{(window \cdot area)(velocity \cdot past \cdot blade)}\right]} \qquad \text{Equation 2.27}$$

The effect of impeller speed may now be determined from Equation 2.28.

$$ICS = \frac{9\pi^4 \rho_b n_b n^3 D_i^4 d^4}{512V} \qquad \text{Equation 2.28}$$

where n_b is the number of impeller blades.

It should be noted that the ICS formula is only approximate because viscous effects have been ignored as have the trajectory of particles from streamlines. Growth rate decreased for increased impeller collision severity. Turbulent collision severity increased with increased bead loading, leading to a higher frequency of bead collisions and a decrease in the apparent growth rate. Both the TCS and ICS models provided good fits of experimental data.

2.6.2.2 Hydrodynamic Effects on Glucose consumption

Croughan *et al.* (1988) noted that the glucose uptake of FS-4 cells in microcarrier cultures decreased from 46×10^{-12} to 35×10^{-12} g/(cell.h) for an increased agitation rate from 35 to 150 rpm in spinner flasks (specific growth rate at these conditions was 0.0028 L/h). Specific glucose uptake was calculated according to equation:

$$R_g = \frac{(G_2 - G_1)\ln\left(\frac{C_2}{C_1}\right)}{(t_2 - t_1)(C_2 - C_1)} \qquad \text{Equation 2.29}$$

where G_i is the glucose concentration at time i (t_i)
C_i represents the viable cell concentration at time i.

No correlation was found between glucose uptake and specific growth rate. It appeared as though glucose uptake was not associated with growth for FS-4 cells.

2.6.2.3 Hydrodynamic effects on cells grown in suspension

Reuss (1988) set out to understand the effect of geometric and operating parameters on the specific growth rate of the mould *Rhizopus nigricans* in stirred bioreactors. He demonstrated that maximum growth rate decreased for a decrease in reactor volume, thus making the common parameter of impeller tip speed unsuitable for satisfactory

explanation of disruption phenomena. Reuss (1988) further remarked that so called reaction volume independent parameters, such as the mean energy dissipation rate, varied for changed reaction volume and were therefore unsuitable for descriptions of systems of all geometries. Instead of the previous parameters, Reuss (1988) suggested using the energy input per unit volume as described by Equation 2.30:

$$E = \frac{P}{V_{susp} C_v} \qquad \text{Equation 2.30}$$

where P is the power input (W)
V_{susp} is the flow rate of the cell suspension (m^3/s)
C_v is the volumetric solid concentration.

When applying this concept to the problem of mechanical damage to micro-organisms, the volume concentration of biomass can be neglected. Thus, it is assumed that all the power input into the system is dissipated in the fluid bulk. The flow rate of the cell suspension is expressed as:

$$V_{susp} = \frac{V}{\theta} \qquad \text{Equation 2.31}$$

where V is the reaction volume (m^3)
θ is the average circulation time (s)

From systematic measurements of distributions in two different volume vessels, at different ratios of liquid height to tank diameter and impeller to tank diameter, the average circulation time could be correlated with geometrical and operating parameters in the following way (Boelcke, 1983, as cited in Reuss, 1988):

$$\theta = \frac{0.76}{n}\left(\frac{H}{D_T}\right)^{0.6}\left(\frac{D_T}{D_i}\right)^{2.7} \qquad \text{Equation 2.32}$$

where n is the impeller speed (rps)
H is the liquid height (m)
D_T is the tank diameter (m)
D_i is the impeller diameter (m)

The model found good correlation with experimental results and had the added benefit of being applicable for a range of reactor geometries. Data in a plot of specific growth rate versus energy per unit volume could be fitted by a continuous line of the form:

$$\mu_{max} = (\mu_{max})^* - C\left(\frac{P}{V/\theta}\right)^a \qquad \text{Equation 2.33}$$

where μ_{max} is the maximum specific growth rate (L/h)
$(\mu_{max})^*$ is the upper limit of the maximum specific growth rate (L/h)
C and a are constants.

μ_{max} is probably the apparent growth rate, making $(\mu_{max})^*$ equivalent to the maximum growth rate in the absence of mechanical disruption. The final term in Equation 2.33 is attributed to cell death due to mechanical forces.

Reuss (1988) plotted the degree of disruption for various cell concentrations of stationary phase *Saccharomyces cerevisiae* versus energy input per unit volume and found a deviation of less than 10% from a single regression line of the data. This proved that the omission of biomass concentration from equation 2.32 was justified. Reuss (1988) derived the

concept of specific energy or power input per circulated flow rate from experimental data of *Rhizopus nigricans*. Using published experimental data, disruption of the protozoa *Tetrahymena pyriformis* by mechanical agitation in vessels and with impellers of different sizes could also be interpreted quantitatively. The same key parameter was also used to explain the influence of the most important operating parameters on the disruption of microbial cells in bead mills, a very important process for the recovery of intracellular products.

Effects of agitation on growth rate seem very dependent on the micro-organism studied. Thus Yang and Wang (1992) investigated the effect of agitation and sparging rate on the growth of shear sensitive algae. They observed negligible changes in growth rate for low agitation rates (200 – 350 rpm), however at an agitation rate of 525 rpm, the growth rate diminished. This rate was then further diminished as the system was sparged with air. Kioutkia *et al.* (1996) found that moderate agitation rates had essentially no effect on the growth of insect cells. In contrast, these authors noted that similar variations in the rate of agitation in hybridoma systems resulted in a decrease in both growth rate and viable cell concentration at the end of each fermentation. The results indicate that animal cells exhibit different sensitivities to shear, some showing no sensitivity at all. However this particular study was limited in that they did not investigate agitation rates above 400 rpm (0.94 $m.s^{-1}$ tip speed) .

2.7 CONCLUSIONS AND RECOMMENDATIONS

From previous work, it has been demonstrated that hydrodynamic stress inhibits microbial growth, reduces performance and in extreme case causes disruption (Scholtz-Brown, 1998; Toma *et al.*, 1991; Nemati and Harrison, 1999, 2000). Critical levels of hydrodynamic stresses have been identified, in term of agitation rate and solid loading (Toma *et al.*, 1991; Scholtz-Brown, 1998; Nemati and Harrison, 1999, 2000).

Cell growth conditions and resultant wall thickness seem decisive in the response to stress (Chisti, 1999; Smith *et al.*, 2000). However, changes in the cell wall structure are not precisely known and still need to be investigated.

The production of specific compounds as a response to hydrodynamic stress has been observed. Trehalose, glycogen and heat shock proteins are formed as a response to different stresses such as nutrient deprivation (de Winde *et al.*, 1997), heat shock (Piper, 1997; Lee, 1999), cold shock (Nkosi, 2001), osmotic shock (Lee, 1999). No author mentions the formation of such products under hydrodynamic stress. But Ruiss (1997) notes that these general stress responses may be observed in other stress conditions that have not been fully studied.

Smith *et al.* (2000) found that under severe conditions of stress, yeast enter stationary phase to better resist the trauma. From the studies of Nemati and Harrison (1999, 2000), as well as Croughan *et al.*, 1988), it appears that hydrodynamic stress in the presence of inert particulates increases lag phase in growth. This corresponds to an adaptation period of the cells to their environment. Mechanisms of adaptation and resistance need also to be elucidated.

In general, limited rigorous studies of microbial cell damage in slurry reactors under growth conditions are reported. Hydrodynamic stress is little characterised. As concerns modelling of hydrodynamic stress, work of Reuss (1988), Scholtz-Brown (1998) and Croughan *et al.* (1986) all suggest the need for a cell death rate term to describe cell damage or disruption in slurry reactor systems. Further, damage in slurry reactor systems is attributed chiefly to particle-cell-particle interactions and not cell-eddy interactions for microbial cells (Scholtz-Brown, 1998).

Chapter 3: Experimental procedure

The experimental procedure describes the aerobic cultivation of yeast in a slurry reactor, under hydrodynamic stresses and its analysis. Section 3.1 deals with the materials involved in the yeast growth. The equipment used and standard experimental conditions are described in Section 3.2. Analyses performed (Section 3.3) are also detailed. In Section 3.4 the experimental approach is described.

3.1 EXPERIMENTAL MATERIALS

3.1.1 Micro-organisms

Baker's Yeast *Saccharomyces cerevisiae* was grown from a culture kindly supplied by Anchor Yeast (Cape Town, South Africa). The yeast was maintained on agar slopes (Appendix A) at 4°C for up to six months after which they were transferred to new slopes to avoid loss of viability. These slopes were used to inoculate the pre-inoculum for all experiments.

3.1.2 Non-biological solids

Silica sand supplied by CONSOL Sand (Cape Town, South Africa) was used as a model for non-biological particles in the reactor. A particle size fraction of 600 – 850 μm was achieved using stainless steel sieve screens (20 to 28 mesh).

Silica sand required preparation before being used in the experiments to remove any organic compounds and impurities from the particle surface (Scholtz-Brown, 1998). This was achieved by washing several times in an agitated tank with distilled water (at least 10 times), then calcining at 500°C for 4 hours. Silica was washed again for about 3 hours and allowed to dry in an oven overnight. Total organic carbon (TOC) analysis was performed in order to determine if the sand was totally free of all biological material.

The density of the solid material was determined using an Accupyc 1330 Pycnometer. This fully-automatic gas displacement pycnometer determines the density of a known mass of substance by measuring the pressure change of helium in a calibrated volume. The average density was found to be 2650.4 kg/m^3 ± 0.4 kg/m^3.

During experimentation, solid particle breakup was suspected in the bioreactor, because the solution became coloured. The extent of this breakup was therefore examined using a Malvern Mastersizer. The solids particle size was analysed for the various impeller speeds investigated, namely 460, 565 and 850 rpm. The results showed that particle breakup did not occur to any significant extent. Minimal surface breakage from the solid particles is therefore suspected for the coloration of the bioreactor.

3.1.2 Inoculum preparation and propagation

The propagation procedure involves a 10-fold increase in volume per propagation vessel transfer, i.e. the 15 ml pre-inoculum yeast culture is made up to the 150 ml inoculum culture, which is made to the 1500 ml bioreactor volume.

3.1.2.1 Pre-inoculum

A pre-inoculum of 1% (15 mL) of the initial working volume of the reactor (1.5 L) was prepared, using a 250 mL Erlenmeyer flask. The sterile media was inoculated from the stock culture slant and grown at 30°C for 24 hours in a shaker oven at 130 rpm. The pre-inoculum medium consists of a YM growth media. The exact medium composition is shown in Appendix A.

3.1.2.2 Inoculum

The inoculum was prepared by inoculating a 250 ml shake flask containing 135 ml of simple medium with the 15 ml pre-inoculum culture. Yeast were cultivated for a further 14 hours at 30°C in the shaker oven.

3.1.2.3 Growth medium

The growth medium consisted of 1350 mL of simple medium and 150 mL of inoculum. The inoculum was added to the bioreactor under aseptic conditions.

Inoculum and growth media (detailed in Appendix A) were composed of glucose, salts and vitamins. Glucose and salt solutions had to be autoclaved separately to prevent the caramelisation of glucose. The two solutions were added together under aseptic conditions in a laminar air flow cabinet. Vitamins were added to the autoclaved solutions by filter-sterilisation in a laminar air flow cabinet.

3.2 EXPERIMENTAL RUN PROPAGATION

3.2.1 Reactor set up

The reactor consisted of a completely sealable and sterilisable 2 litre glass reactor vessel, with a working volume of 1.5 L, containing a heating coil, air sparger, baffles. Various ports were provided for inoculation, sampling, etc. Reactor design and geometry is detailed in Appendix B. The reactor set-up is shown in Figure 3.1.

Under standard conditions, agitation of the broth was performed using a 6-bladed Rushton turbine (RT). A 45-degree angled pitch blade impeller (PBT) was also used. The impeller was driven by a constant speed motor for which belts were available to adjust the speed to one of four speeds.
The variable speed motor allowed the stirrer speed to be adjusted between 460 and 850 rpm. Impeller speeds were determined by using a hand-held photo tachometer (Lutron DT-2236). Under standard conditions, a speed of 565 rpm was used.

A 4-bladed baffle of 15 mm diameter was placed inside the reactor to eliminate vortex formation and improve the degree of mixing.

Compressed air supplied to the reactors passed through a cotton wool filter, sterile distilled water to humidify the air and finally an air filter of 0.22 μm pore size to reduce the risk of contamination in the reactor. It was sparged into the vessel below the

impeller. The air flow rate was maintained at 1.5 L/min (1 vvm) to ensure that there is no oxygen limitation.

A constant temperature of 30°C is advised for maximum yeast cell growth (Atkinson and Mavituna, 1983). Temperature was maintained at this value by means of the heating coil through which water was circulated from a heated waterbath.

Yeast are found to grow optimally at pH between 4 and 5 (Shuler *et al.*, 1992). A 15 mL aliquot of an acetic acid/sodium acetate buffer solution was added to the salt solution to maintain the pH between these values during the growth. The pH was checked at the beginning and at the end of each run.

Foaming and frothing are undesirable as they lead to the partitioning of biomass into the froth phase where physiological conditions are sub-optimal. As a consequence, 2 ml of antifoam were added to the reaction medium prior to autoclaving.

Figure 3.1: Experimental setup

3.2.2 Media and reactor sterilisation

Pre-inoculum, inoculum and reaction medium were autoclaved at 120°C for 20 minutes. The glucose solution was autoclaved in the reactor vessel. Sterilisation of the reactor involved:

- Reactor vessel charged with the glucose solution, 2ml of antifoam and the specific mass of silica to provide the desired volume-to-volume ratio of solids in the reactor.
- Reactor lids clamped tightly onto the vessels, while the ports not in used are sealed.
- Air exit line filter connected to its particular port.

Salt solutions were autoclaved separately in a 1 litre bottom-feeding Erlenmeyer flask. Heat labile vitamin solution was added to the salt solution in the Erlenmeyer flask under aseptic conditions in the laminar flow cabinet, by means of a syringe by passing the solution through a 0.22 μm filter.

3.2.3 Reactor inoculation

Once the reactor is autoclaved, the impeller was connected to the drive shaft and the air line to the sparger. The heating coil was connected so that the temperature of the reactor medium was at a constant 30°C when the reactor inoculum was added.
The salt and vitamin solution was transferred to the reactor under gravity. The pre-prepared reactor inoculum was then transferred to the bottom-feeding Erlenmeyer flask previously used to transfer the salt/vitamin solution to the reactor, under aseptic conditions. Both flask mouths were flamed before the transfer was done.

3.2.4 Sampling

Sampling was performed using an aseptic sampling port. The initial sample was taken immediately after the reactor inoculation. Thereafter samples were taken at varying time intervals, every 3 hours in the beginning, and then every 5 hours.

Sampling protocol required that no more than 10% of the initial reactor volume be sampled during experimentation. This limited the number of available samples taken to 12, since, for every sample, 12.5 ml had to be extracted. The first 5 ml were syringed out and collected as waste, in order to clean the sample line. A second sample of 7 ml was then extracted and analysed.

3.2.5 Termination of experiment

Experiments were run until the microscopic cell count indicated that growth had reached stationary phase. Therefore, for each experiment, the last sampling was taken 28 hours after inoculation.

3.3 ANALYTICAL TECHNIQUES

All the analytical techniques are detailed in Appendix C.

3.3.1 Absorbance

As the cells multiply during the growth, the broth becomes opaque. Thus absorbance was measured at 660 nm as an indication of the total number of cells. Following the settling out of the silica phase, the coefficient of variance of absorbance measurements varied from 15.3% at the beginning to 2.2% at the end of the run, based on a standard deviation of 0.05 absorbance unit.

3.3.2 Dry biomass concentration

The biomass concentration of *Saccharomyces cerevisiae* was determined from a cell dry weight analysis. 1 mL of cell suspension was pipetted into Eppendorf microfuge tubes pre-dried and weighed to four decimal places. The suspension was centrifuged at 15000 rpm for 5 min in a microtube. After removal of the supernatant, the cell pellet was dried in an oven at 80°C for 3 days. After being cooled in a dessicator and re-weighed, the cell dry weight concentration was determined from the quotient of the cell mass (final minus initial weight) and the volume of the suspension (1 mL). Each cell dry mass analysis was performed in triplicate. The coefficient of variance varied typically from 55.5% at the beginning of the run to 9.2% at the end, based on a standard deviation of 0.42g.

3.3.3 Microscopy

Total cell counts, budding index and viability measurements were determined simultaneously at regular intervals during the growth. Direct cell counting was accomplished using light microscopy at 40x magnification (bright field) and a Thoma counting chamber. Lysed and dead cells were determined by staining with a modified Ringer salt solution containing methylene blue (dead and lysed cells appeared in blue).
The coefficient of variance in cell counting was calculated as 1.3% and 7.4% in viability and 4.9% and 20.6% in budding index measurements, respectively at the beginning and the end of the run.

3.3.4 Zeta potential

Zeta potential is the measurement of particle surface charge on the basis of electrophoretic mobility within a defined electric field (Smart *et al.*, 1995). Differences in zeta potential can be correlated with the degree of cell surface disruption of the yeast cells at any stage in the propagation. Zeta potential at pH 4 was measured in duplicate for each sample using the Zetasizer. Cells were removed from the culture medium by centrifugation and re-suspended in a acetic acid/sodium acetate buffer prior to Zeta potential measurements. The coefficient of variance was found to be 7.5% of the measurement.

3.3.5 pH level

The pH was measured at the beginning and at the end of each run. Owing to the addition of the acetic acid/sodium acetate buffer, no significant decrease was observed. From an initial pH of 5, the pH of the medium dropped to pH 4.5 at the end of the fermentation.

3.3.6 Glucose Measurement

Glucose was expected to be the growth limiting substrate. Glucose measurements were used to investigate the rate of substrate consumption based on the Monod equation. Concentrations were determined using the *Glucose/GOD-Perid* method, using the analysis kit provided by Boehringer Mannheim. This is based on conversion of glucose to gluconate and H_2O_2 with a subsequent colorimetric reaction of the H_2O_2, allowing spectrophotometric measurements. The coefficient of variance in the measurements was 9.6%.

3.3.7 Ethanol Measurement

Ethanol was measured as the main product of the fermentation. Ethanol concentration was determined by gas chromatography, using a Perkin Elmer Autosystem fitted with a flame ionisation detector and a stainless still column packed with 100% methyl silicone. Column temperature was varied from 40 to 120°C at a rate of 30°C per minute using helium as carrier gas at 20 mL/min. The detector and injector temperatures were set at 250°C. Butanol was used as the internal standard. The coefficient of variance of the measurements was found to be 7.4%.

3.3.8 TEM Analysis

TEM analyses was performed for two runs (0% solid and 1% solids) to determine any change in cell morphology, particularly in cell wall thickness and structure. The method used for TEM involved freeze-substitution of yeast, dehydration, embedding in resins, ultramicrotomy, post-staining and high voltage electron microscopy.

3.4 EXPERIMENTAL APPROACH

The "standard" experimental conditions are presented in Table 3.1. When one factor was investigated (for example solid size), this factor was set to the investigated value and all the other factors maintained to the reference values.

Table 3.1 Reference values of the different investigated factors

Parameter of study	"Standard" value
Solid loading	1% (40g)
Solid size	600-850 μm
Impeller type	Rushton turbine
Impeller speed	565 rpm
Inoculum size	10%
Inoculum age	14 h

Three sources of hydrodynamic stress were studied:

- The influence of solid particles

Solid loading was investigated by running a series of experiments over the range of solids volume fractions of 0%, 0.5%, 1%, 1.5%, 2% and 5%. The control (0%) and the standard (1% solids) were performed in triplicate.
Solid size was also investigated, sizes varying from 465-600 μm to 600-850 μm and 850-1130 μm.

- The influence of inoculum

The inoculum size was investigated. The standard 10% inoculum size was reduced to 2.5% and to 1%.
The inoculum age was studied using an inoculum grown for 24 hours in contrast to the standard 14h inoculum.

- The influence of the impeller

The effect of impeller speed was studied in the range 460 to 850 rpm, using the following speeds: 460, 565, 600 and 850 rpm.
The effect of impeller type was also studied by comparing Rushton turbine to pitched blade impeller.

Chapter 4: Reproducibility of the results

4.1 INTRODUCTION

Due to the length of one experimental run, only one experiment at each condition was used to investigate the effect of solid loading, solid size, inoculum age and size and impeller type and speed. In order to assess the reproducibility of the results, experiments at two conditions were performed in triplicate. The first experimental condition was a control experiment at 0% solid loading. The speed of the Rushton impeller was set to 565 rpm and the aeration rate to 1 vvm. A 10% inoculum (15 mL) was grown for 14 h before inoculation of the reactor. The second experiment was performed at the same conditions except that 1% v/v solid loading (40g) was added to the reactor. The reproducibility of the experiment was studied using the triplicate experiments and considering each analytical method in turn. The results for 0% and 1% solid loading were compared.

4.2 REPRODUCIBILITY OF ANALYTICAL METHODS ACROSS TRIPLICATE EXPERIMENTS

4.2.1 Statistical method

The reproducibility of the results was studied using the paired t-test (Excel Data Analysis package). This method assesses the significance of the mean difference between pairs of values at each time point. It was chosen because the data sets varied with time and could not be compared using the normal t-test or the F-test. For the same condition (0% or 1%), each combination of the three replicated runs were paired. Reproducibility was assessed when no difference could be detected with a 90% level confidence. The data used to generate the graphs presented in this section are tabulated in Appendix D. The standard errors based on the replicated experiments were calculated using the 2-way ANOVA, as detailed in Section 4.3. They account only for variations between the triplicate experiments, not for variations with time or with solids loading. Typical calculations on Excel are presented in Figure 4.1.

Glucose

t-Test: Paired Two Sample for Means

	Run 3	*Run 4*
Mean	2.0163636	1.97236364
Variance	7.0893366	10.769671
Observations	11	11
Pearson Correlation	0.9754686	
Hypothesized Mean Difference	0	
df	10	
t Stat	0.1615279	
P(T<=t) one-tail	0.4374473	
t Critical one-tail	1.8124615	
P(T<=t) two-tail	0.8748945	
t Critical two-tail	2.2281392	
Probability that there is a real difference	0.1251055 -> no significant difference	

t-Test: Paired Two Sample for Means

	Run 4	*Run13*
Mean	2.6616333	2.72783333
Variance	13.420615	12.9940079
Observations	8	8
Pearson Correlation	0.990849	
Hypothesized Mean Difference	0	
df	7	
t Stat	-0.3770405	
P(T<=t) one-tail	0.3586569	
t Critical one-tail	1.8945775	
P(T<=t) two-tail	0.7173137	
t Critical two-tail	2.3646226	
Probability that there is a real difference	0.2826863 -> no significant difference	

t-Test: Paired Two Sample for Means

	Run 3	*Run13*
Mean	2.6483333	2.72783333
Variance	8.4532821	12.994008
Observations	8	8
Pearson Correlation	0.9526264	
Hypothesized Mean Difference	0	
df	7	
t Stat	-0.1848847	
P(T<=t) one-tail	0.429281	
t Critical one-tail	1.8945775	
P(T<=t) two-tail	0.8585621	
t Critical two-tail	2.3646226	
Probability that there is a real difference	0.1414379 -> no significant difference	

Figure 4.1 Example of calculations of reproducibility using Excel Data Analysis package.

4.2.2 Total cell count, viability and reproduction

The total number of cells, the number of viable cells, the budding index and the viability, measured by methylene blue staining, were measured for the experiments in triplicate using light microscopy and a counting chamber. The results are presented in Figure 4.2. It appears clearly that the reproducibility of microbial cell counting was good. Under both conditions, 0% and 1% solid loading, this result is confirmed by the paired t-test. The standard errors based on the replicates are 4.2×10^6cells/mL for total cell concentration, 4.3×10^6cells/mL for viable cell concentration, 0.035 for viability and 0.023 for budding index. These represent coefficients of variance of 11.1, 11.7, 3.7 and 18.2, respectively.

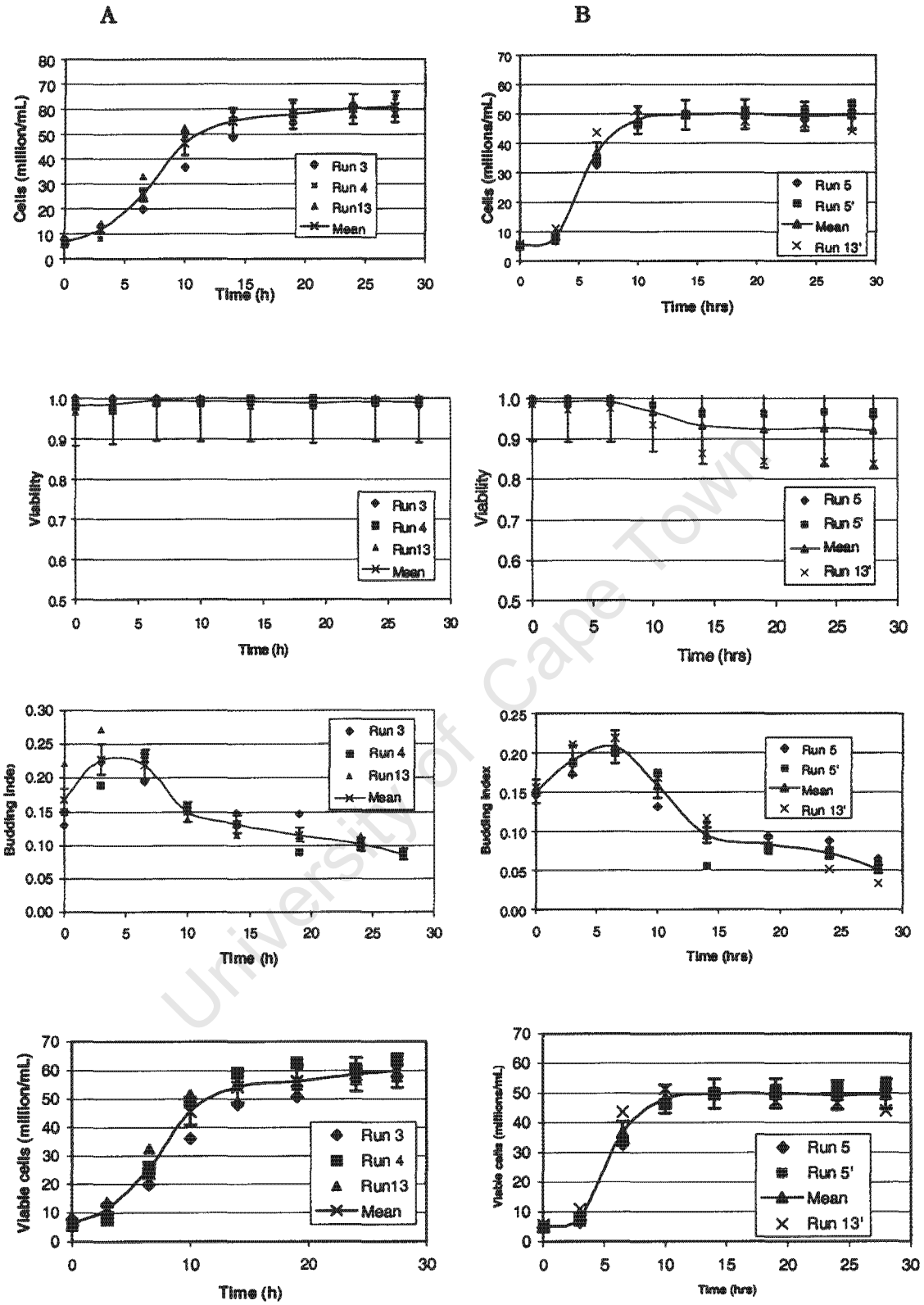

Figure 4.2 Reproducibility of cell counting with 0% solid (A) and 1% solid loading (B).

4.2.3 Biomass concentration in terms of absorbance

Absorbance at 660 nm was measured for the triplicate experiments. Results are presented in Figure 4.3. The reproducibility of absorbance results over experiments conducted under the same experimental conditions is good. The standard error on absorbance measurements is calculated as 0.13, representing a coefficient of variance of 25 and 5% at the beginning and end of experiment respectively.

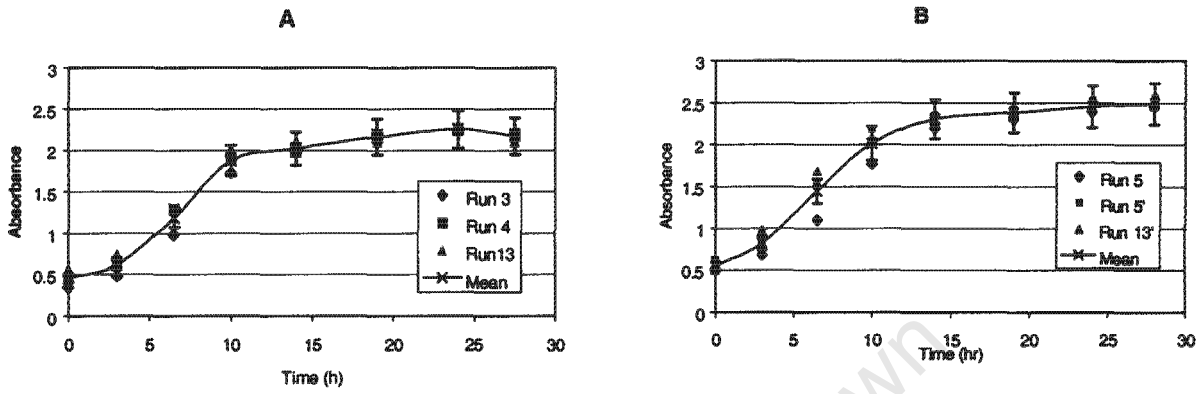

Figue 4.3 Reproducibility of absorbance measurements: 0% (A) and 1% solid loading (B).

4.2.4 Biomass concentration in terms of dry mass

Figure 4.4 shows the results obtained for dry mass measurements. These are found to be poorly reproducible. While a typical standard error of 0.42 g/L is obtained, this represents an unacceptably high coefficient of variance at the low yeast biomass concentrations used (0 to 2 g/L).

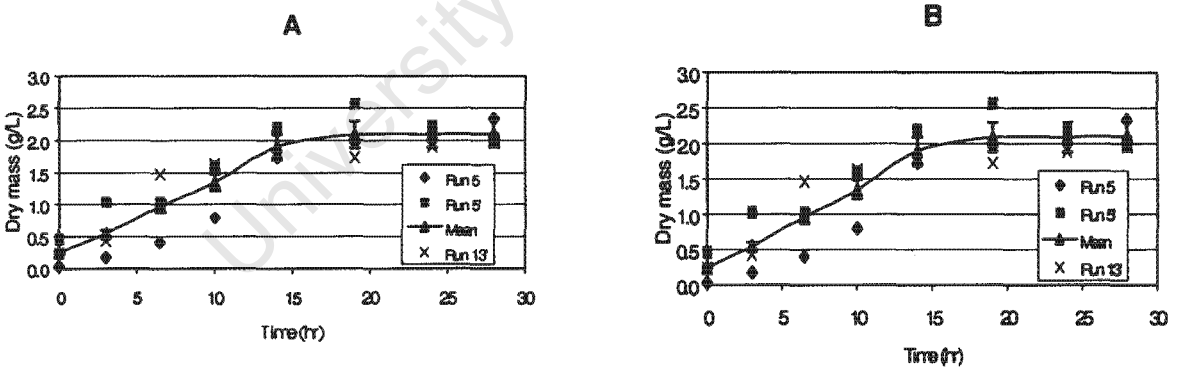

Figure 4.4 Reproducibility of dry mass measurements: 0% (A) and 1% solid loading (B).

4.2.5 Glucose concentration

Results for glucose measurements are presented in Figure 4.5. Glucose measurements are assessed to be reproducible. The standard error for glucose concentration is 0.59 g/L.

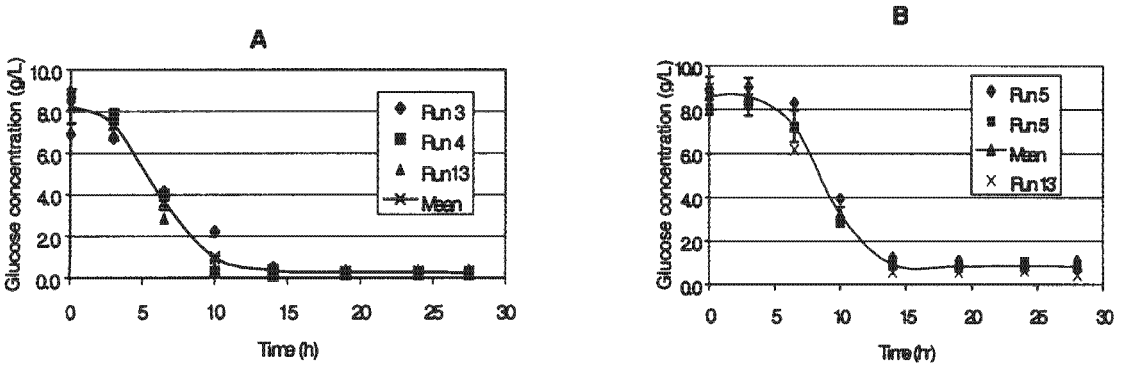

Figure 4.5 Reproducibility of glucose measurements: 0% (A) and 1% (B) solid loading.

4.2.6 Cell surface charge measured as Zeta potential

Figure 4.6 shows the results obtained for zeta potential measurements. Good reproducibility is observed. The standard error typically calculated for zeta potential measurements is 0.54 mV.

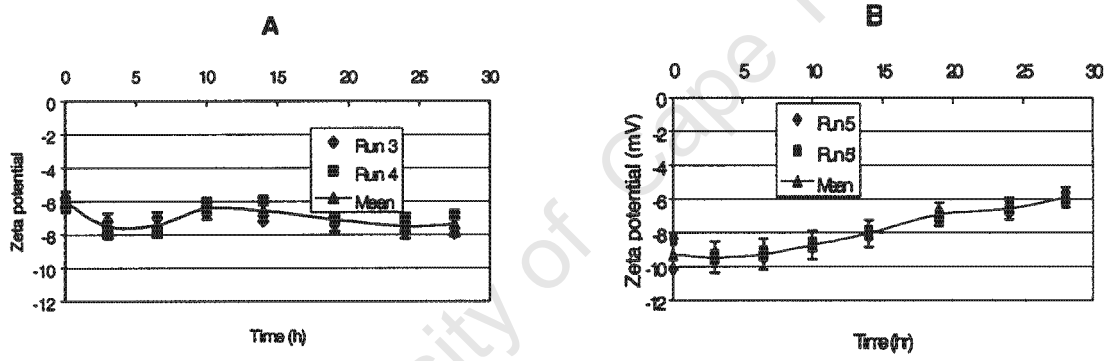

Figure 4.6 Reproducibility of zeta potential measurements: 0% (A) and 1% (B) solid loading.

4.2.7 Ethanol concentration

Results for ethanol measurements by gas chromatography are presented in Figure 4.7. Ethanol measurements are reproducible. The standard error calculated for ethanol measurements is 0.13 g/L.

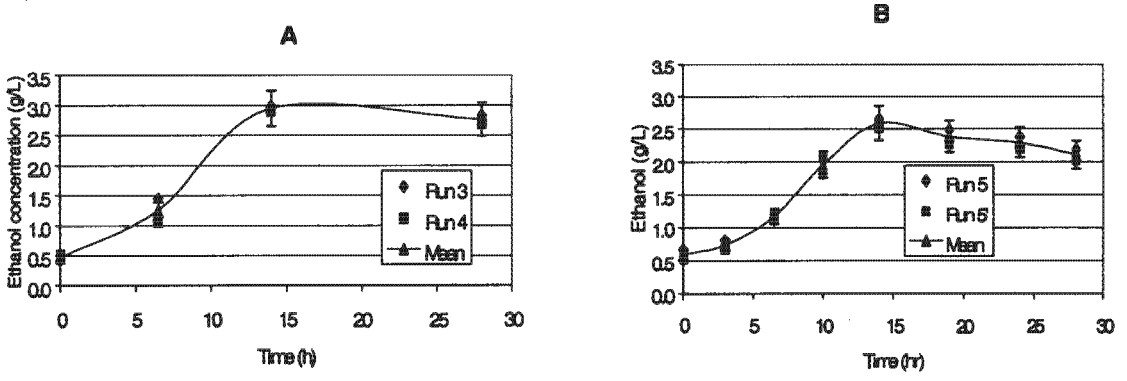

Figure 4.7 Reproducibility of ethanol measurements: 0% (A) and 1% (B) solid loading.

4.2.8 Conclusions on reproducibility

All the assay methods were found to give reproducible results with 90% confidence, except for dry mass measurements. As a consequence, dry biomass measurements were not used in further detailed analysis and calculations. For this analysis, the calculated standard error was very high compared to the low biomass concentrations used (more than 25% of the values). For all other assay methods, standard errors based on the replicates, calculated using the 2-way ANOVA (Section 4.3) were found to be acceptable (less than 12% of the typically measured values).

4.3 COMPARISON OF EXPERIMENTAL DATA GENERATED AT 0% AND 1% SOLID LOADING

4.3.1 Statistical method

Results for experiments with 0% and 1% solid loading were statistically analysed, using the Analysis of Variance (ANOVA). The ANOVA is a procedure which can be used to determine whether several means are significantly different to one another, as a group, by using the F-test to assess the significance of the variance due to the different means (Napier-Munn,1994). The ANOVA essentially partitions the total data variance into its components, and makes comparisons between them. In our problem, involving the comparison of replicated time-dependent experiments with two solids loadings, there are three sources of variation: time, solid loading and error. Each has a sum of squares associated with it, which is a measure of variation.

The sum of squares due to time, S_{time}, is:

$$S_{time} = \sum_{i=1}^{r} n_i \left(\bar{x}_i - \bar{\bar{x}}\right)^2 \qquad \text{Equation 4.1}$$

where r = number of samples taken during the growth (8)
$\bar{\bar{x}}$ = overall data mean
$\bar{x}_i$ = mean value at the i^{th} time
n_i = number of replicates of the i^{th} time (3)

The sum of squares due to solids loading, S_{solid}, is:

$$S_{solid} = \sum_{j=1}^{c} n_j \left(\bar{x}_j - \bar{\bar{x}}\right)^2 \qquad \text{Equation 4.2}$$

where c = number of solids loadings investigated (2)
$\bar{\bar{x}}$ = overall data mean
$\bar{x}_j$ = mean value for each solid loading j.
n_j = number of replicates for each solid loading j.

The sum of squares due to error, S_{error}, is:

$$S_{error} = \left(\sum_{i=1}^{r} \sum_{j=1}^{c} x_{ij}^{\ 2} \right) + \frac{S^2}{n} - \sum_{i=1}^{r} \frac{R_i^{\ 2}}{c} - \sum \frac{C_j^{\ 2}}{n} \qquad \text{Equation 4.3}$$

where c = number of solids loadings investigated (2)
r = number of times considered (8)
x_{ij} = value measured at time i with solids loading j.
n = total number of observations.
S = sum of all observations.
R_i = sum of observations at time i.
C_j = sum of observations with solids loading j.

The square root of the "error" Mean Square, calculated as $\frac{S_{error}}{(c-1)(r-1)}$, is the standard error of the experiment, i.e. the basic error based on the replicates. These errors, calculated for all analytical methods, are presented in Table 4.1.

4.3.2 Results

All the different analyses were tested using the 2-way ANOVA (Excel Data Analysis package). Calculations for Section 4.3 are presented in Appendix E. An example of calculations performed on Excel is given in Figure 4.8.

Budding Index

Sample	Time	Solid loading 0 %	1 %
1	0	0.130	0.146
2		0.150	0.150
3		0.222	0.156
1	3	0.223	0.173
2		0.188	0.188
3		0.272	0.211
1	6.5	0.194	0.204
2		0.235	0.200
3		0.229	0.219
1	10	0.159	0.132
2		0.151	0.175
3		0.138	0.169
1	14	0.147	0.112
2		0.131	0.056
3		0.115	0.117
1	19	0.146	0.093
2		0.090	0.075
3		0.110	0.082
1	24	0.094	0.088
2		0.097	0.076
3		0.113	0.052
1	28	0.091	0.065
2		0.088	0.056
3		0.081	0.034

Anova: Two-Factor With Replication

ANOVA

Source of Variation	*SS*	*df*	*MS*	*F*	*P-value*	*F crit*	
Time	0.125904	7	0.017986	32.82852	7.29E-13	2.312738	
Solid Loading	0.00676	1	0.00676	12.33789	[redacted]	4.149086	1-0.001346 = Probability
Interaction	0.002775	7	0.000396	0.723544	0.653049	2.312738	that there is a real difference.
Error	0.017532	32	0.000548				
Total	0.152971	47					

Standard error [redacted]

Figure 4.8 Example of 2-way ANOVA using Excel Data Analysis package.

The sum of squares (SS) accounting for time (Figure 4.8) corresponds to S_{time} (Equation 4.1), while SS accounting for solids loading is S_{solid} (Equation 4.2) and SS accounting for error is S_{error} (Equation 4.3). The F-test is used to compare the SS, but before this can be done, they must be converted to unit of variance by dividing by the corresponding degrees of freedom (df) to give the mean square (MS). The F-test assesses whether the MS due to time, solids loading or interactions is significantly greater than that due to error.

$$F=\frac{MS_{solid}}{MS_{error}}=12.34 \text{ with 1, 32 degrees of freedom}$$

From tables, this value is significant at the 99.99% level (with a probability level of 0.0013), and thus we would conclude that the difference between the two solids loadings is real. The probability of a real difference is calculated as 1 – P-value. When using Excel Data Analysis package, one can specify the level of confidence desired. The F-crit value is the F value corresponding to that confidence level (which has been chosen here to be 95%). Above F-crit, an F-value is significant at 95% confidence.

Results obtained for each assay method with respect to solids loading are summarised in Table 4.1. For all analyses, variation with time was found to be very significant (≥ 99.999%). Except for total cell number and dry mass measurements, a significant difference between runs at 0% and 1% solids loading was found, with at least a 95% confidence level. On total cell concentration, variation with solids loading was not found to be significant (21.2%). However, the standard error, based on the replicates, was calculated to be $4.2x10^6$cells/mL. It is very acceptable for the cell concentrations at the end of growth (8% of the values), but for lag phase and exponential phase, the high coefficient of variance could explain the inability to detect a significant difference. When comparing only the four last samples (end of exponential phase and stationary phase), a significant difference was assessed between 0% and 1% solids loadings, at the 99.2% confidence level. Concerning dry mass measurements, no significant difference was detected between 0% and 1% solids loadings. It also should be noted that the standard error for dry mass was 0.42g/L, which is extremely high compared to the low cell concentrations involved (0 to 2 g/L).

Table 4.1 Results of the 2-way ANOVA for all assay methods with respect to solids loading.

Assay method	Significant difference	% confidence	Standard error
Total cell concentration	No	21.2	$4.2x10^6$cells/mL
Total cell concentration at the end of the run	Yes	99.2	$3.3x10^6$cells/mL
Viable cell concentration	Yes	95.6	$4.3x10^6$cells/mL
Viability	Yes	99.8	0.035
Budding index	Yes	99.9	0.023
Absorbance	Yes	99.9	0.134
Dry mass	No	87.2	0.42 g/L
Glucose concentration	Yes	99.9	0.59 g/L
Zeta potential	Yes	99.9	0.54 mV
Ethanol concentration	Yes	99.2	0.13 g/L

Even though reproducible, absorbance measurements showed unexpected results. As illustrated in Figure 4.9, absorbance at 1% (v/v) solids loading was found to be higher than without particles. Reduction in the extent of growth being confirmed by all other analyses, a phenomenon altering the optical density of the solution was suspected to occur. In order to assess the importance of this phenomenon, absorbance was plotted as a function of the total cell number for different experimental conditions (Figure 4.10). Absorbance was found to be linearly dependent on the total cell concentration. Best regression lines and coefficients of regression are summarised in Table 4.2.

An increase in absorbance was clearly noticed when increasing solids concentration or agitation rate. Therefore attrition or leaching was suspected in the bioreactor. Microscopy observation confirmed minimal attrition. Atomic absorption spectroscopy analysis proved that the solid particle breakup and leaching were not significant, even though colouring the solution. While showing good reproducibility within a single experimental condition, the hypothesis that optical density was proportional to total cell number failed when expanded across a range of hydrodynamic operating conditions, and as a consequence, absorbance measurements were not used for further calculations or analyses.

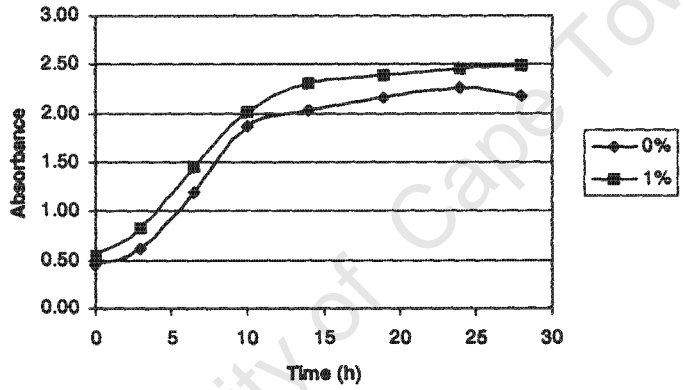

Figure 4.9 Absorbance profiles at 0% and 1% solids loadings (mean values).

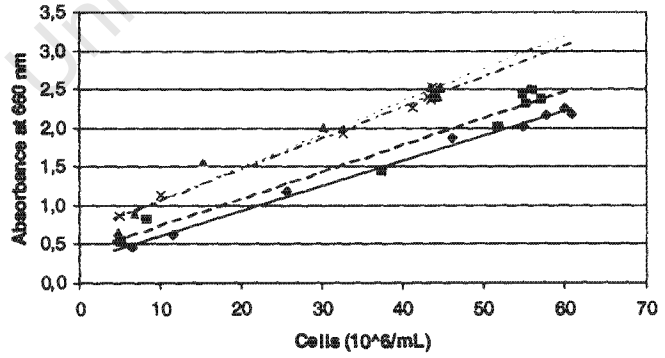

Figure 4.10 Absorbance as a function of total cell concentration for different experimental conditions: 0% (♦), 1% (¯), 2% (·) (v/v) solids loadings and 850 rpm (×).

Table 4.2 Regression for absorbance as a function of total cell number.

Experimental conditions	Equation	Coefficient of correlation R^2
0% solid	y = 0.0326x + 0.2753	0.9931
1% solid	y = 0.0345x + 0.4027	0.9617
2% solid	y = 0.0425x + 0.6332	0.9688
850 rpm	y = 0.0400x + 0.6708	0.9914

4.4 CONCLUSIONS ON REPRODUCIBILITY

For all analytical methods except for dry mass measurements, a good reproducibility was assessed using the paired t-test (Section 4.2). Thereafter, experiments at 0% and 1% solids loading were compared to determine whether the difference between the two operating conditions was statistically significant (Section 4.3). This was proved for all analyses (except dry mass measurements) by using the 2-way ANOVA. The analysis of variance also allowed the calculation of the standard error for each assay method, based on the replicates. These errors were found to be acceptable, except, again, for dry weight. As a consequence, this analysis was not used for any further calculation. Moreover, for absorbance measurements, a phenomenon of attrition or leaching was demonstrated with solutions becoming coloured at high solids loadings or high agitation speed. Therefore the hypothesis that optical density was proportional to total cell concentration was not valid across the range of experimental conditions used. Hence we used only the following as routine assay methods: cell counting (total cell number, viability, budding index), glucose measurement, zeta potential measurement and ethanol measurement.

Chapter 5: Influence of the solid particles on the growth

5.1 EFFECT OF SOLID LOADING

High solids loadings are required in industrial processes such as bead mills (about 50% v/v solids loading) or bioleaching technologies (30% w/v solids loading). In the first system, cell disruption is desired, while in the second one, maximum growth and cell activity are wanted. In both cases, cells are reported to experience physiological stress (Scholtz-Brown, 1998; Engler, 1985; Nemati and Harrison, 2000), leading to disruption under the harshest conditions.

Six solids loadings were investigated at constant impeller speed, namely 0%, 0.5%, 1%, 1.5%, 2% and 5%. All the analytical methods presented in Section 3 were performed on the samples. The data collected and used in Figures 5.1 to 5.8 are tabulated in Appendix F.1.

5.1.1 Total cell concentration, viability and reproduction

5.1.1.1 Total cell concentration

The cell concentration was determined by means of total cell counts under light microscopy (Appendix C). Figure 5.1 shows the total cell concentration as a function of time for different solids loadings. Lag phase, specific growth rate, biomass yield on glucose and the duration of the exponential phase were calculated from the data. Details of calculations are explained in Appendix G. Results are tabulated in Table 5.1. Standard deviations based on the triplicate experiments at 0% and 1% solids loadings are also reported for comparison.

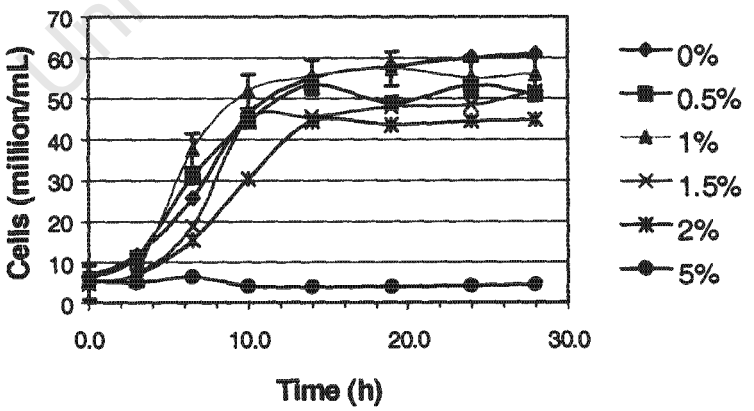

Figure 5.1 Effect of solid loading across the range 0 to 5% on a volume basis on total cell concentration.

Table 5.1 Effect of solid loading on growth parameters.

Solid loading	t_{lag} (h)	$\mu_{max\ exp}$ (h^{-1})	t_{exp} (h)	$Y_{X/S}$ (10^9 cells/g)	k_d (h^{-1})
0.0%	3.0 (±1.0)	0.254 (±0.026)	17 (±1.0)	7.53 (±1.08)	0.000
0.5%	4.0	0.158	18	5.87	0.096
1.0%	3.5 (±0.5)	0.135 (±0.018)	15 (±1.5)	7.15 (±0.96)	0.119 (±0.018)
1.5%	5.0	0.134	15	5.90	0.120
2.0%	6.5	0.112	14	5.50	0.142
5.0%	≥ 28	-0.021	no growth	4.10	0.275

With 5% (v/v) solids loading of silica, no growth occurred and the cell number decreased. The specific growth rate and durations of the different phases could not be calculated. The reduction in both the rate and extent of growth with increased solids loading is clearly illustrated (Figure 5.1, 5.2). The reduced extent of growth is seen by a decrease in the stationary phase population (Figure 5.1, 5.2) and the decrease in biomass yield, $Y_{X/S}$ (Table 5.1, Figure 5.2).

The decrease in the overall extent of growth is a composite effect of the reduced duration of the exponential phase and maximum specific growth rate, as well as increased lag phase. It is proposed that the reduced apparent specific growth rate may result from an increase in the death rate (k_d) with increasing solids loading where:

$$\mu = \mu_{max}^{\bullet} - k_d \qquad \text{Equation 5.1}$$

A power law fashion model for k_d is presented in Section 5.1.7.
From the data presented, it is apparent that some critical solids loading exists below which the solids loading exhibits an insignificant effect on cell growth. From the indicators used ($\mu_{max\ exp}$, t_{lag}, t_{exp}, $Y_{X/S}$), it is seen that loading exhibited a negative effect on growth at loading greater than 1%; however the critical value varied between 0.0 and 0.5% (v/v) depending on the parameter used as indicator (Figure 5.2).

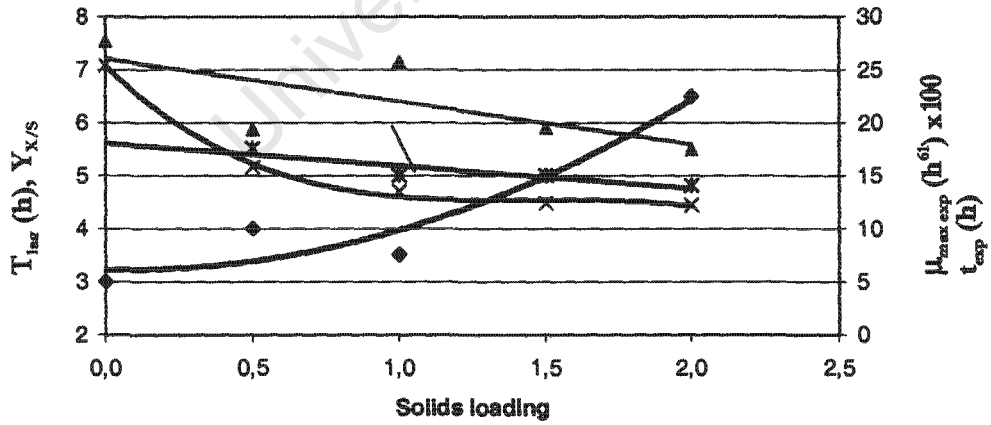

Figure 5.2 Influence of solid loading on growth parmeters. (♦ t_{lag} (h), — Poly (t_{lag}), ▲ $Y_{X/S}$ (10^9 cells/g), Linear ($Y_{X/S}$), × $\mu_{max\ exp}$ (h^{-1}), — Poly ($\mu_{max\ exp}$), ✱ t_{exp} (h), — Linear (t_{exp})).

5.1.1.2 Viable cell concentration

The viable cell concentration was determined by differential methylene blue staining cell counts and light microscopy. Detailed data is given in Appendix F.1. Figure 5.3 shows viable cell concentration as a function of time at different solids loadings. Cell viability was calculated as a fraction of the total cell count (Appendix C). As the viability at 5% solids loading was very low compared to that calculated at other solid concentrations, two graphs are used in Figure 5.4 to illustrate the influence of solids loading on viability. $\mu_{maxViable}$ was calculated as specified in Appendix G. Results for $\mu_{maxViable}$ and the percentage of viable cells at the end of each experiment are reported in Table 5.2. Figure 5.5 illustrated the decrease in growth rates when increasing solids loading.

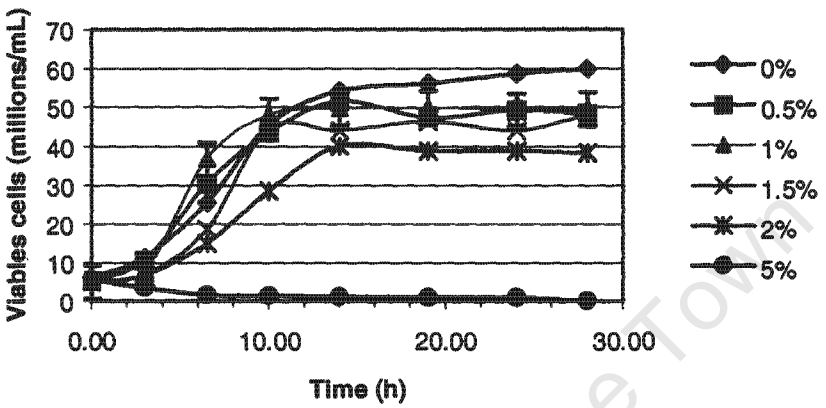

Figure 5.3 Effect of solid loading on viable cell concentration.

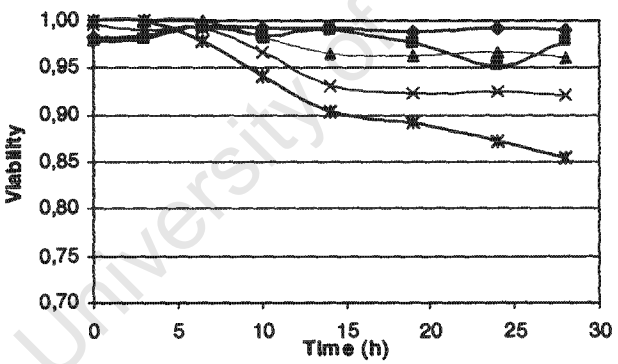

Figure 5.4a

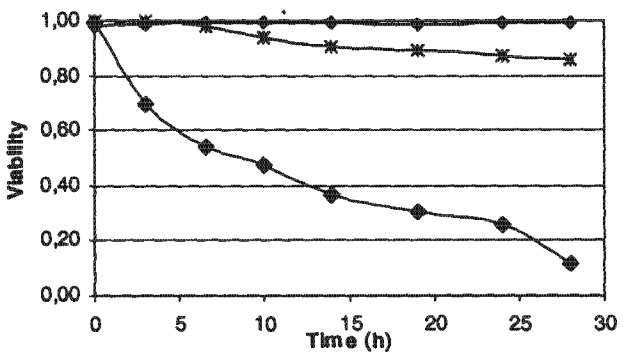

Figure 5.4b

Figures 5.4 a and b Effect of solid loading on viability (♦ 0%, ■ 0.5%, ▲ 1%, ×1.5%, × 2%, ● 5%).

Table 5.2 Effect of solid loading on $\mu_{viable\ cells}$.

Solid loading	$\mu_{viablecells}$ (h^{-1})	% of viable cells at the end of the growth
0.0%	0.253 (± 0.028)	98.2 (± 1.3)
0.5%	0.155	97.7
1.0%	0.138 (± 0.016)	96.1 (± 5.6)
1.5%	0.131	93.0
2.0%	0.110	85.5
5.0%	-0.025	2.6

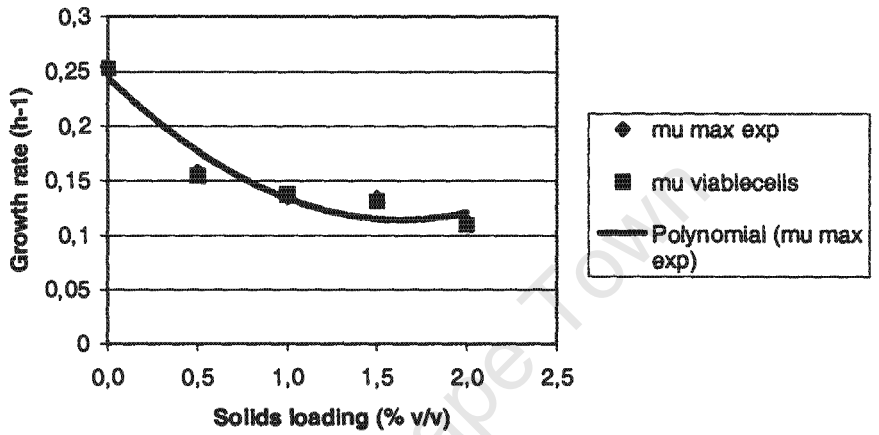

Figure 5.5 Influence of solids loading on the specific growth rates.

As with the total cell number, a decrease in viable cell number in the stationary phase was observed with increasing solid concentrations. At 5% solids loading, no increase in viable cell number was observed over the entire growth period. The specific growth rate based on viable cell number corresponds well to that reported on total cell number, decreasing with increasing solids concentration (Figure 5.5). Typically the fraction of viable cells found under optimal growth conditions lies in the range 0.94 to 0.99. The data collected at 0 to 0.5% solid loading is seen to conform to this pattern (Figure 5.3). At 1, 1.5 and 2% solids loading, a decrease in the fraction of viable cells of 7 to 10% is observed with time, indicating loss of viability or cell death in the presence of the solid phase. This trait is further demonstrated at a 5% solid loading where the viable cell fraction decreases to 10% over the 28h incubation period. These observations are consistent with the hypothesis of an increasing cell death with increasing volume fraction.

5.1.1.3 Budding index

Budding index provides further quantification of cell viability and metabolic activity. It is defined as the fraction of cells carrying a protusion of a cell bud (Appendix C). Figure 5.6 shows changes in budding index with time, for different solids loadings.

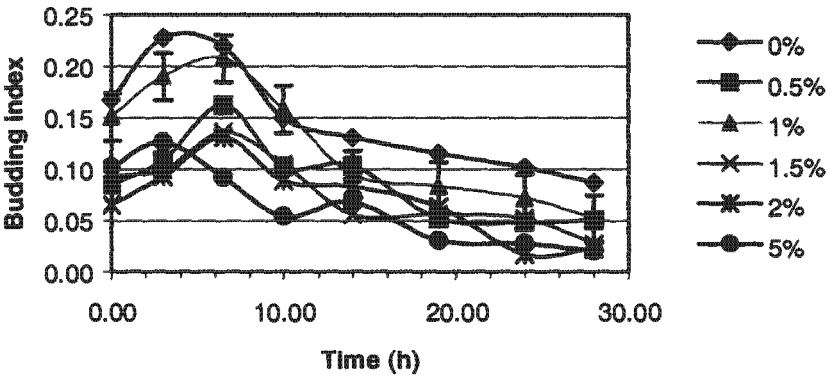

Figure 5.6 Effect of solid loading on budding index.

Budding index shows the same trend for all experiments: it increases during lag and early exponential phase, peaking during exponential phase. Except for 0.5% solid, the budding index is higher for low solid loading and decreases as solid loading increases.
Time corresponding to the maximum budding index slightly increases with solid loading. This does not hold for 5% solid loading. The cells start dying before being able to bud. Large differences in the initial budding index (higher than the standard error for budding index, calculated to 0.023) are observed. That may suggest that yeast are very sensitive to pre-inoculum and inoculum growth. Even if pre-inoculum and inoculum were supposed to be prepared in the same experimental conditions, no analysis was performed to rigorously determine their influence on the growth, despite the consistent inoculation procedure.

5.1.2 Glucose concentration

Substrate consumption was measured in terms of glucose concentration at each solid loading. The data is recorded in Appendix F.1 and illustrated in Figure 5.7. The specific substrate consumption rate and lag period preceding consumption were calculated according to Appendix G and are presented in Table 5.3. In Figure 5.8, the combination of cell and glucose lags illustrates the increase in the lag phase duration when increasing solids loading.

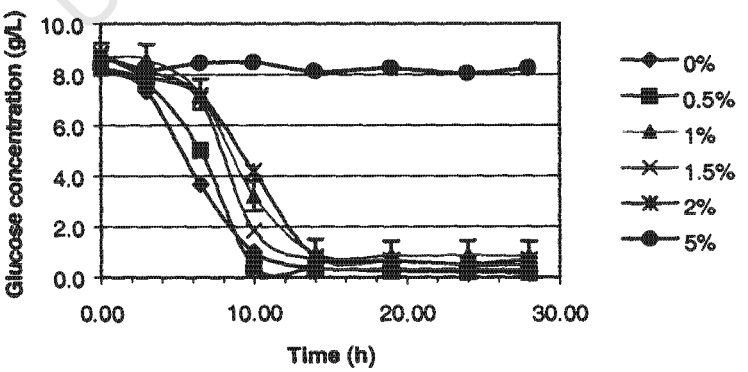

Figure 5.7 Effect of solid loading on glucose consumption.

Table 5.3 Differences in substrate uptake parameters for various solid loading.

Solid loading	q_s ($g.h^{-1}.10^9cells^{-1}$)	Glucose lag phase (h)
0.0%	-0.0486 (± 0.007)	4 (± 1.34)
0.5%	-0.0238	4
1.0%	-0.0338 (± 0.007)	5 (± 1.04)
1.5%	-0.0518	6
2.0%	-0.0326	6
5.0%	0	> 28

No significant glucose consumption was observed at 5% solid loading. This confirms that metabolic activity reduced rapidly during the lag phase, with cell death occurring before growth proceeded. At all other solid loadings, the glucose is consumed within 14 hours. No significant difference in the glucose uptake rate was assessed. However, the glucose lag phase increased as solid loading increases (Figure 5.8). That increase in lag phase, confirmed by both total cell number and glucose measurements suggests that cells need to acclimatise the experimental conditions. The harsher the hydrodynamic conditions, the longer the time required for adaptation is.

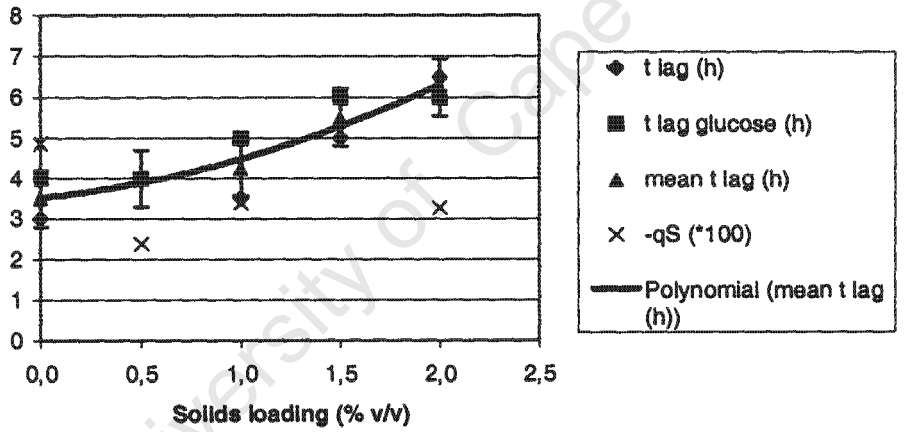

Figure 5.8 Influence of solids loading on lag phase duration and substrate utilisation rate.

The consumption of all glucose available within a fixed time period as well as the lack of any specific trend in glucose uptake rate with solids loadings in the range 0 to 2% by volume implied that a decreased growth yield resulted with increasing solids loadings (Table 5.3). This suggests that additional energy derived from substrate consumption and glucose oxidation may be required for cell maintenance with increasing solids loadings at sub-lethal concentrations.

5.1.3 Zeta potential

Zeta potential gives an indication of the surface charge of yeast cell. *Saccharomyces cerevisiae* cells exhibit negatively charged surfaces at the pH values of growth (between pH 4 and 6). Amory *et al.* (1988) attributed this negative charge to the presence of phosphate

groups in the outer cell wall mannoprotein layers, but other constituents can influence the net charge of yeast, such as proteins. If any change in the chemical composition of the wall occurs under hydrodynamic stress, these changes should be reflected in zeta potential. Hence, zeta potential was measured as a function of time for all experiments at pH 4.0. The data obtained are detailed in Appendix F.1. and summarised in Figure 5.9.

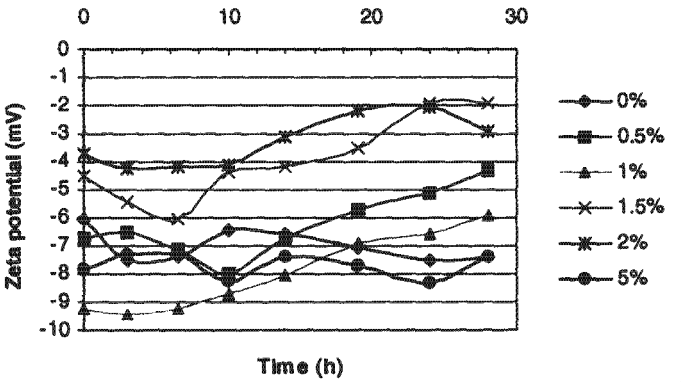

Figure 5.9 Effect of solid loading on zeta potential measurements.

Typical problems of zero charge (pZ_0) for the yeast cell wall have been reported. Robinson (2001) measures pZ_0 values for flocculent and non-flocculent yeast strains, cultivated under aerobic and anaerobic conditions. His findings are reported in Table 5.4.

Table 5.4 Zero charge values for different yeast strains cultivated under aerobic and anaerobic conditions (adapted from Robinson, 2001)

	pZ_0	
Yeast strain	**Aerobic**	**Anaerobic**
SAB1	< 2	< 2
SAB2	~ 2	2.4
SAB5	< 2	2.4
SAB1/96	2	3.8

Under aerobic conditions, pZ_0 is lower than 2 for all yeast strains considered. In this study, zeta potential was measured at pH 4. Therefore problems of zero charge were eluded. At pH 4, Robinson (2001) reports typical zeta potential values ranging from –4 to –12 mV for aerobically grown yeast and –1 to –4 mV for those grown under anaerobic conditions. This is in agreement with this work.

At 0% and 5% solid loadings, zeta potential at pH 4.0 remained constant with time, within a 91% confidence interval. Across all other solid loading in the range of 0.5 to 2%, an increase in zeta potential at pH 4.0 was recorded with time (i.e. less negative values). Exposing yeast cells to the French Press, Robinson (2001) observed an increased in the zeta potential at a constant pH, when the hydrodynamic stress was increased from 0 MPa to 10 MPa. Smart *et al.* (1995) reports that starved cells are significantly less negatively charged compared to those that are not starved, suggesting that the cell surface characteristics reflect the physiological condition of yeast. Since phosphate is the predominant charged species at pH 4.0, a loss of phosphomannan at the cell surface is suspected.

If assuming that the surface charge is constant for an unstressed system (0% solid), the increase in the surface charge with time will reflect the stress undergone by the metabolically active yeast with time. The more stressed the system is, the less negative the zeta potential determined. The deviation of the behaviour for 5% solids loading from the general trend may be explained by most cells being dead or dying.
It should be noted that the results at 0% solids loading are contradictory with Robinson and Harrison (2001) observations. They observed for an unstressed system (non-flocculent yeast SAB2, grown aerobically on a 16°P brewery wort, in a 2L agitated reactor) a decrease in zeta potential from early exponential (-0.9 mV) to stationary phase (-11.0 mV) at pH 4.0. However different growth conditions (yeast strain and growth media) may explain such a difference.

5.1.4 Ethanol concentration

Ethanol is a product of primary metabolism. Ethanol concentration was measured after 0h, 6h, 15h, 24h and 28h. The data is shown as ethanol concentration as a function of time for the various solids loadings in Figure 5.10, with detailed data given in Appendix F.1. The specific ethanol production rate was calculated as specified in Appendix G. Only data collected prior to glucose depletion (from 0 to 15 hours) was used, as ethanol consumption results thereafter. Results are tabulated in Table 5.4.

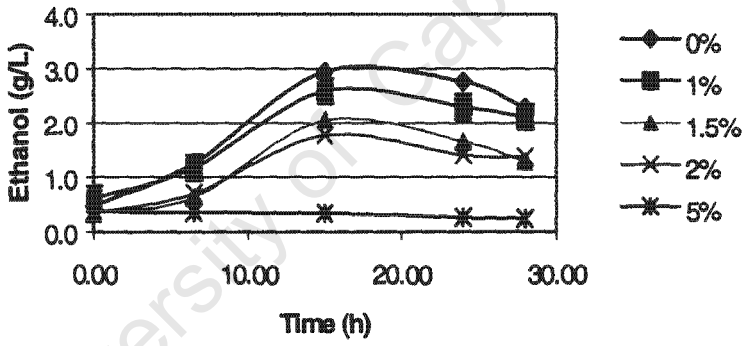

Figure 5.10 Effect of solid loading on ethanol production.

At all solids concentrations (except 5% solid), ethanol production showed the same trend. From time 0 to 15 hours, there is an increase in ethanol concentration. Thereafter the residual ethanol concentration decreases. This behaviour is explained by a shift in substrate on glucose depletion at 14 hours. Thereafter the cells consumed ethanol, hence the decrease in concentration. The standard deviations for q_P, based on the triplicate experiments at 0% and 1% solids loading, are quite high. As a consequence, no conclusion can be drawn on the influence of solids loading on the product production rate. From Figure 5.10, it is seen that the lower the solid loading the higher the ethanol produced. At 5% solid loading, no ethanol is produced. This is confirmed by the decrease in $Y_{P/S}$ with increasing solids loadings (Table 5.5).

Table 5.5 Differences in ethanol production parameters for various solids loadings.

Solid loading	q_p ($g.h^{-1}.10^9 cells^{-1}$)	$Y_{EtOH/s}$	$Y_{EtOH/x}$ ($g.10^9$ $cells^{-1}$)
0.0%	0.0062 (± 0.002)	0.228 (± 0.028)	0.030 (± 0.002)
1.0%	0.0039 (± 0.001)	0.193 (± 0.013)	0.027 (± 0.001)
1.5%	0.0061	0.115	0.020
2.0%	0.0038	0.126	0.023
5.0%	-	-	-

5.1.5 TEM analysis

As cell wall is the first barrier of defence against physical stress (Walker, 1998), it is necessary to consider the changes in the wall structure (wall thickness, morphological changes) to understand how yeast respond to hydrodynamic stress. Transmission Electron Microscopy (TEM) appears to be a suitable method for this analysis. In contrast to higher eukaryotic cells, yeast cells are particularly difficult to preserve mainly due to the presence of the thick cell wall that acts as a barrier against diffusion of fixatives. Although several procedures are targeted to overcome these difficulties, none of them have become established as a standard procedure (Bauer *et al.*, 2001).

TEM analysis was performed for two experiments, 0% and 1% solids loadings. Preparative method is described in Appendix C. Samples were taken at time 3h (end of lag phase), 14h (exponential phase) and 28h (stationary phase). Samples at 0% solid and 1% solid concentration by volume were prepared in the same way and at the same time.

Pictures of whole cells were taken, so were pictures of the wall (all with the same magnification for easier comparison). Measurements were done manually, as no image analysis program was available. As the cell wall thickness was irregular, three measurements were done per picture.

Cell shape and size:

Yeast cell shape was modelled as an ellipsoid. Length and width of cells were measured. No significant difference could be detected in mean length and mean width between the experiments. No difference either was observed with time. Results are tabulated in Table 5.6. Mean diameters reported in the literature (yeast modelled as sphere) are added for comparison. Cell sizes measured using TEM are consistent with those reported in the literature.

A brush-like structure of polysaccharide was observed at the surface of the cell wall (Figure 5.11). This fibrillar structure was also noticed by Osumi (1997).

The appearance of the yeast was very different depending on the level of stress applied. Figure 5.12 shows cells with no solid (#7) and 1% solids loading (#7). Cells grown with 1% solid are visibly damaged compared to the ones grown without solid. Cell walls are not clearly defined and shapes are less regular than without stress.

Table 5.6 Cell sizes for different experiments. Comparison with results found in the literature.

	Mean length (nm)	Mean width (nm)
0% solid	3678 ± 266	2738 ± 400
1% solid	3614 ± 710	2797 ± 415
Srinorakutara (1998)	3330 ± 70	
Smith *et al.* (2000)	3420 ± 620	

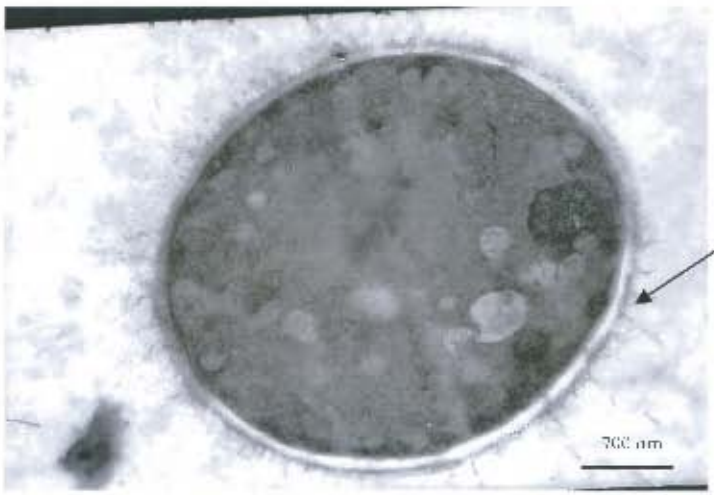

Figure 5.11 TEM photograph of a yeast cell (0% solid, t=0h). The fibrillar structure of pollysaccharaide is observable at the surface.

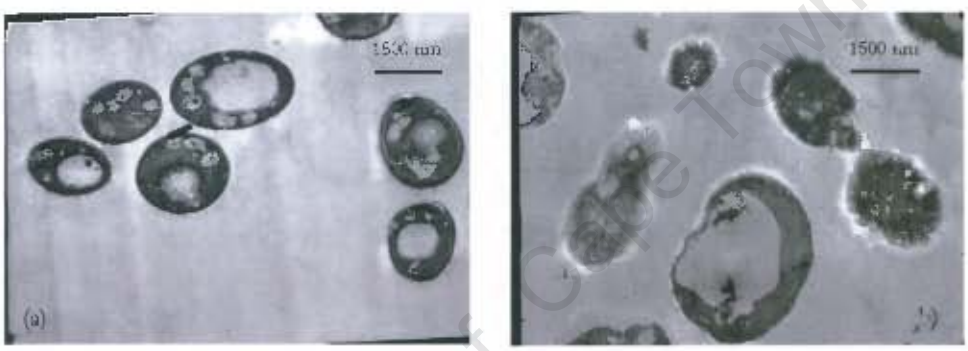

Figure 5.12 Comparison between yeast at t=28h for 0% solid (a) and 1% solid (b).

Cell walls:

The morphology of the yeast cell wall was determined from transmission electron micrographs. At least eight pictures of the wall were taken per sample and three measurements were done per picture.

Measurements of the cell wall thickness obtained for unstressed yeast are consistent with that reported in the literature (Table 5.7). However, contrary to Smith *et al.* (2000) and Srinorakutara (1998), who observed that the cell wall thickness in the exponential phase is generally smaller than in the stationary phase, no difference in the thickness was observed for growth at 0% solid loading.

Table 5.7 Comparison of cell wall thickness of unstressed yeast with those reported in the literature

	Wall thickness (nm)	
0% solid	71 ± 11	
Smith et al. (2000a)	90	
Moor and Muhlehaler (1963)	70 ± 10	
Srinorakutara et al. (1995)	70 - 100	
Srinorakutara et al. (1998)	70 ± 15	
Gaskova et al. (1998)	175 ± 15 260 ± 42	(depending on glucose concentration in the growth media)

During preparation for TEM analysis, the cells were presumably cut at random. Sections could have intersected a given cell at any axial position, *i.e.* close to the cell central axis, close to the cell wall, or anywhere in between. Any mean cell wall thickness and mean cell diameters determined from the micrographs would therefore be only relative values. Smith *et al.* (2000b) developed a novel mathematical model to correct for random slicing during TEM sample preparation. As no image analysis program was available, their method could not be applied in this study. However, all the samples were prepared and sliced in the same way, so a comparison can be drawn between the different experiments. Figure 5.13 presents some micrographs obtained for the cell wall at different times (3h, 14h and 28h), for the two experimental conditions (0% and 1% solids loadings). It appears clearly on the photographs that the cell walls of yeast experiencing stressful conditions (1% solids loading) are thicker than the walls of unstressed ones. This is also demonstrated in Figure 5.14, which shows mean wall thickness at different times for the two solids loadings. The data used to generate this plot is reported in Appendix H.

However, it was observed that a certain percentage of cells exhibit a thin wall even for 1% solid. The percentage of these cells increased with time. As dead cells could not be differentiated from living cells with TEM analysis, it was postulated that these cells with thin wall were dead cells. It was also noted that at 0% solid, the wall was very regular, while at 1% solid, the wall thickness was very irregular. That suggests the existence of cell wall repair mechanisms that compensate where the cell is damaged. Klis et al. (2002) report that the cell is capable of locally repairing the cell wall in case of cell wall damage. Kapteyn *et al.* (1999) found that increased deposition of chitin in lateral walls is part of a compensation mechanism for cell damage. He also observed changes in β1,3-glucan synthesis. These observations confirm that the mechanical strength of the wall is mainly due to the inner layer, which consists of β1,3-glucan and chitin.

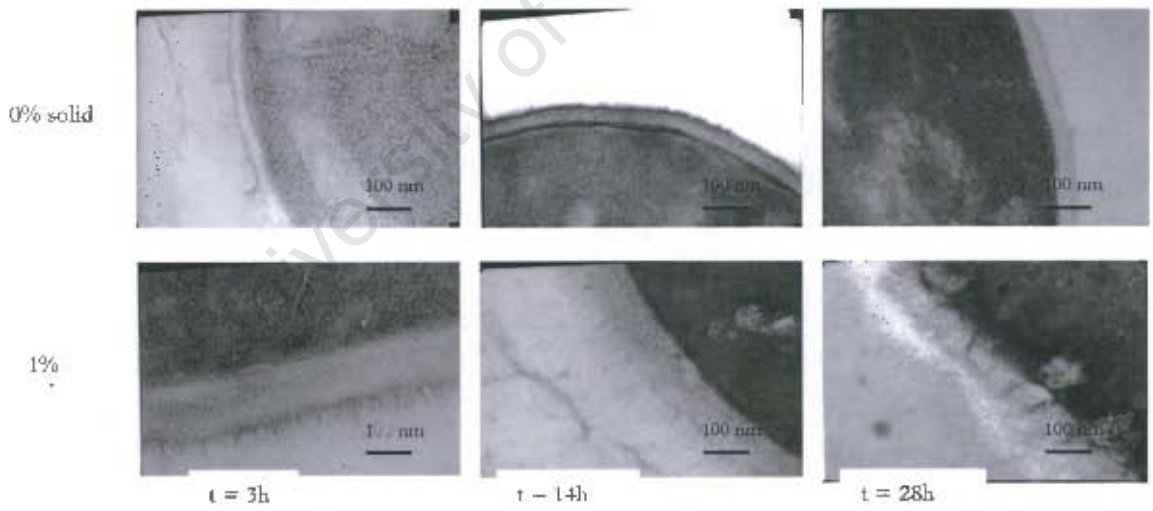

Figure 5.13 Micrographs of the yeast cell wall for 0% and 1% solids loadings, at different times (3h, 14h and 28h).

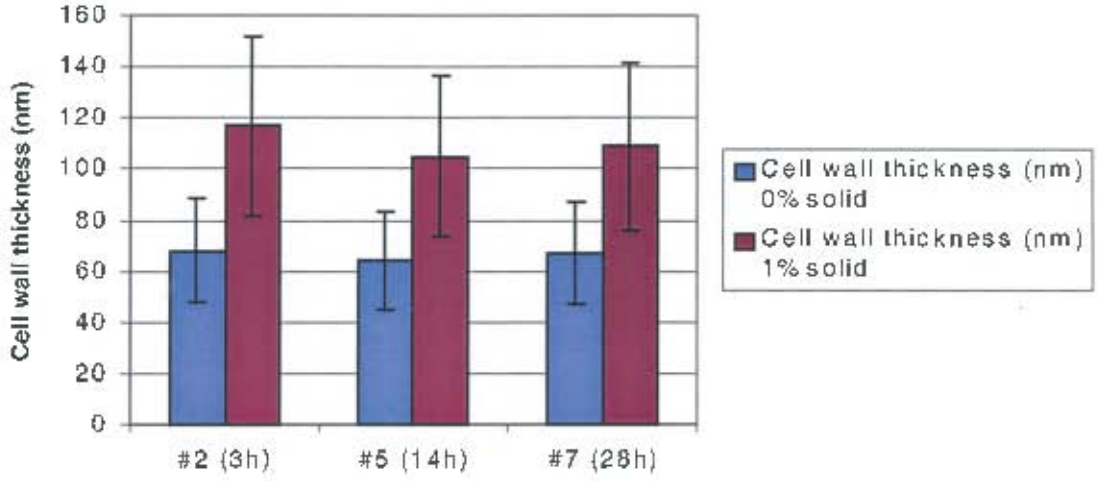

Figure 5.14 Influence of time and hydrodynamic stress on cell wall thickness.

5.1.6 Modelling

A model for cell activity was derived from an expression proposed by Reuss (1988). The kinetic growth model postulates that the apparent cell growth rate is equal to the true growth rate in the absence of solid less the cell death rate.

$$\frac{dX}{dt} = \mu \cdot X \qquad \text{Equation 5.2}$$

Where

$$\mu = \mu_{max}^{*} - k_d \qquad \text{Equation 5.3}$$

And X: biomass concentration (10^6cells/mL)
t: time (h)
μ: apparent growth rate (h^{-1})
μ_{max}^{*}: true growth rate in the absence of solid (h^{-1})
k_d: cell death rate (h^{-1})

The death rate is given as the product of cell concentration and the death rate constant. The cell death rate constant was calculated as a power law fashion type accounting for the characteristics of the system in which growth occurred (solids loading in present case).

$$k_d = a\phi^b \qquad \text{Equation 5.4}$$

Where ϕ: solid loading (% v/v)
a, b constants.

The model assumed that no mass transfer limitations or hydrodynamic stress (except solids loading) could influence the true cell growth rate. As a consequence, μ was calculating by using the control experiments at 0% solids loading and 565 rpm impeller speed. Croughan *et al.* (1988) showed that in the absence of a solid phase, growth rate is independent of system hydrodynamic stress. Toma *et al.* (1991) and Scholtz-Brown

(1998) showed that for *Saccharomyces cerevisiae*, cell growth and disruption are negligible in stirred tank reactors operated in the absence of solid particles. This validated the assumption that the control experiments experience uninhibited cell growth.
The model parameters were calculated at the point of maximum growth. All the calculations are reported in Appendix I. Using the total cell counts to model the death kinetics, the following model was determined:

$$k_d = 0.11 \times \phi^{0.50} \qquad \text{Equation 5.5}$$

The model was found to correlate well with the experimental data (Figure 5.15). The constant b of 0.50 was found to be lower that the coefficient of 1.64 calculated by Scholtz-Brown *et al.* (2002) in Equation 2.15. This suggested that in the range 0% to 2% (v/v), influence of solids loading is lower for growing cells than for stationary one. As the power per unit volume was not calculated in this work, it was not possible to compare the constant a of 0.11 with the coefficient of 7.11×10^{-5} $(P/V)^{0.56}$ proposed by Scholtz-Brown *et al.* (2002).

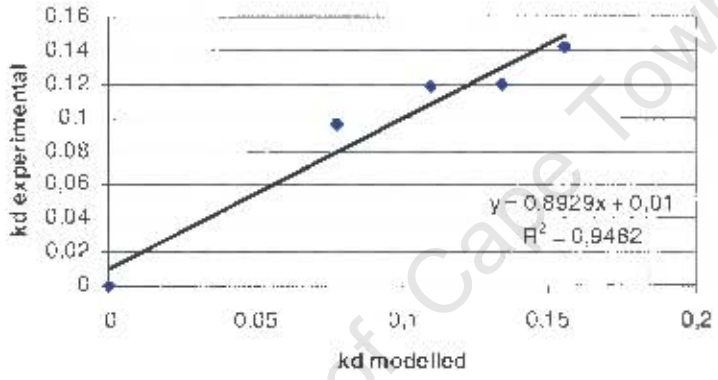

Figure 5.15 Comparison between experimental death constants ($k_{d\ exp}$) and modelled death constants ($k_{d\ mod}$).

5.1.7 Discussion and conclusions

In this study, it has been shown that the concentration of inert solids present during the growth and metabolism of the microbe *S. cerevisiae* influenced its performance. Over the solids loading of 0 to 2% by volume, an increase in the lag phase was observed, both through cell growth and substrate consumption, with increased solids loading. This indicates an increased period of acclimatisation was required. Further a decrease in apparent specific growth rate with increasing solids loading was observed. This may be attributed to an increase in the specific death rate constant and is supported by a decreased fraction of viable cells with increasing solids loading. The death rate constant was modelled as a power law expression accounting for solids loading. A good fit was found between the model and experimental data.

At 5% solids loading, no cell growth, substrate consumption or product formation was observed, indicating a loss of metabolic activity. Further the cell viability decreased to 10% over the incubating period and budding index decreased through incubating period.

The critical solids loading above which a negative influence on yeast performance was observed lay in the range 0.0 to 1% by volume, dependent on assay used.

The decrease in cell growth with unchanged substrate consumption is illustrated by the decrease in $Y_{X/S}$ with increased solids loading. This suggests that additional substrate is diverted from cell growth to provide energy for cell maintenance under the adverse conditions.

TEM analysis performed on samples at 0% and 1% solids loadings demonstrated that the presence of solid particles strongly affects the cell wall morphology. While no influence on cell size could be detected, an increase in cell wall thickness was observed with increased level of stress. Many authors mention the ability of the cells to repair cell damages, by modifying the wall composition. As the cell wall was very irregular at 1% solids loading, such a repair mechanism is suggested where the cell has been injured.

Scholtz-Brown *et al.* (2002) considered the same system yeast plus silica sand in a slurry reactor, but with cells in the stationary phase. They observed negligible disruption in the absence of solid particles, which correlates well with what found in this study. For the same solid size (600-850 µm), they varied the solids fraction across the range 0 to 40% (v/v) at 750 rpm. Significant disruption of *S. cerevisiae* occurred when agitated in the presence of 5% (v/v) silica particles. The extent of disruption increased as time increased. In this study, little disruption was observed at 5% (v/v) solids loading, but no growth occurred and the viability dropped through incubating period. However the agitation rate used was lower (565 rpm), which can explain the difference in the extent of disruption.

Nemati and Harrison (2000) investigated the bioleaching of pyrite by *Sulfolobus metallicus*. With increased solids loading, they also observed a critical solid loading above which performance decreased. This critical value was observed to be 9% by volume. At 12 to 15% (v/v) solids loading, cells activity decreased, but still occurred. The negative effect of increasing solids loading on cell activity was suspected, but could not be assessed for sure, as a decrease in pH occurred at the same time and could strongly affect *S. metallicus* performance. However, a recent study from Sissing (2002), using inert silica, supports the first hypothesis. At 18% (v/v) solids concentration, no more metabolic activity occurred and cell death was observed. These observations correlate well with those of our study, where 5% solids loading appears to be the critical value for yeast activity.

5.2 EFFECT OF SOLID SIZE

The influence of solid size has been reported to affect the efficiency of cell disruption in a bead mill, based on an attrition mechanism (Chisti, 1999; Engler, 1985). Further, Harrison *et al.* (2002a) reported the influence of solids size on the disruption of stationary phase yeast in the slurry bioreactor. Increased cell disruption was observed with increasing particle size and momentum. Nemati and Harrison (2000) showed that the bioleaching performance of *Sulfolobus* was affected by both particle size and solids loading. Cell death was observed at very small particle size. Hence, the influence of particulate size on yeast growth was tested using three different silica sizes, namely diameters of 465-600 µm, 600-850 µm and 850-1130 µm at a 1% (v/v) solids loading. The same analyses were used to investigate performance as with solids loading. The detailed data collected are tabulated in Appendix F.2.

Particle size distributions were measured by laser diffraction using the Malvern analyser. Figure 5.16 illustrates the profiles obtained for the three sizes investigated. In the range 465 – 600 µm, a geometric mean of 501 µm was used (94% of the particle diameters in the range 400 – 650 µm). In the range 600 – 850 µm, a mean diameter of 693 µm was assessed (91% between 550 and 900 µm). 82% of the solids diameters lay in the range 800 to 1300µm, with a mean diameter of 1021µm for the range 850 – 1130 µm.

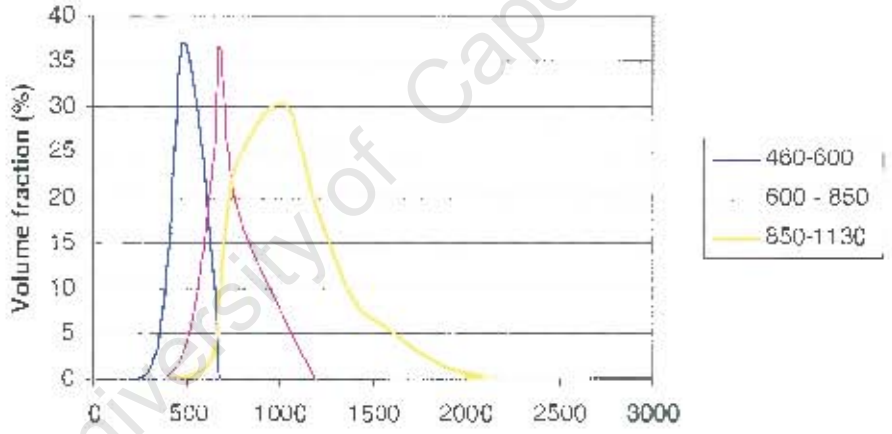

Figure 5.16 Size distributions of the solid particles for the three ranges considered.

5.2.1 Total cell concentration, viability and reproduction

5.2.1.1 Total cell concentration

Figure 5.17 presents total cell concentration as a function of time for different solid sizes. Growth parameters calculated according to Appendix G are presented in Table 5.7.

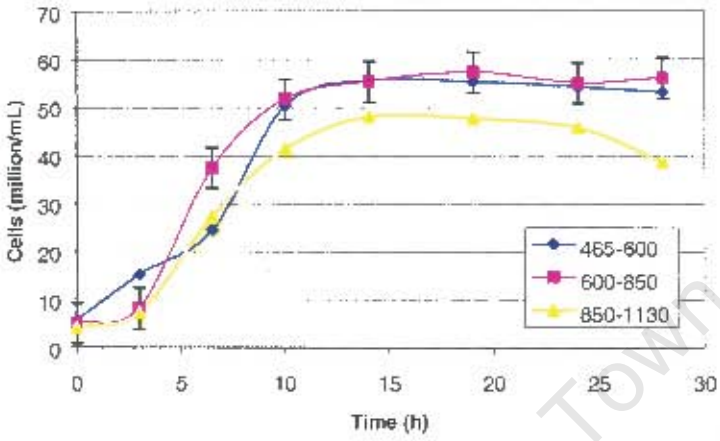

Figure 5.17 Effect of particulate size on total cell concentration.

While no difference (in terms of cell number, specific growth rate and biomass yield) is observed between runs at 465-600 µm and 600-850 µm solids sizes, a decrease in both the rate and extent of growth is clearly illustrated with particles in the range 850 – 1130 µm. The reduction in extent of growth at high solid sizes is demonstrated by the decrease in stationary phase cell concentration (Figure 5.17) and the drop in biomass yield (Table 5.8). The decrease in specific growth rate may result in an increase in the death rate (k_d) with increasing solid size.

Table 5.8 Differences in growth parameters *of S. cerevisiae* at 1% solids loading as a function of solid size.

Solid size	t_{lag} (h)	$\mu_{max\,exp}$ (h^{-1})	t_{exp} (h)	$Y_{X/S}$ (10^9 cells/g)
465-600	5.5	0.133	15	6.86
600-850	3.5 (±0.5)	0.135 (±0.018)	15 (±1.5)	7.15 (±0.96)
850-1130	3.5	0.109	14	5.09

5.2.1.2 Viable cell concentration

The viable cell concentration and viability as a function of time for different solid sizes are presented respectively in Figure 5.18 and Figure 5.19. Calculations of the specific growth rate based on viable cells, and the fraction of viable cells at the end of the growth for each particle size investigated are summarised in Table 5.9.

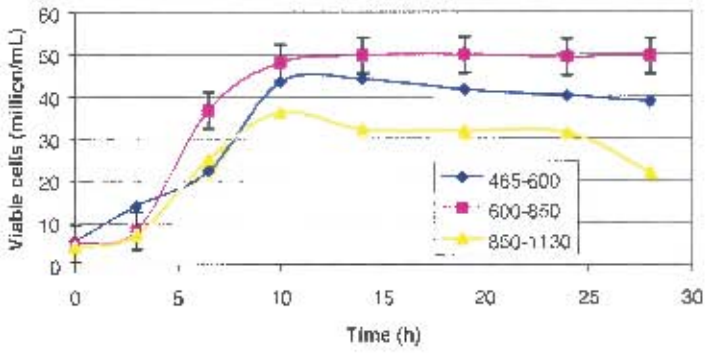

Figure 5.18 Effect of particulate size on viable cell concentration.

Table 5.9 Specific growth rate based on viable cells and percentage of viable cells at the end of the growth for different solid sizes.

Solid size(μm)	$\mu_{viablecells}$	Fraction of viable cells at the end of the growth (%)
465-600	0.121	72.8
600-850	0.138 (± 0.016)	96.1 (± 5.6)
850-1130	0.102	56.1

From the data presented, it clearly appears that solid size in the range 600 – 850 μm is the most favourable in maintaining viability. It is the only size that holds cell in the typical viability range of 90 to 99%. The decrease in viable fraction for small and large size fractions supports the decrease in the specific viable growth rate. The increase in solid size sharply affects the stationary phase cell concentration, specific growth rate and fraction of viable cells at the end of the growth (loss of 44% viability). This increase in solid size implies an increase in particulate momentum. As a consequence, the results correlate well with Harrison *et al.* (2002) work, that reported increased cell damage (with particular reference to cell disruption) with increasing particle momentum (defined as the product of the particle mass and impeller tip speed, Harrison *et al.*, 2002). Therefore the reduced viability with the smaller size fraction appears contradictory. However, it has to be noted that when reducing particle size with a same solid loading, the particle number is increased in the system, implying that interactions between solid particles and cells occur more frequently.

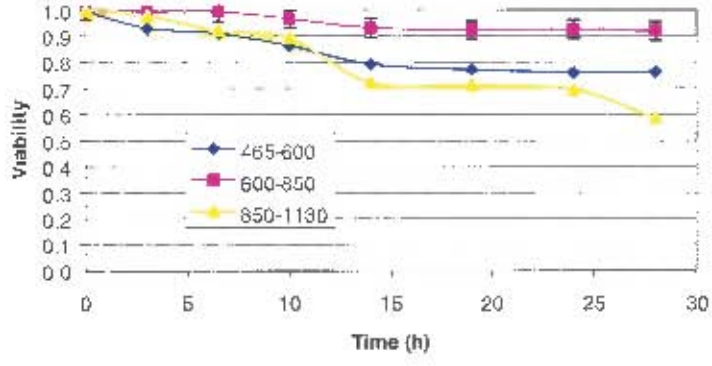

Figure 5.19 Effect of particulate size on viability at 1% solids loading.

5.2.1.3 Budding index

Changes observed in budding index as a function of time, for different solid sizes, are illustrated in Figure 5.20.

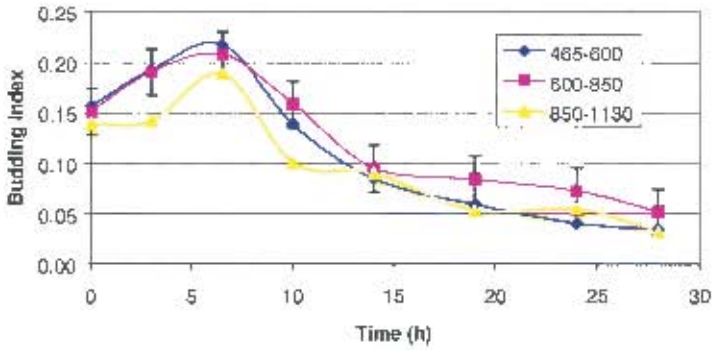

Figure 5.20 Effect of particulate size on budding index at 1% solids loading.

The similarities in budding index for sizes 465-600 and 600-850 µm support observations in Section 5.2.1.1. The lower values of budding index obtained for 850-1130 µm may result from the combined effect of the decrease in cell viability and cell activity, pointed out in Section 5.2.1.2.

5.2.2 Glucose concentration

Glucose concentration profiles are plotted in Figure 5.21, as a function of time. Glucose uptake parameters, calculated as specified in Appendix G, are tabulated in Table 5.10.

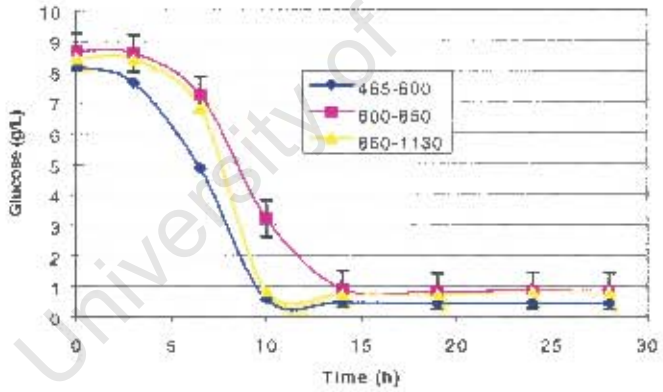

Figure 5.21 Effect of particulate size on glucose consumption at 1% solids loading.

Table 5.10 Glucose uptake parameters calculated for different solid sizes.

Solid size (µm)	q_s ($g.h^{-1}.10^9cells^{-1}$)	Glucose lag phase (h)
465-600	-0.0334	4
600-850	-0.0338 (± 0.007)	5 (± 1.01)
850-1130	-0.0531	5

When no difference is noticed in the specific substrate utilisation rate for 465-600 µm and 600-850 µm, the glucose is consumed more rapidly for the lower particle size (within 10 hours, while glucose is depleted within 14 hours for 600-850 µm). This suggests additional energy derived from glucose consumption may be required for cell maintenance. It is further supported by the decrease in cell viability after 10h with 465-600 µm diameter particles (Figure 5.19), once all the glucose has been depleted.

At 850-1130 µm, the substrate utilisation rate is higher, and all the glucose available is consumed within 10 h, time which corresponds to the higher viable cell concentration (Figure 5.18). The increase in the substrate utilisation rate suggests an increase in cell maintenance requirements when yeast are exposed to the harshest hydrodynamic conditions.

5.2.3 Zeta potential

Figure 5.22 shows results for zeta potential measurements when increasing particulate sizes. For the three experimental conditions, an increase in zeta potential with time is seen, which correlates well with observations reported in Section 5.1. As yeast cell charge is mainly attributable to the wall constituents (phosphate groups and proteins), a change in the cell wall composition is therefore suspected through the growth. Zeta potential is higher for increased solids size. This is clearly noticeable from 0 to 15 h. It as unespected that the zeta potential of cells agitated in the presence of the 600-850 µm solids fraction is not more negative than those cells in the 465-600 µm fraction (since the viability of the cells in the former case is much higher). From 15h, a plateau is observed for experiment with 850 – 1130 µm particle size. The decrease in viability and increase in the death rate confirm that cells are dying. Therefore the result correlates well with observation at 5% (v/v) solids loading, where constant zeta potential values were found.

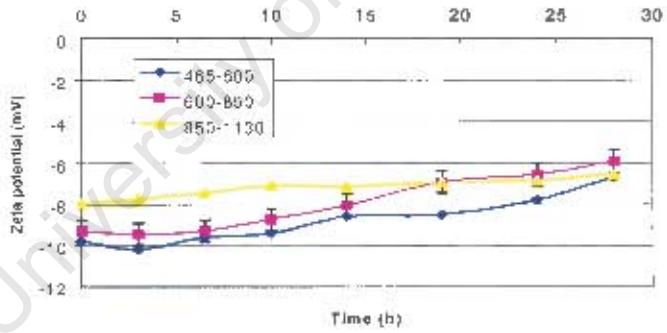

Figure 5.22 Effect of particulate size on zeta potential measurements at 1% solids loading.

5.2.4 Discussion and conclusions

The study of the effect of particulate size demonstrated clearly that the performance of the yeast was best at the size fraction 600 to 850 µm. On increase of the size fraction to 850 to 1130 µm, a decrease in stationary phase concentration, cell viability, specific growth rate, magnitude of negative cell surface charge and biomass yield was observed.

Chapter 6: Influence of the inoculum state on the growth

6.1 EFFECT OF INOCULUM SIZE

It is expected that microbes are less able to modify their environment when present at low concentration and so are more vulnerable to hostile conditions. While this is assumed, no specific reference to this in the literature was found. To test the hypothesis, the effect of inoculum size on yeast growth was investigated. Four inoculum sizes were tested, namely 10% inoculum (standard condition), 2.5%, 2% and 1% inoculum. The same analyses as reported in the previous sections were performed. The standard experimental conditions were set as follows: 1% (v/v) solid loading, 600 – 850 µm solid size, agitation rate of 565 rpm (tip speed 2.33 $m.s^{-1}$) using a Rushton turbine, and an inoculum grown for 14h. These values were kept constant for all experiments, while only the inoculum size was changed.
The data presented in this section are tabulated in Appendix F.3.

6.1.1 Total cell concentration, viability and reproduction

6.1.1.1 Total cell concentration

Figure 6.1 shows total cell concentration as a function of time for different inoculum sizes. The growth parameters calculated are reported in Table 6.1 Lag and exponential periods were determined visually, as described in Appendix G. It is clearly seen that inoculum size plays an important role in the growth in the slurry bioreactor. As inoculum size decreases, the lag phase increases, the specific growth rate decreases, the duration of exponential phase increases and biomass yield decreases. However, for 2% , 2.5% and 10% inoculum sizes, the same quantity of yeast is produced (over a longer time period), while, using a 1% inoculum, the final concentration is diminished by some 30%.

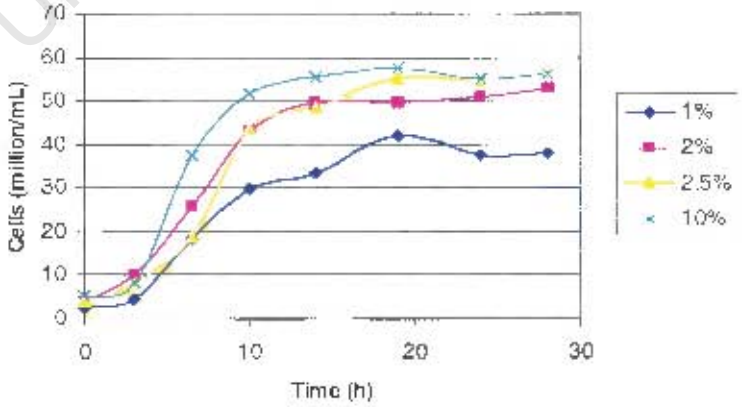

Figure 6.1 Effect of inoculum size on total cell concentration.

Table 6.1 Effects of inoculum size on growth parameters.

Inoculum size	t_{lag} (h)	X_{max} (10^6 cells/mL)	X_{max}/X_0	$\mu_{max\,exp}$ (h^{-1})	t_{exp} (h)	Yx/s (10^9 cells/g)
1.0%	5.5	37.7	0.63	0.099	20	4.99
2.0%	5.0	53.1	0.88	0.119	17	6.56
2.5%	5.5	55.9	0.93	0.124	17	7.00
10.0%	3.5 (± 0.5)	56.0 (± 4.2)	0.93 (±0.07)	0.135 (± 0.018)	15 (± 1.5)	7.15 (± 0.96)

Note: X_0 is the maximum biomass concentration at 0% (v/v) solids loading.

From the data presented in Figure 6.2, it is apparent that a critical inoculum size exists below which yeast exhibits a lower growth performance when incubated in the presence of a stress factor such as hydrodynamic stress generated in an agitated, aerated slurry bioreactor. For X_{max}/X_0, $\mu_{max\,exp}$, t_{exp} and $Y_{X/S}$ this value is determined at 2% (v/v), while for t_{lag} is higher than 2.5% (v/v).

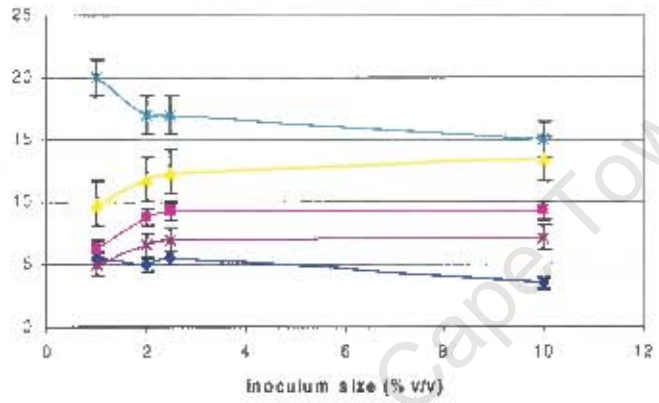

Figure 6.2 Influence of inoculum size on growth parameters. (● t_{lag} (h), ˙ $X_{max}/X_0 \times 10$, ▲ $\mu_{max\,exp}$ (h^{-1}) × 100, × t_{exp} (h), ✳ $Y_{X/S}$ (10^9 cells/g)).

6.1.1.2 Viable cell concentration

Figure 6.3 shows viable cell concentration as a function of time following inoculation with different volumes fractions of inoculum. Table 6.2 presents specific growth rate based on viable cell number, $\mu_{viablecells}$, and the ratio between maximum viable cells grown under stress and no stress $(X_{max}/X_{max\,0})_{viable}$. The viable cell concentration as a function of time showed the same trend as total cell concentration: $\mu_{viablecells}$ decreased when the inoculum size was lowered.

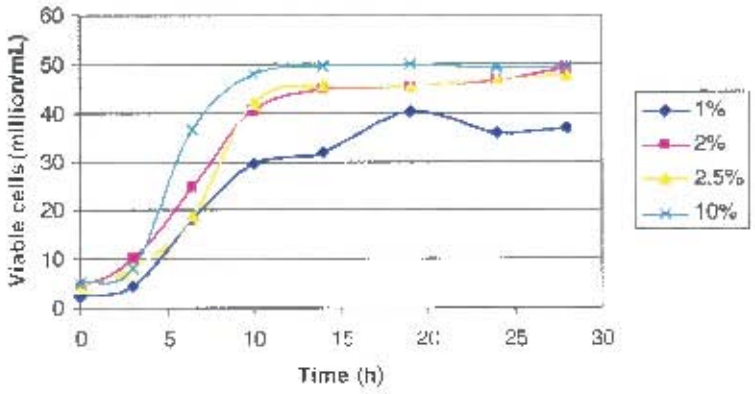

Figure 6.3 Effect of inoculum size on viable cell concentration.

Table 6.2 Specific growth rate on viable cells for different inoculum sizes.

Inoculum size	$\mu_{viablecells}$ (h^{-1})	$X_{max\ viable}$ (10^6 cells/mL)	$(X_{max}/X_{max\ 0})_{viable}$
1.0%	0.086	36.7	0.61
2.0%	0.115	49.1	0.82
2.5%	0.129	47.7	0.80
10.0%	0.118 (± 0.016)	49.5 (± 4.3)	0.83 (± 0.07)

Viability as a function of time is plotted for the different inoculum sizes in Figure 6.4. The viability was maintained in excess of 92% with 1, 2 and 10% inoculum, exhibiting no specific effect of inoculum size. The gradual decrease in viability with time across all these experiments at 1% solids loading (compared to the control experiment at 0% solid loading) confirms the stress exerted in the slurry reactor.

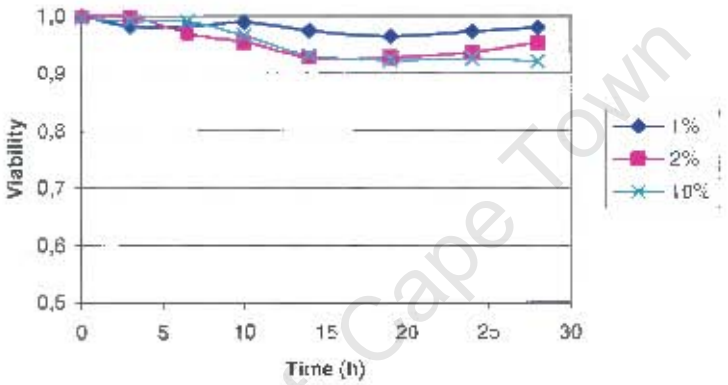

Figure 6.4 Effect of inoculum size on viability on incubation at 1% solids loading in the slurry reactor.

6.1.1.3 Budding index

Figure 6.5 shows changes in budding index with time as a function of inoculum size. The maximum budding index was obtained for the lowest inoculum size. It occurs after a slightly longer period of time, which can be related to the longer lag phase. Little difference in trend of budding index with time is noticeable.

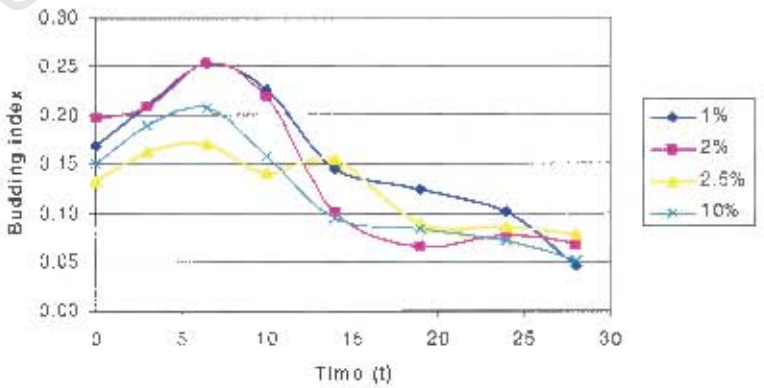

Figure 6.5 Effect of inoculum size on budding index.

6.1.2 Glucose concentration

The residual glucose concentration as a function of time is given in Figure 6.6. The specific substrate consumption rate and lag period preceding glucose consumption are tabulated in Table 6.3. Little difference was seen for 2%, 2.5% and 10% (v/v) inoculum sizes in terms of glucose consumption profile, glucose lag phase and specific substrate consumption rate. Glucose consumption is more rapid for the 1% (v/v) inoculum. This is probably because of increased maintenance requirements, supported by the data in Figures 6.1, 6.3 and 6.7.

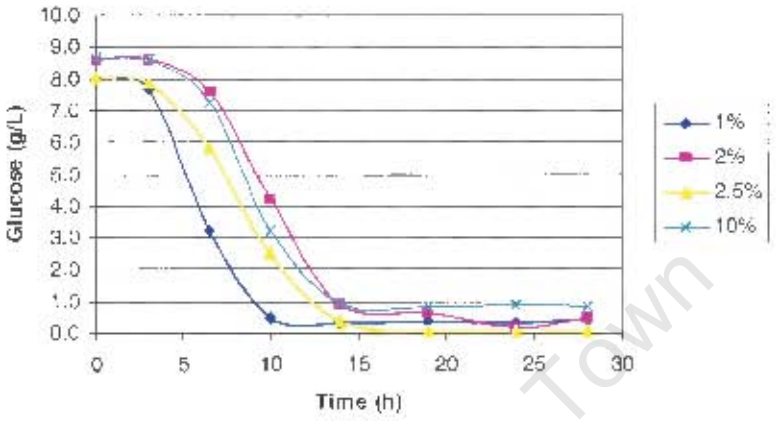

Figure 6.6 Effect of inoculum size on glucose consumption on incubation at 1% solids loading in the slurry reactor.

Table 6.3 Glucose uptake parameters for different inoculum sizes.

Inoculum size	q_s ($g.h^{-1}.10^9$ $cells^{-1}$)	Glucose lag phase (h)
1%	-0.0270	3
2%	-0.0230	5
2.50%	-0.0310	3
10%	-0.0338 (± 0.007)	5 (± 1.04)

6.1.3 Zeta potential

Figure 6.7 shows results for zeta potential of yeast as a function of time on varying the inoculum size. For all inoculum sizes, zeta potential increases with time. As inoculum size decreases, zeta potential is higher. This suggests that the surface charge of yeast is modified when microbes are more exposed to hydrodynamic stress. The more exposed yeast are, the less charged they are. This is in agreement with findings reported in Section 5.1.4 based on increased stress due to increased solids loading.

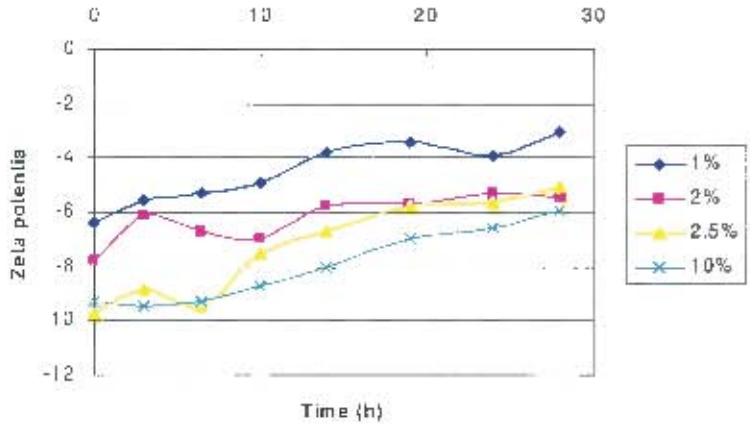

Figure 6.7 Effect of inoculum size on zeta potential measurements.

6.1.4 Ethanol concentration

Ethanol concentration as a function of time for three inoculum sizes are plotted in Figure 6.8. Data collected prior to glucose depletion (from 0 to 15 hours) were used to calculate the specific ethanol production rate. Results are reported in Table 6.4. A decrease in ethanol production is observed when inoculum size is reduced from 10% to 2.5% (v/v), in terms of ethanol concentration, product yield on substrate and product yield on biomass. However with a 1% (v/v) inoculum size, ethanol production occurs more rapidly, with a higher specific production rate with glucose being depleted more quickly with the same inoculum size. This suggests an increase in yeast metabolic rate below a critical inoculum size and a shift in metabolism away from biomass production.

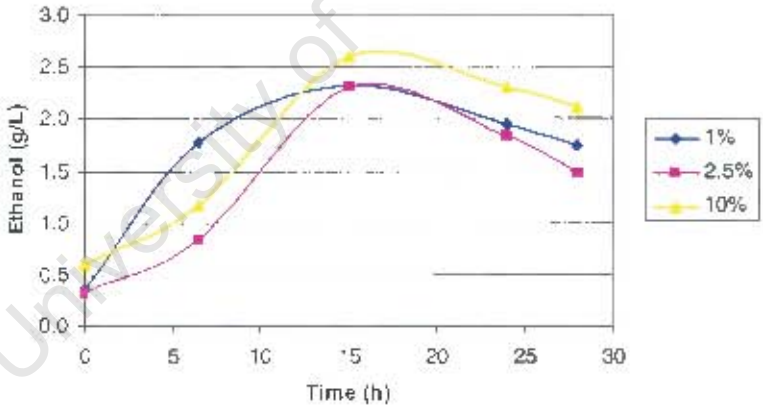

Figure 6.8 Effect of inoculum size on ethanol production.

Table 6.4 Effect of inoculum size on product formation parameters.

Inoculum size	q_p ($g.h^{-1}.10^9$ cells^{-1})	$Y_{EtOH/s}$	$Y_{EtOH/x}$ ($g.10^9$ cells^{-1})
1.0%	0.0049	0.184	0.037
2.5%	0.0046	0.144	0.021
10.0%	0.0039 (± 0.001)	0.193 (± 0.013)	0.027 (± 0.001)

6.1.5 Discussion and conclusions

The influence of inoculum size on the growth of micro-organisms has been poorly studied. In this work, an investigation of the effect of inoculum size on yeast growth was performed. It has been demonstrated that the inoculum size plays a determinant role in yeast performance. From 2 to 10% inoculum size, little difference was observed in the extent of yeast growth, glucose consumption and ethanol production. However below 2% (v/v) inoculum size, the yeast activity changed. As the inoculum size was decreased, the lag phase and exponential phase increased while the specific growth rate and the biomass yield decreased. As yeast viability remained quite high for all experiments (above 92%), it was concluded that a decrease in inoculum size did not cause a increase in the death rate but a reduced yeast activity.

6.2 EFFECT OF INOCULUM AGE

As mentioned in Section 6.1, the effect of inoculum state on the growth is not reported in previous studies. However, yeast are postulated to grow differently depending on inoculum conditions In order to access the influence of inoculum age on the growth, two inoculum ages were tested in this work. In the standard experiment, inoculum was incubated for 14 hours, resulting in a late exponential phase culture. A 24-hour inoculum representing the stationary phase of growth, was compared to the standard condition. All other experimental conditions (solids loading, solid size, agitation rate and type, inoculum size) were maintained at their reference values (Section 3.4). The data used to generate the plots presented in this section are tabulated in Appendix F.4.

6.2.1 Total cell concentration, viability and reproduction

6.2.1.1 Total cell concentration

Figure 6.9 shows total cell concentration as a function of time for the two inoculum ages. Specific growth rate, lag periods and yields are reported in Table 6.5. It is clearly observed that no difference in these parameters exists between the two inoculum ages.

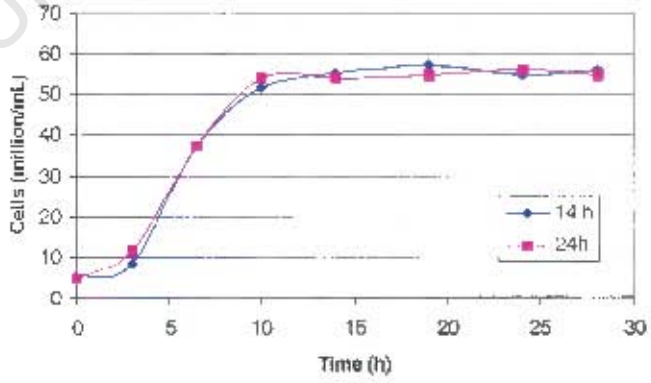

Figure 6.9 Effect of inoculum age on total cell concentration.

Table 6.5 Influence of inoculum age on growth parameters.

Inoculum Age	t_{lag} (h)	$\mu_{max\ exp}$ (h^{-1})	t_{exp} (h)	Yx/s (10^9 cells/g)
14 hr	3.5 (± 0.5)	0.135 (± 0.018)	15 (± 1.5)	7.15 (± 0.96)
24 hr	3	0.134	15	7.17

6.2.1.2 Viable cell concentration

Viable cell concentration as a function of time is given in Figure 6.10 for the two inoculum ages. Table 6.6 presents the results for the specific growth rate based on viable cells and the ratio of maximum viable cell count, between these experiments and the control (0% (v/v) solid loading). While little difference is observed in viable cell concentration during the lag and exponential phases (same values for the specific growth rate), a decrease in the viable cell concentration is observed with a 24h inoculum in the stationary phase. During the same period of time, viable cell concentration remains constant with a 14h inoculum.

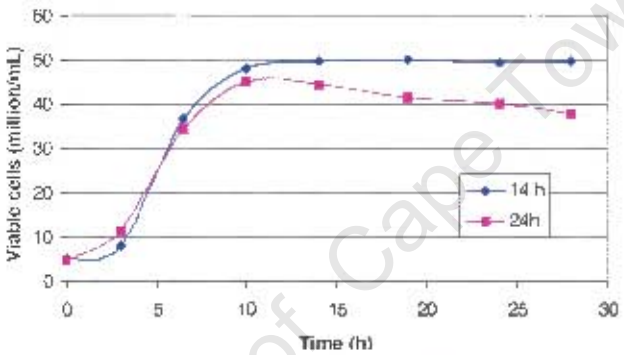

Figure 6.10 Effect of inoculum age on viable cell concentration in the slurry bioreactor at 1% solids loading.

Table 6.6 Specific growth rate based on viable cells for two inoculum ages.

Inoculum age	$\mu_{viablecells}$ (h^{-1})	$X_{max\ viable}$ (10^6 cells/mL)	$X_{max\ viable}/X_{viable}$
14 hr	0.118 (± 0.016)	49.5 (± 4.3)	0.83 (± 0.07)
24 hr	0.121	37.6	0.63

Figure 6.11 shows viability as a function of time for the two inoculum ages. It clearly appears that viability decreased more rapidly for a 24h inoculum than for the late exponential phase inoculum (14h). While viability is higher than 92% throughout the fermentation inoculated with the 14h inoculum, it decreased to 75% with the 24h inoculum. It confirms the previous observation (Section 6.2.1.1) that inoculum age does not affect the total cell number concentration but viable cell number in stationary phase decreases when increasing the inoculum age from 14h to 24h. Hence, it can be postulated that an increase in the death rate in stationary phase occurs when increasing the inoculum age.

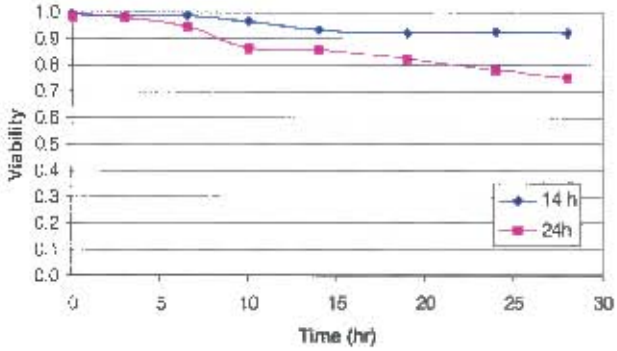

Figure 6.11 Effect of inoculum age on viability.

6.2.1.3 Budding index

Figure 6.12 shows budding index profiles as a function of time for two inoculum ages. It clearly appears that inoculum age has a strong influence on budding index. The 24-hour inoculum curve exhibits a high initial value of budding index. During lag phase, the budding index drops sharply from 0.4 to 0.05, while it increases for a 14-hour inoculum. From 15 hours, budding index shows the same behaviour for the two inoculum ages. Differences observed during lag phase confirm that the inocula are in a different metabolic state when added to the reactor.

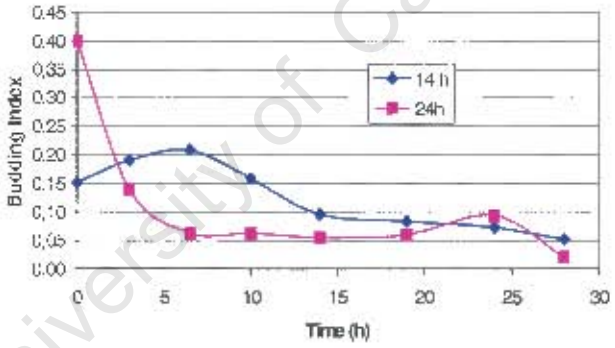

Figure 6.12 Effect of inoculum age on budding index.

6.2.2 Glucose concentration

Substrate consumption measured in terms of glucose concentration is illustrated in Figure 6.13. Values for specific substrate consumption rate and substrate lag phase are reported in Table 6.7. It is observed that glucose was consumed more rapidly with a 24h inoculum than a 14h inoculum. This is confirmed by a shorter glucose lag phase and a higher specific substrate consumption rate. Considering that the same total cell concentrations were observed for the two inoculum ages, it may be assumed that glucose was used with the 24h inoculum for both growth and maintenance requirements. Once all the glucose was depleted (after 10h), viable cell concentration decreased, suggesting

that yeast are unable to remain viable under conditions where the substrate is insufficient to provide energy for cell maintenance.

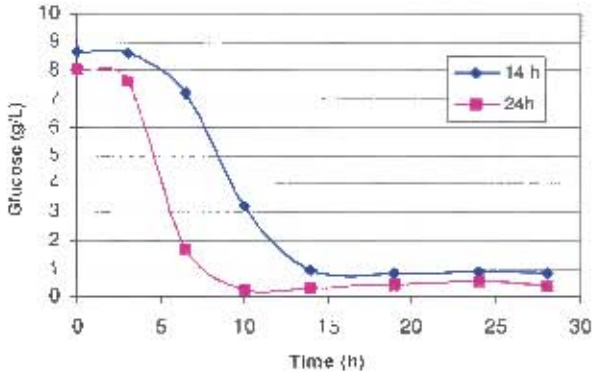

Figure 6.13 Effect of inoculum age on glucose consumption.

Table 6.7 Glucose uptake parameters for two inoculum ages.

Inoculum age	q_s ($g.h^{-1}.10^9$ $cells^{-1}$)	Glucose lag phase (h)
14 hr	-0.0338 (± 0.007)	5 (± 1.0 h)
24 hr	-0.0512	3

6.2.3 Zeta potential

Figure 6.14 shows results for zeta potential measurements for two inoculum ages. For both experiments, zeta potential increased with time. With a 24h inoculum, zeta potential of yeast was higher throughout the fermentation than with the 14h inoculum. This confirmed that surface charge was modified as a function of the physiological status of the cell and when yeast are exposed to stressful conditions.

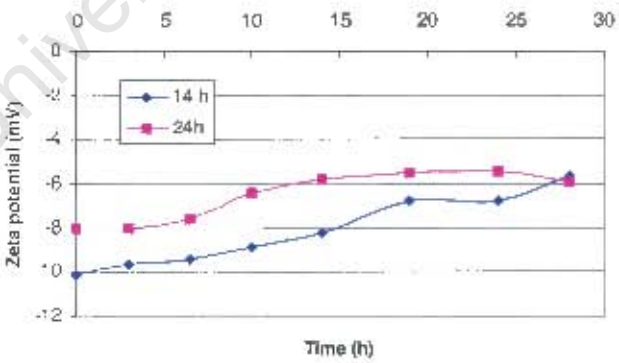

Figure 6.14 Effect of inoculum age on zeta potential.

6.2.4 Ethanol concentration

Ethanol concentration as a function of time following inoculation using the two inoculum ages is given in Figure 6.15. Table 6.8 summarises the values calculated for the specific production rate of ethanol, product yield on substrate and product yield on biomass. It clearly appears that a higher inoculum age reduced the extent of ethanol production. Not only was the maximum ethanol concentration reduced, but q_p and $Y_{EtOH/s}$ were also diminished. This correlates well with the hypothesis that substrate is used for cell maintenance and not for normal metabolic activity with the 24h inoculum.

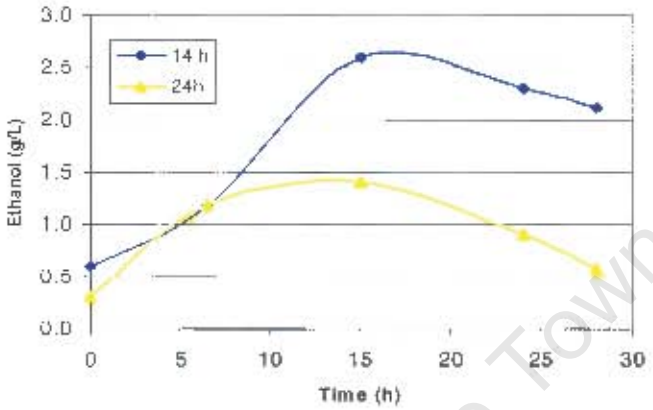

Figure 6.15 Effect of inoculum age on ethanol production.

Table 6.8 Differences in ethanol production parameters for two inoculum ages.

Inoculum age	q_p ($g.h^{-1}.10^9$ cells^{-1})	$Y_{EtOH/s}$	$Y_{EtOH/x}$ ($g.10^9$ cells^{-1})
14h	0.0039 (± 0.001)	0.193 (± 0.013)	0.027 (± 0.001)
24h	0.0015	0.034	0.05

6.2.5 Discussion and conclusions

While no literature reference on the influence of inoculum on yeast growth was found, it is commonly held that such influence exists. Hence the effect of inoculum age was investigated in this study. It was found that little difference in total cell concentration could be detected between a 14h inoculum and a 24h inoculum. However differences were observed in terms of viablility, budding index, substrate consumption and ethanol production. The decrease in viable cell concentration in stationary phase and the decrease in budding index suggested that death rate was not negligible following inoculation with the 24h inoculum. Rapid glucose uptake and lower ethanol production confirmed that substrate was used not only for cell growth (same profile for lag and exponential phases), but also provided energy for cell maintenance. On depletion of all glucose, these yeast were more sensible to hydrodynamic stress and higher number of dead cells was observed. From these observations, the existence of an optimum inoculum age for growth of micro-organisms existed. Two experimental conditions were insufficient to determine the value of this optimum. However a 24h inoculum appeared less resilient to

yeast growth under stress compared to a 14h inoculum. Further this resilience does not appear to be recovered in a single growth cycle.

Chapter 7: Influence of the impeller on the yeast performance in the slurry bioreactor

7.1 EFFECT OF IMPELLER TYPE

Experiments with two impeller types were performed, in order to establish whether the impeller flow pattern would alter cell activity and viability. Under standard conditions, a Rushton turbine was used, providing a radial flow pattern. In addition, a pitched-blade turbine was chosen as the axial impeller to generate the axial flow pattern. Experiments were performed at both 0% and 1% (v/v) solids loadings. The data used to generate the graphs presented in this section are tabulated in Appendix F.5.

7.1.1 Total cell concentration, viability and reproduction

7.1.1.1 Total cell concentration

Figure 7.1 shows total cell concentration as a function of time for the Rushton turbine (RT) and pitched-blade turbine (PBT) at 0 and 1% (v/v) solids loading. Calculations for growth parameters are reported in Table 7.1.

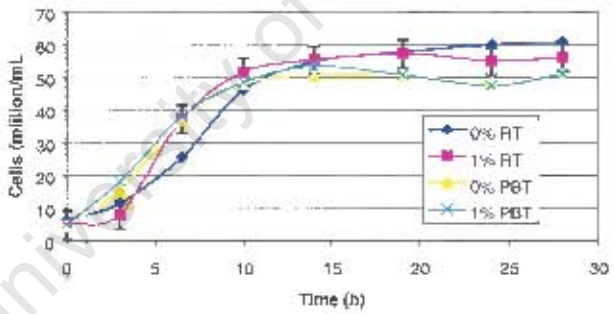

Figure 7.1 Effect of impeller type on total cell concentration.

Table 7.1 Influence of impeller type on growth parameters.

Impeller type	t_{lag} (h)	$\mu_{max\ exp}$ (h^{-1})	t_{exp} (h)	Yx/s (10^9 cells/g)
0% RT	3.0 (± 1.0)	0.254 (± 0.026)	17 (± 1.0)	7.53 (± 1.08)
1% RT	3.5 (± 0.5)	0.135 (± 0.018)	15 (± 1.5)	7.15 (± 0.96)
0% PBT	3.0	0.164	13	6.76
1% PBT	3.0	0.141	14	6.68

When comparing the Rushton turbine to the pitched-blade turbine, a slight decrease in the stationary phase cell concentration was observed with the axial impeller. This reduced activity was supported by the decrease in biomass yield and exponential phase duration (Table 7.1). Considering only the pitched-blade impeller, no difference between experiments at 0% and 1% (v/v) solids loadings could be assessed. At these concentrations, a decrease in extent of growth using a Rushton turbine could not be observed either (Section 5.1). However Figure 5.2 and Table 7.1 show that there is a significant difference in the maximum specific growth rates at 0% and 1% solids (v/v). A mechanism independent of solids loading is suspected to be responsible for reduced growth. Pitched-blade turbine produces a lower turbulence intensity than a Rushton turbine (Hackl *et al.*, 1989), and requires a lower power input per unit volume. Hence an oxygen transfer limitation might cause a decrease in growth.

7.1.1.2 Viable cell concentration

Figure 7.2 shows viable cell concentration as a function of time for the two impeller types, while viability is illustrated in Figure 7.3. The fraction of viable cells in the stationary phase and specific growth rates based on viable cells are reported in Table 7.2.

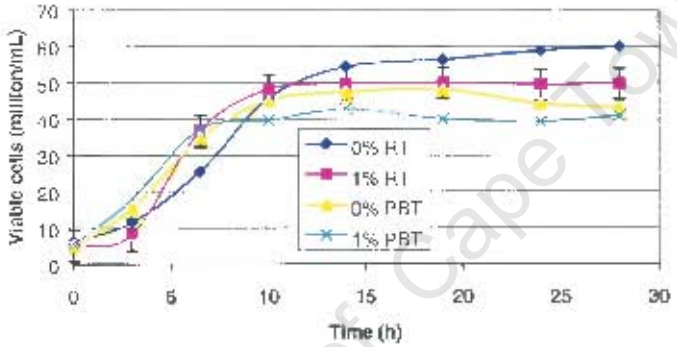

Figure 7.2 Effect of impeller type on viable cell concentration.

Table 7.2 Specific growth rate based on viable cells for two impeller types.

Impeller type	$\mu_{viable cells}$	% of viable cells at the end of the growth
0% RT	0.253 (± 0.028)	98.2 (± 1.3)
1% RT	0.138 (± 0.016)	96.1 (± 5.6)
0% PBT	0.155	84.5
1% PBT	0.144	80.0

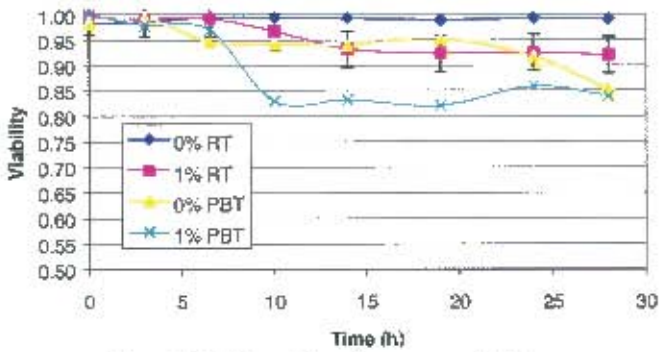

Figure 7.3 Effect of impeller type on viability.

As observed in Section 7.1.1.1, viable cell concentration profiles and specific growth rate based on viable cells were very similar for the pitched-blade impeller at the two solids loadings. However a sharp decrease in viability was observed after 10h for cells grown at 1% solids loading. It was suggested that the combined effects of hydrodynamic stress plus oxygen limitation stress resulted in the decrease in cell viability and subsequent increase in the death rate constant k_d. Agitation with a pitched-blade turbine did not maintain cell viability in the reported limits of viability for unstressed systems (94 to 99%), even in the absence of solid particles.

7.1.1.3 Budding index

Influence of impeller type on budding index as a function of time is illustrated in Figure 7.4. For all experimental conditions, budding index exhibited the same trend: it increased through the lag phase and the beginning of exponential phase and decreased from mid-exponential phase. At 0% solid loading, maximum budding index was observed at the same time (5 h) for both impeller types, while maximum budding index was delayed to 7h at 1% solids loading. This supported the assumption that solids loading decreased cell activity (Section 5.1). While a slight decrease in budding index was apparent for a pitched-blade turbine compared to the Rushton one, results for 0% and 1% (v/v) solids loading on agitation with the pitched-blade turbine were very similar. This confirmed that reduced activity using the axial flow impeller may result from a stress independent of the solid particules.

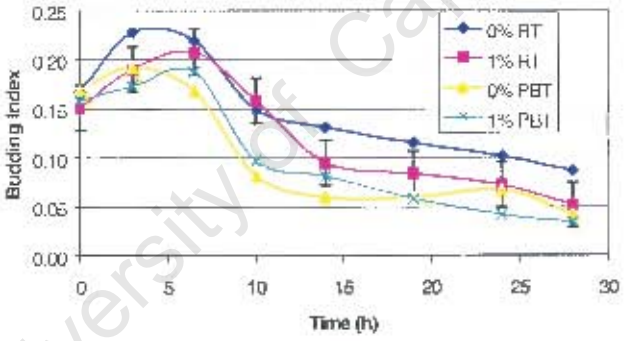

Figure 7.4 Effect of impeller type on budding index.

7.1.2 Glucose concentration

Results for glucose consumption when changing impeller type are presented in Figure 7.5. Glucose uptake parameters are tabulated in Table 7.3.

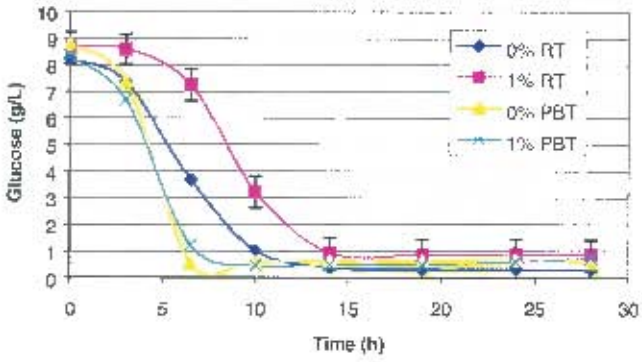

Figure 7.5 Effect of impeller type on glucose consumption.

Table 7.3 Influence of impeller type on glucose uptake parameters.

Impeller type	q_s ($g.h^{-1}.10^{9}cells^{-1}$)	Glucose lag phase (h)
0% RT	-0.0486 (± 0.007)	4 (± 1.34)
1% RT	-0.0338 (± 0.007)	5 (± 1.04)
0% PBT	-0.0543	3
1% PBT	-0.0561	3

Glucose consumption showed the same profiles at 0% and 1% (v/v) solids loading for the pitched-blade turbine, supporting the postulation that the stress introduced by the lower energy input associated with the pitched-blade turbine dominated the stress generated by the influence of solid particulates. This was further supported by the similarities in substrate consumption rate and glucose lag duration on agitation with the pitched-blade turbine at 0 and 1% solids loading. The substrate was consumed more rapidly (higher substrate consumption rate and shorter glucose lag phase) when yeast were grown in a slurry reactor agitated by a pitched-blade impeller compared to a Rushton turbine. It was previously found that rate and extent of growth were reduced using the pitched-blade impeller type. As a consequence higher glucose consumption is postulated to be required for providing extra energy for cell maintenance.

7.1.3 Zeta potential

Figure 7.6 presents results for zeta potential measurements as a function of time for two impellers.

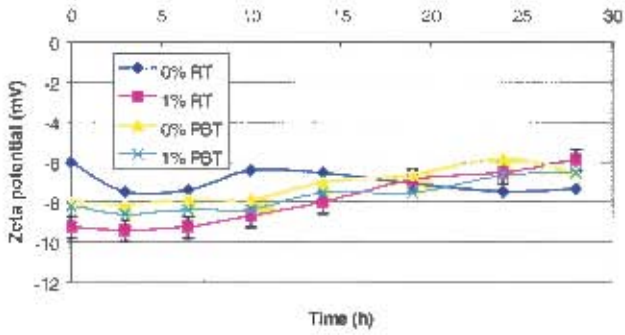

Figure 7.6 Effect of impeller type on zeta potential measurements.

An increase in zeta potential measurements with time was observed for pitched-blade impeller. As noticed previously, observations at 0% and 1% solids loadings were very similar. In Section 5.1.3, yeast experiencing mild-stress (0.5 to 2% (v/v) solids loading) were found to exhibit increased surface charge with increasing time of exposure to stress, suggesting that modifications in the cell wall composition occurred. Similarly, yeast grown in a reactor agitated by an axial impeller may experience stress other than or in addition to hydrodynamic stress.

7.1.4 Discussion and conclusions

In this study, comparison between two impeller types, Rushton turbine and pitched-blade impeller was performed, at both 0% and 1% solids loadings. It was clearly demonstrated that in that range of concentrations, the presence of the solid particles had no influence on the growth using the pitched-blade impeller. This was supported by the similarities in stationary phase cell concentration, specific growth rate, biomass yield, budding index, glucose concentration and zeta potential. Only viability indicated a difference when solid was added to the bioreactor. Lower viability was observed at 1% solids loading.

When comparing observations with the pitched-blade turbine to the ones with the Ruston turbine, reduced rate and extent of growth and lower budding index were noticed. These findings disagree with those found in the literature. Scholtz-Brown (1998) used both Rushton turbine and pitched-blade turbine to disrupt yeast cells in a slurry reactor. They observed the same maximum extent of cell disruption, irrespective of the flow pattern. However the rate of cell disruption was less for the pitched-blade turbine. Pearce (1993) also found with a mineral bio-oxidation system that either the Rushton or the axial impeller at an impeller speed of 350 rpm did not inhibit the growth of thiobacilli. At 630 rpm, no activity appeared in the tank agitated by a Rushton turbine while the growth rate started to increase after a lag phase of 14 days.

The apparent contradiction between results obtained in this work and those reported in the literature might be explained by Hackl *et al.* (1989) observations. They reported that pitched-blade turbine has a higher pumping capacity than Rushton turbine and, for a given impeller speed, requires less power. But as a consequence, it produces lower turbulence intensity. The lower mixing may induce an oxygen limitation, resulting in reduced extent of growth.

7.2 EFFECT OF IMPELLER SPEED

In this set of experiments, the Rushton turbine was used and the solids loading was fixed at 1% (v/v). A series of experiments was performed over the impeller speed range of 460 to 850 rpm to investigate the influence of agitation rate, and thereby energy input, on yeast growth. For the same system of study, Scholtz-Brown and Harrison (2002a) measured the critical impeller speed for complete suspension of the solids. At 5% (v/v) solids loading, this critical impeller speed was set at 400 rpm. In accordance with their results, complete suspension of the solids was observed for all experiments in our study. The data presented in this section are tabulated in Appendix F.6.

7.2.1 Total cell concentration, viability and reproduction

7.2.1.1 Total cell concentration

Figure 7.7 shows total cell concentration as a function of time following agitation at the four impeller speeds 460, 565, 600 and 850 rpm, corresponding to impeller tip speeds of 1.91, 2.33, 2.48 and 3.51 $m.s^{-1}$ respectively. Calculations for growth parameters are reported in Table 7.4.

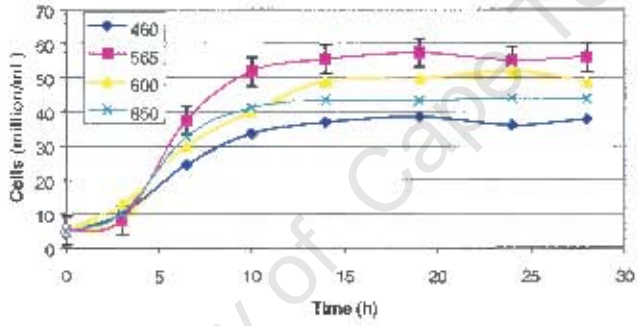

Figure 7.7 Effect of impeller speed on total cell concentration.

Table 7.4 Influence of impeller speed on growth parameters.

Speed (rpm)	Impeller tip speed ($m.s^{-1}$)	t_{lag} (h)	$\mu_{max\,exp}$ (h^{-1})	t_{exp} (h)	Yx/s (10^9 cells/g)
460	1.91	4	0.077	18	5.14
565	2.33	3.5 (± 0.5)	0.135 (± 0.018)	15 (± 1.5)	7.15 (± 0.96)
600	2.48	3.5	0.125	16	6.17
850	3.51	4	0.114	14	4.92

On increasing the agitation rate above the standard rate of 565 rpm, the reduction in both the rate and extent of growth with increased impeller speed was clearly illustrated. The reduced extent of growth was seen by a decrease in biomass yield, $Y_{X/S}$ (Table 7.4) and in the stationary phase cell concentration (Figure 7.7). It is proposed that the reduced apparent specific growth rate may result from an increase in the death rate (k_d) with

increasing impeller speed, where k_d is a power law function of agitation rate. Modelling the death rate was performed and results presented in Section 7.2.7.
On decrease of the agitation rate below the standard rate of 565 rpm to 460 rpm, a decrease in the specific growth rate, biomass yield and stationary phase cell concentrations was also observed. A different stress mechanism occurring at low agitation rate such as poor mass transfer may elucidate this apparent contradiction.

7.2.1.2 Viable cell concentration

The effect of impeller speed on viable cell concentration is illustrated in Figure 7.8. Results for specific growth rates based on viable cell concentration and the viable cell fraction at the end of the growth are tabulated in Table 7.5. Figure 7.9 presents the fraction of viable cells as a function of time at different impeller speeds.

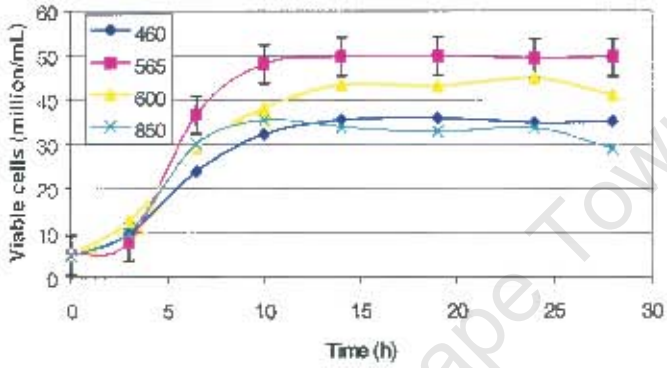

Figure 7.8 Effect of impeller speed on viable cell concentration.

Table 7.5 Specific growth rate based on viable cell concentration and viable cell fraction at the end of the growth at different impeller speeds.

Speed (rpm)	$\mu_{viable cells}$	% of viable cells at the end of the growth
460	0.074	94.7
565	0.138 (± 0.016)	83.9 (± 5.6)
600	0.125	86.2
850	0.111	77.4

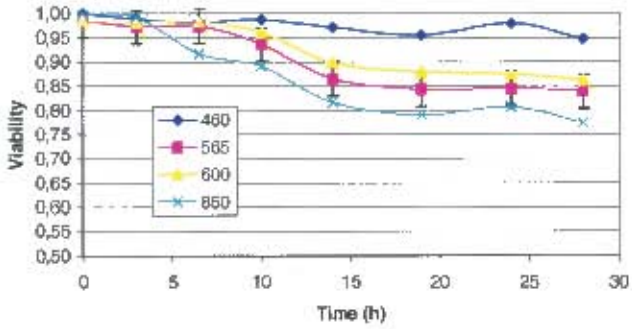

Figure 7.9 Effect of impeller speed on viability.

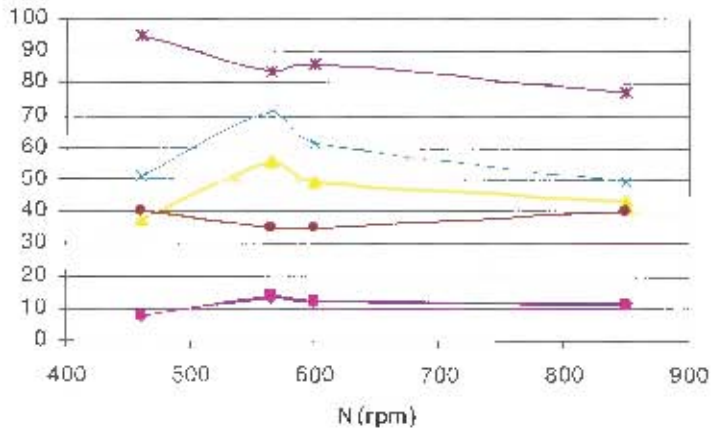

Figure 7.10 Effect of impeller speed on growth parameters. (◆ $\mu_{max\ exp}$ (h^{-1}) ×100, ⁻ $\mu_{max\ viable}$ (h^{-1}) ×100, ▲ X_{max} (10^9 cells/mL), × $Y_{X/S}$ (10^9 cells/g), ◆ t_{lag} (h) × 10, ✳final viability).

As with the total cell number, a decrease in viable cell number in the stationary phase was observed with increasing impeller speeds from 565 to 850 rpm. The specific growth rate based on viable cell number corresponded well to that reported on total cell number, decreasing with increasing agitation rate (Table 7.5). When increasing impeller speed, a decrease in the fraction of viable cells of 10 to 15% was observed with time, indicating loss of viability or cell death for the harsher speeds. These observations are consistent with the hypothesis of an increasing cell death with increasing agitation rate. The fraction of viable cells typically found under optimal growth conditions lies in the range 0.94 to 0.99. The data collected at 460 rpm were seen to conform to this pattern (Figure 7.9). Despite the decrease in cell activity and extent of growth at 460 rpm, the yeast were found to be more viable than at higher impeller speeds. A limiting nutrient or oxygen transfer rate is suggested to explain the lower growth, while cells are subjected to less hydrodynamic stress.

7.2.1.3 Budding index

Budding index profiles as a function of time for different impeller speeds are presented in Figure 7.11. The same general trends were observed for 565, 600 and 850 rpm. The budding index increased during the lag phase and exponential phase, then decreased from mid-exponential phase to stationary phase. However a sharper decrease was observed for 850 rpm than 565 or 600 rpm with the budding index remaining below 0.05 after 10h. This suggested cell activity was adversely affected by the presence of solids loading at high agitation rate. The behaviour at 460 rpm differed from previous observations. No increase was observed during the lag phase. Instead the budding index decreased with the time of growth. It is also observed that budding occurs earlier at higher agitation intensities (Figure 7.11).

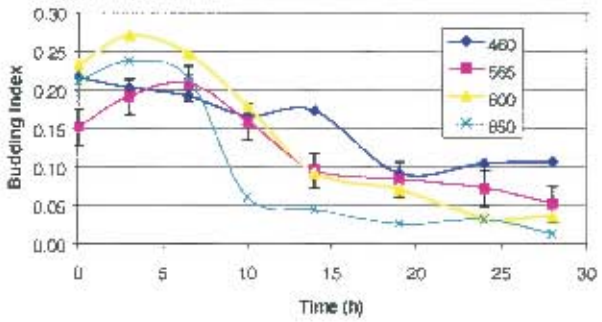

Figure 7.11 Effect of impeller speed on budding index.

7.2.2 Ethanol concentration

Ethanol production as a function of time at different impeller speeds is illustrated in Figure 7.12. Calculations for ethanol production parameters are reported in Table 7.6. From the experiment data, it was apparent that high level of agitation affected negatively the extent of product formation. This was confirmed by the decrease in both product yield on substrate and product yield on biomass with increasing impeller speed. Moreover, the ethanol concentration at 850 rpm decreased less rapidly than at 600 rpm. This may be related to the lower viability of the cells at 850 rpm.

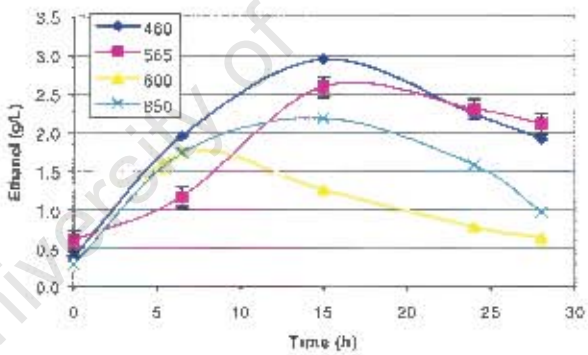

Figure 7.12 Effect of impeller speed on ethanol concentration.

Table 7.6 Differences in ethanol production parameters for different impeller speeds.

Speed (rpm)	q_p ($g.h^{-1}.10^9 cells^{-1}$)	$Y_{EtOH/s}$	$Y_{EtOH/x}$ ($g.10^9$ $cells^{-1}$)
460	0.0055	0.206	0.040
565	0.0039 (± 0.001)	0.193 (± 0.013)	0.027 (± 0.001)
600	0.0071	0.041	0 007
850	0.0062	0.089	0 016

7.2.3 TEM analysis

As detailed in Section 5.1.6, transmission electron microscopy was performed on yeast growing at 850 rpm agitation rate with 1% (v/v) solids loading. Samples were prepared at the end of the lag phase (3h), mid-exponential phase (14h) and stationary phase (28h). Preparation for TEM analyses is detailed in Appendix C. Samples were prepared in the same way as those at 0% and 1% solids loading, but at a different time, consequently slight differences in the cell wall staining may occur. Figure 7.13 shows a series of micrographs obtained at 0% (v/v) 565 rpm, 1% (v/v) 565 rpm, and 1% (v/v) 850 rpm. The influence of agitation rate on the cell wall thickness is illustrated in Figure 7.14. The data used is detailed in Appendix H.

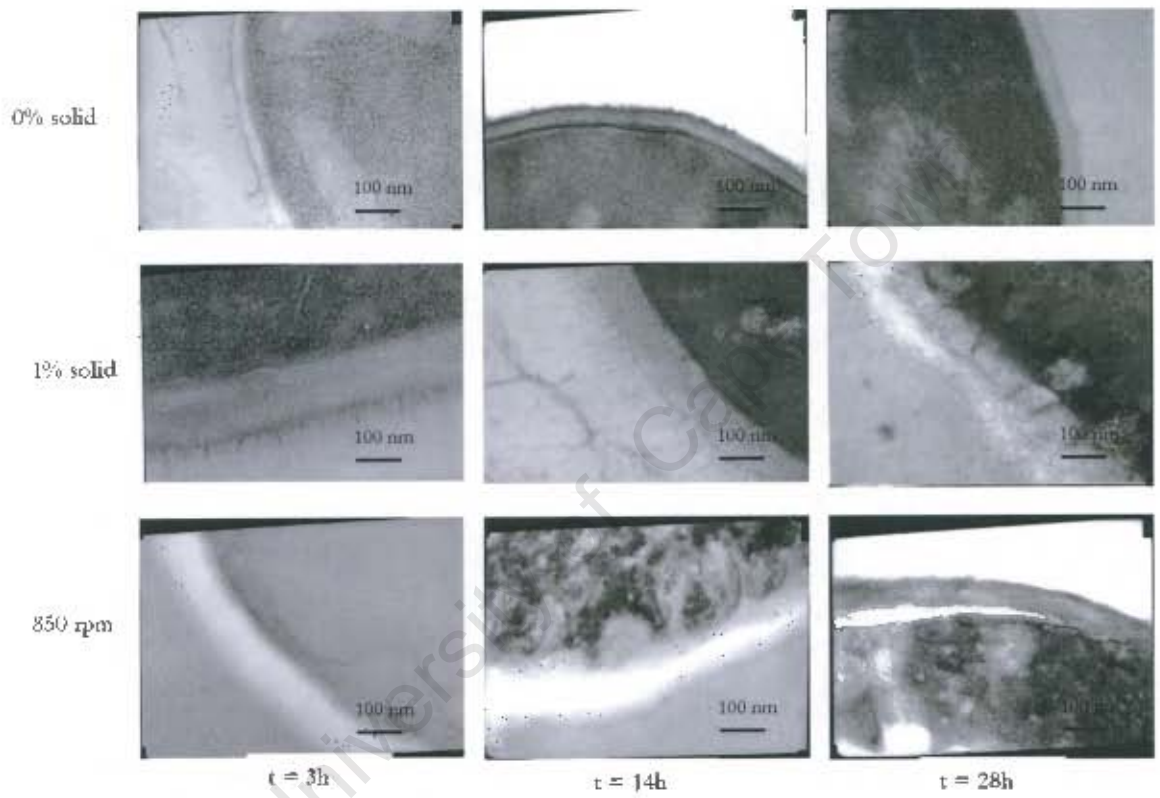

Figure 7.13 Evolution of the cell wall with time, for different hydrodynamic stress conditions.

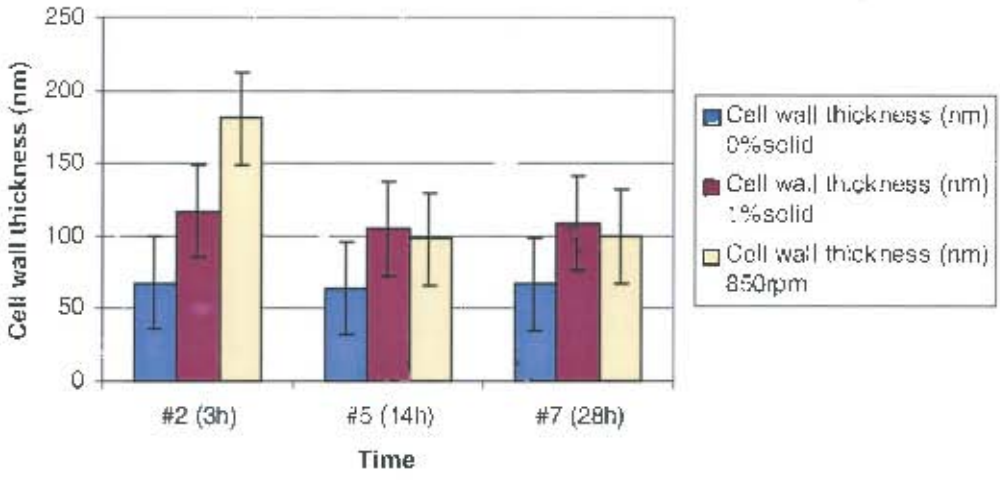

Figure 7.14 Influence of agitation rate on cell wall thickness.

The comparison of cell wall thickness for different experimental conditions clearly showed that yeast cell wall increased in thickness for a stressed system (1% (v/v) solids loading and 850 rpm). No major difference between yeast grown at 565rpm, 1% (v/v) solids concentration and those grown at 850 rpm, 1% (v/v) solids concentration was seen, except for sample 2 (3h). At the end of the lag phase, the wall thickness was significantly higher for the more stressed conditions (1% solids loading by volume, plus 850 rpm agitation rate). As mentioned in Section 5.1.6 for 1% solids loading, large differences in cell wall thickness within each sample were noticed for 565 rpm at 14h and 28h. As the ratio of thin to thick walls increased with time (and this change was more prevalent at 850 rpm and 1% solids loading than at 565 rpm and 1% solids loading), it was assumed that thin cells were dead or damaged ones (Table 7.7).

Table 7.7 Percentage of cells exhibiting thin cell walls.

Sample	565 rpm and 1% solid	850 rpm and 1% solid
#2	28.6	14.3
#5	33.3	57.1
#7	44.4	77.8

Not only did the fraction of thin walled cells increases at high agitation rate, but the number of lysed cells also increased. This confirms an increased in the death rate constant k_d, under harsher hydrodynamic conditions. Figure 7.15 gives an illustration of a cell lysed at two points. It was apparent that cell disruption involved the rupture of the cell membrane and the release of intracellular compounds into the growth medium. This supports the use of bead mills (slurry reactors at high agitation speed and high solids concentration) for the recovery of intracellular enzymes. Irregularities in the wall thickness at the higher impeller speed were also observed. They were also observed at 1% solids loading.

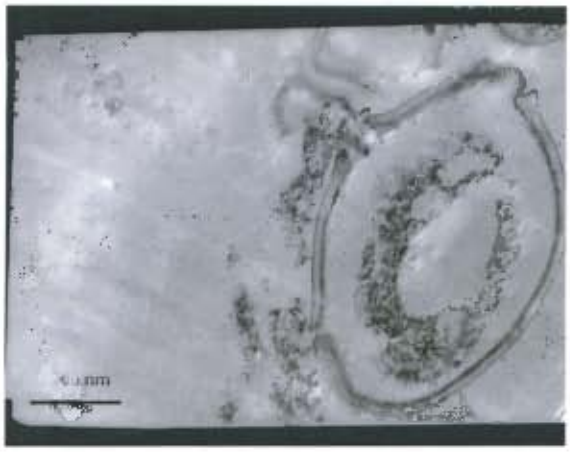

Figure 7.15 Illustration of a lysed cell (850 rpm, t = 28h).

The cell wall of *Saccharomyces cerevisiae* is an elastic structure that provides osmotic and physical protection and is responsible for the mechanical strength of the cell (Klis *et al.*, 2002). The cell wall construction is a dynamic process and the cell can make considerable adjustments to the composition and structure of its wall during the cell cycle or in response to environmental conditions such as nutrient and oxygen availability, temperature and pH (Kapteyn et al., 1999). Kapteyn *et al.* (1999) also reported that when the cell wall is defective, dramatic changes can occur in its molecular architecture pointing to the existence of cell wall repair mechanisms that compensate for cell damage. It appears that in this study that yeast cells adapted to harsh hydrodynamic conditions by increasing their wall thickness. Repair mechanisms were suggested by the irregularities in the wall thickness of stressed cells, compared to those cultured in unstressed environments. No investigation of the composition of the wall was performed, but literature suggests that β1,3-glucan and chitin play a determinant role in responding to stresses (Kapteyn *et al.*, 1999).

7.2.4 Modelling

For agitation rates higher than 565 rpm, where hydrodynamic stress is the predominant death mechanism, the death rate constant k_d was modelled as presented in Section 5.1.7. The apparent cell growth rate was postulated to be equal to the true growth rate in the absence of solid less the cell death rate.

$$\frac{dX}{dt} = \mu \cdot X \qquad \text{Equation 7.1}$$

Where

$$\mu = \mu_{max}^{*} - k_d \qquad \text{Equation 7.2}$$

And X: biomass concentration (10^6cells/mL)
t: time (h)
μ: apparent growth rate (h^{-1})
μ_{max}^{*}: true growth rate in the absence of solid (h^{-1})
k_d: cell death rate (h^{-1})

The death rate was given as the product of cell concentration and the death rate constant. k_d was expressed as a power law function of the agitation rate N:

$$k_d = cN^d \qquad \text{Equation 7.3}$$

where N is the agitation rate (rpm)
c, d are constants.

All the calculations performed to determine c and d are reported in Appendix I. The following expression was determined.

$$k_d = 0.014 \times N^{0.34} \qquad \text{Equation 7.4}$$

The model was found to correlate with experimental data with a coefficient of correlation R^2 equal to 0.87. The parity between the actual kd determined and the predicted by equation 7.2 is compared in Figure 7.16.

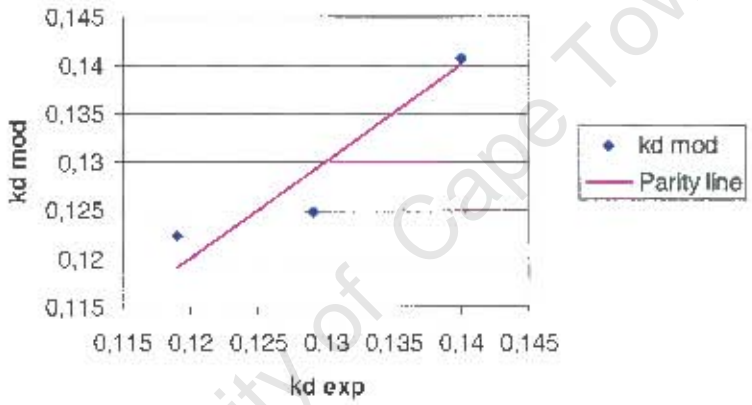

Figure 7.16 Comparison between experimental death constants ($k_{d\ exp}$) and modelled death constants ($k_{d\ mod}$).

7.2.5 Discussion and conclusions

It has been shown that the agitation rate strongly influenced the growth of *Saccharomyces cerevisiae* in a slurry reactor. An impeller speed of 565 rpm, corresponding to an impeller tip speed of 2.33 $m.s^{-1}$, was found to be the most favourable for yeast growth in the presence of 1% by volume suspended solids.

Below 565 rpm, the reduced rate and extent of growth was postulated to be due to nutrient limitation, even though cell viability remained in the reported values for unstressed systems.

Above 600 rpm (2.48 $m.s^{-1}$ tip speed), a decrease in both cell viability and activity (in terms of ($\mu_{max\ exp}$, $Y_{P/S}$, $Y_{P/X}$, q_P, stationary phase cell concentration) was noticed. This is in agreement with the literature. The effect of agitation intensity on cell damage has been investigated in the mineral bio-oxidation and animal cell-microcarrier systems. In the mineral bio-oxidation system, Hackl *et al.* (1989) found that an impeller tip speed of 5.3 $m.s^{-1}$ was detrimental to *thiobacilli*. However normal leach rates were observed when

reducing the tip speed of the Rushton turbine to 3.3 m. s^{-1}. Investigating the growth of *thiobacilli* in the presence of 2% (v/v) pyrite, Pearce (1993) determined that the cell growth was inhibited at a tip speed of 2.6 m. s^{-1} for a 6-bladed Rushton turbine, while a impeller tip speed of 1.4 m. s^{-1} was not detrimental to the cells. In the animal cell-microcarrier system, low agitation rates of 0.1 to 0.2 m. s^{-1} were found to have no effect on the cell growth, even when the inert solids concentration was increased to 2.9% (v/v) (Croughan *et al.* 1988, 1989; Lakhotia and Papoutsakis, 1992). However, at high agitation intensities of 0.3 to 0.6 m. s^{-1}, the apparent cell growth rate was reduced even at low microcarrier concentrations of 0.02% (v/v) (Croughan *et al.*, 1989). As the inert solids concentration is increased to 2.9% (v/v), a sharp decrease in the cell growth rate was observed (Croughan *et al.*, 1988). In contrast with these studies, Scholtz-Brown (1998) observed significant cell disruption of *S. cerevisiae* for the entire range of agitation intensities (439 to 900 rpm) at 10% and 20% (v/v) solid concentrations. In agreement with the study of Croughan et al. (1988), yeast disruption at these agitation speeds was magnified as the solids concentration increased. Toma *et al* (1991) considered the growth of *Brevibacterium flavum*, *S. cerevisiae* and *Trichoderma reesei* in agitated bioreactors. They determined an optimum impeller speed above which cell growth and activity decrease due to hydrodynamic stress. They theorised that the inhibition of microbial growth and productivity, although the cells were not killed as a result, was due to limited mass transfer in stagnant eddies of microscales of turbulence and shear forces damaging cell membranes. They use the term *turbohyphobiosis* to describe this effect.

Investigating the disruption of stationary phase *Saccharomyces cerevisiae* in a slurry reactor, Harrison *et al.* (2002) varied impeller speed in a range of 150 rpm to 1090 rpm, at a volume fraction of silica of 20 %. They measured the rate of release of a wall-associated enzyme (invertase), k_{RW} and the rate of release of total soluble protein (intra-cellular compound), k. At low impeller speeds (below 250 rpm), k_{RW} exceeded k while at higher agitation rates, k and k_{RW} were equal. This suggested the outer mannan layer of yeast was damaged first, higher agitation resulting in more severe cell envelope damage and rupture the cell membrane. Cell wall damage at high agitation rates was also observed in the present study, by using TEM analysis. It was furthermore demonstrated that yeast cells develop a resistance mechanism to the stress by increasing their cell wall thickness. No chemical analyses of the wall were performed, but literature suggests that an increase in β1,3-glucan and chitin may occur (Kapteyn *et al.*, 1999).

Chapter 8: Conclusions and Recommendations

8.1 CONCLUSIONS

Different industrial processes involve the growth of micro-organisms in the presence of solid particles, such as mineral bioprocessing, soil bioremediation and immobilised biocatalyst systems. In contrast, other slurry systems such as the bead mill are used to maximise cell disruption. In these systems, microbes experience a great deal of hydrodynamic stress, due to high agitation rate combined to the presence of solid particulates. Biological response to hydrodynamic stress has been quantified in terms of change in integrity, viability, metabolic rate, metabolic pathway and morphology (Logan and Dettmer, 1990; Smith *et al.*, 1990; Toma *et al.*, 1991; Illing, 1996).
Using a non-growing system of yeast and silica sand in a slurry reactor, Scholtz-Brown and Harrison (2002 a) report that the dominant mechanism of cell damage depends on interaction between particles and cells, as opposed to cell interactions with turbulent fluid eddies. Nemati and Harrison (1999, 2000) present responses of *Sulfolobus metallicus* to hydrodynamic stress, when the microbes are grown in the presence of pyrite. Their results indicate that over the range 42.5 – 202 microns (mean diameter), the particle size has no influence on the growth and activity of the cells at a solids loading of 3% pyrite. Constant values for both the specific growth rate and yields factors are obtained. When increasing solids loading from 3% to 6 and 9% (v/v) pyrite, a shift to microbial growth from exponential phase to stationary phase is observed. The lag phase is more pronounced at higher pulp densities and in the presence of larger particles. Below a critical particle size (<25 μm) and above a critical solid loading (18% pyrite), cell disruption and impaired metabolic activity are observed.

In this research project, the effects of hydrodynamic stress on the growth of *Saccharomyces cerevisiae* in a slurry reactor were investigated. Experiments were performed to study the effect of different solid sizes and solids loadings, agitation rate and agitator type, inoculum age and inoculum size. These experiments were carried out in order to ascertain the impact of hydrodynamic conditions on the physiological and morphological stress of yeast, and its ability to adapt to the stress. Critical values of hydrodynamic parameters were identified and models for the death rate constant were proposed.

Cell damage due to hydrodynamic stress can range from loss of viability to loss of integrity, via changes in metabolic rate or changes in morphology. Loss of viability can be measured through methylene blue viability staining. Budding index can also be calculated through this method, giving an indication of the physiological state of yeast. Changes in metabolic rate can be evaluated through calculations of specific growth rate, substrate utilisation rate, ethanol production rate and yield factors. Measurements of glucose and ethanol concentrations throughout the growth are therefore necessary. Yeast specific growth rate can be obtained through cell counting. Modifications in yeast morphology can be visualized by Transmission Electron Microscopy. Special interest care cell wall thickness and structure. As the cell wall represents the first barrier of defence against

physical stress, zeta potential can give important information about yeast cell surface charge. Finally, more severe hydrodynamic stress may cause loss of integrity. Cell disruption can be monitored through microscopic cell counts.

The results obtained from experiments to investigate the effect of hydrodynamic stress on the growth of *Saccharomyces cerevisiae* in a slurry reactor demonstrated that all the hydrodynamic parameters investigated in this study, solids loading, solid size, inoculum age, inoculum size, agitation rate and agitator type, play a determinant role on the growth of yeast in a slurry reactor.

Effect of solids loading on the growth
When increasing solids loading from 0 to 2% by volume, a decrease in the apparent specific growth rate occurred. This decrease in the apparent specific growth rate was combined with a decrease in viable cell fraction. Therefore the concept of increase in specific death rate was outlined. Specific death rate was considered to be a constant k_d accounting for the various hydrodynamic parameters. Thereafter the death rate constant was modelled as a power law expression accounting for solids loading. A good fit was found between experimental and calculated points. The critical solids loading above which solids concentration affected the growth ranged from 0.0% to 0.5% (v/v), depending on assay used. At 5% solids loading, no cell growth, substrate consumption or product formation were observed, indicating a complete loss of metabolic activity. The cell viability decreased to 10%.

When exposed to hydrodynamic stress, it appeared that yeast develop mechanisms to adapt and resist the stress. Increasing lag phase, i.e. increasing the period of acclimatisation, is one of these strategies. Thus when solids loading was increased from 0 to 2% (v/v), lag phase doubled. Another resistance mechanism lies in morphological changes. TEM analysis on samples at 0% and 1% solids loading revealed that the presence of solid particulates strongly affected the cell wall structure. While no influence on the cell size could be outlined, an increase in the cell wall thickness was observed with increased level of stress. Moreover the cell wall was very irregular at 1% solids loading, suggesting a repair mechanism occurred where the cell has been injured. Under adverse conditions, yeast switch from growth to maintenance. Thus, increasing solids loading, the decrease in cell growth rate with unchanged substrate consumption, illustrated by a decrease in $Y_{X/S}$ suggested that additional substrate was diverted from cell growth to provide extra energy for cell maintenance.

Effect of solid size on the growth
On increase of the particle size fraction to 850 to 1130 μm, a decrease in stationary phase concentration, cell viability, specific growth rate, magnitude of negative cell surface charge and biomass yield was noted. Performances of the smaller size fraction (465 to 600 μm) were similar to the optimal fraction in terms of growth rate, biomass yield and total cell number. However reduction in viability with time occurred.

Effect of inoculum age on the growth
When increasing inoculum age from 14 hour to 24 hour, no much difference was observed in total cell concentration. However, loss of viability, lower budding index, different substrate consumption and ethanol production were focused. Rapid glucose uptake and decrease in growth rate confirmed a shift in metabolic activity. The decrease in viable cell concentration in stationary phase and the drop in budding index suggested that death rate was not negligible.

Effect of inoculum size on the growth
No much difference was noticed from 2 to 10% inoculum size in the extent of yeast growth, glucose consumption and ethanol production. Thereafter the critical value below which the yeast activity changed was set at 2% (v/v) inoculum size. When the inoculum size was decreased to 1% (v/v), the specific growth rate and the biomass yield decreased and lag phase increased. Rapid glucose uptake and decrease in growth rate suggested a shift in metabolic activity. However yeast viability remained quite high for all experiments (above 92%). In this case, it was concluded that a decrease in inoculum size did not cause an increase in the death rate but a slow-down in yeast activity.

Effect of agitation rate on the growth
With respect to impeller speed, above 600 rpm, decrease in both viability and activity was noticed. Above 565 rpm, the death rate constant was also expressed as a power law fashion type accounting for the agitation rate N. Correlation with experimental data was not as good as for solids loading. At high agitation rate (850 rpm and 1% by volume solid loading), cell damage was observed by TEM analysis. Paradoxically, rate and extent of growth also decreased below 565 rpm, even though cell viability remained in the class reported for unstressed systems. In that case, another stress mechanism was suspected to occur in the bioreator.

Effect of agitation type on the growth
Investigating the influence of agitation type on the growth of yeast, paradoxical results were obtained. Using a pitched-blade impeller, which produces lower turbulence intensity (i.e. lower hydrodynamic stress), reduced rate and extent of growth were observed. Thereafter, a different stress was suspected to occur in the bioreactor (poor mass transfer).

There exist optimum conditions for the growth of *Saccharomyces cerevisiae* in the presence of solid particulates in a slurry reactor. Over the conditions tested, the following values were selected: 1% (v/v) or less solids loading, particle size in the range 600 – 850 μm, 10% inoculum size, agitation performed by a Rushton turbine at 565 rpm. As only two values were tested for inoculum age, no optimum could be determined. However, a 24 hour inoculum showed less resilience in terms of performance than a 14 hour inoculum.

8.2 RECOMMENDATIONS

From the data collected in this study, it has been possible to determine the response of yeast *Saccharomyces cerevisiae* to some hydrodynamic stresses. Responses have been quantified in terms of viability, metabolic rate (growth rate, glucose utilisation rate and ethanol production rate), morphology (cell wall thickness and structure), and integrity. However, no investigation has been performed on changes in metabolic pathway. Studies on the release of stress indicators such as HSP's, trehalose or glygogen, under conditions of physical stress, are recommended.

While no literature can be found about the influence of the inoculum on the growth, this work points out the importance of the inoculum state. Nevertheless, our study was limited, especially for inoculum age, where only two ages could be compared. Further work should be conducted to determine optimum inoculum age and size for the growth.

From this study, it has been shown that the cell wall plays a determinant role in adapting and resisting to hydrodynamic stress. Transmission Electron Microscopy allowed studying the cell wall morphology. However, further work should be carried out to investigate changes in the cell wall composition.

Lee (1999) mentions the phenomenon of cross-protection, where one stress effector leads to an increased tolerance to a number of different stresses. In industrial processes, micro-organisms usually experience several stresses at the same time. It is therefore valuable to investigate the effects of different stresses combined to hydrodynamic stress, for a better understanding of cross-protection mechanisms.

REFERENCES

Amory, D.E., and Rouxhet, P.G. (1988), Surface properties of *Saccharomyces cerevisiae* and *Saccharomyces carlsbergensis*: chemical composition, electrostatic charge and hydrophobicity, *Biochimica et Biophysica Acta*, **938**, 61 - 70.

Atkinson, B., Black, G.M., Lewis, P.J.S., Pinches, A. (1979), Biological particles of given size, shape, and density for use in biological reactors, *Biotechnolology and Bioengineering*, **21**, 193 – 200.

Augenstein, D.C., Sinskey, A.J., and Wang, D.I.C. (1971), Effect of shear on the death of two strains of mammalian tissue cells, *Biotechnology and Bioengineering*, **12**, 409 – 418.

Bailey, A.D. and Hansford, G.S. (1993), Oxygen mass transfer limitation of batch bio-oxidation at high solids concentration, *Minerals Engineering*, **7**, 293 – 303.

Bandyopadhyay, K.K., Ghose, T.K. (1982), Studies on immobilised *Saccharomyces cerevisiae*. III. Physiology of growth and metabolism on various supports, *Biotechnology and Bioengineering*, **24**, 805 –815.

Basson, L. (1996), Loss of yeast quality during mechanical handling in a brewery: An investigation of cropping, MSc thesis, University of Cape Town.

Bauer, C., Herzog, V., Bauer, M.F. (2001), Improved Technique for Electron Microscope Visualization of Yeast Membrane Structure, *Microscopy and Microanalysis*, **7**, 530 – 534.

Bayer, M.E.(1967), Response of cell walls of *Escherichia coli* to a sudden reduction of the environmental osmotic pressure, *Journal of Bacteriology*, **93**, 1104 – 1112.

Bayley, J.E. and Ollis, D.F. (1986), Biochemical Engineering Fundamentals, 2nd edition, McGraw-Hill, Singapore.

Beavan, M.J., Belk, D.M., Stewart, G.C., and Rose, A.H. (1979), Changes in electrophoretic mobility and lytic enzyme activity association with development of flocculating ability, *Canadian Journal of Microbiology*, **25**, 888 – 895.

Berry, D.R. (1989), Fermentation Process Development of Industrial Organisms, Marcel Dekker nc..

Birch, R.M., Walker, G.M. (2000), Influence of magnesium ions on heat shock and ethanol stress responses of *Saccharomyces cerevisiae*, *Enzyme and Microbial Technology*, **26**, 678 – 687.

Boelcke, C. (1983), *Thesis*, TU Berlin. Cited by Reuss, M. (1988), Influence of mechanical stress on the growth of *Rhizopus nigricans* in stirred bioreactors, *Chemical Engineering Technology.*, **11**, 176 – 187.

Bowen, W.R. and Cooke, R.J. (1989), Studies of *Saccharomyces cerevisiae* during fermentation, *Biotechnology and Bioengineering*, **33**, 1309 – 1318.

Bowen, W.R., Sabuni, A.M., and Ventham, T.J. (1992), Studies of the cell wall properties of *Saccharomyces cerevisiae* during fermentation, *Biotechnology and Bioengineering*, 40, 1309 – 1348.

Brookman, J.S.G. (1974), Mechanism of cell disintegration in a high pressure homogeniser, *Biotechnology and Bioengineering*, **16**, 371 – 383.

Brookman, J.S.G. (1975), Further studies on the mechanism of cell by extreme pressure extrusion, *Biotechnology and Bioengineering*, **17**, 465 - 479.

Cherry, R.S., and Papoutsakis, E.T. (1988), Physical mechanisms of cell damage in microcarrier cell culture bioreactors, *Biotechnology and Bioengineering*, **32**, 1001 - 1014.

Chisti, Y. (1999), Shear sensitivity, In Bioprocess technology: Fermentation, Biocatalysis, and Bioseparation, **5**, Flickinger, C.M. and Drew, A.S. (eds), John Wiley & Sons, 2379 - 2406.

Cimprich, P., Slavik, J., and Kotyk, A. (1995), Distribution of individual cytoplasmic pH values in a population of the yeast *Saccharomyces cerevisiae*, *FEMS Microbiology Letters*, **130**, 245 – 252.

Clarck, D.A. and Norris P.R. (1996), Oxidation of mineral sulphides by thermophilic microorganisms, *Mineral Engineering*, **9** (11), 1119 – 1125.

Croughan, M.S., Hamel, J. and Wang, D.I.C. (1987), Hydrodynamic effects on animal cells grown in microcarrier cultures, *Biotechnology and Bioengineering*, **29**, 130 – 141.

Croughan, M.S., Hamel, J. and Wang, D.I.C. (1988), Effects of microcarrier concentration in animal cell culture, *Biotechnology and Bioengineering*, **32**, 975 – 982.

Croughan, M.S. and Wang, D.I.C. (1989), Growth and Death in Overagitated Microcarrier Cell Cultures, *Biotechnology and Bioengineering*, **33**, 731 – 744.

Dengis, P.B., Nelissen, L.R., and Rouxhet, P.G. (1995), Mechanisms of yeast flocculation: comparison of top and bottom fermenting strains, *Applied and Environment Microbiology*, **61**, 718 – 728.

D'Amore, T., Crumplen, R. and Stewart, G. (1991), The involvement of trehalose in yeast stress tolerance, *Journal of Industrial Microbiology*, **7**, 191 – 196.

De Winde, J.H., Thevelein, J.M., Winderikx, J. (1997), From Feast to Famine: Adaptation to Nutrient Depletion in Yeast, In Yeast Stress Responses, Hohmann, S. and Mager, W.H. (eds), Springer, 7 – 37.

DiSpirito, A.A., Dugan, P.R. and Tuovinen, O.H. (1981), Inhibitory effects of particulate materials in growing cultures of *Thiobacillus ferroxidans*, *Biotechnology and Bioengineering*, **23**, 2761 – 2769.

Doulah, M.S. (1977), Mechanism of Disintegration of Biological Cells in Ultrasonic Cavitation, *Biotechnology and Bioengineering*, **19**, 649 - 660

Doulah, M.S., Hammond, T.H. and Brookman, J.S.G. (1975), A hydrodynamic mechanism for the disintegration of *Saccharomyces cerevisiae* in an industrial homogenizer, *Biotechnology and Bioengineering*, 17, 845 – 858.

Dunlop, E. H., and Namdev, P., K. (1994), Effect of fluid shear forces on plant cell suspensions, *Chemical Engineering Science*, 49, 2263 – 2276.

Eddy, A.A., and Rudin, A.D. (1958), Comparison of the respective electrophoric and flocculation characteristics of different strains of *Saccharomyces cerevisiae*, *Journal of the Institute of Brewing*, 64, 139 – 142.

Engler, C.R. (1985), Disruption of microbial cells, In Comprehensive Biotechnology, M. Moo-Young (ed.), 2, Pergamon Press, 305 – 324.

Escobar B., Cassas J.M., Mamani, J., Ohlbaum, R.B. (1993), Bioleaching of copper concentration with *Sulfolobus*, BC., In Biohydrometallurgical Technologies, Torma A.E, Wey J.E and Lakshmanan, editors, 195 – 204.

Felix, H. (1982), Permeabilised cells, *Analytical Biochemistry*, 120, 211 – 234.

Fish, N.M. and Lilly, M.D. (1984), The interactions between fermentation and protein recovery, *Biotechnology*, 2 (1), 623 – 627.

Fleet, G.H., and Manners, D.J. (1975), Isolation and composition of an alkali-soluble glucan from the cell walls of *Saccharomyces cerevisiae*, *Journal of General Microbiology*, 94, 180 – 186.

Fleet, G.H. (1991), in The yeasts, A.H. Rose and J.S. Harrison (eds), 4, Academic press, London.

Goldstein, A. and Lampen, J.O. (1975), Beta-D-fructofuranoside fructohydrolase from yeast, *Methods in Enzymology*, 42 (C), 504 – 511.

Golovina, I.G., Saveleva, N.D., Loginova, L.G. and Zavarzin, G.A. (1973), Lysis of *Hydrogenomas eutropha* Z-1 cells by the enzymes of *Microsmonospora vulgaris* PA II-4, *Mikrobiologiya*, 42 (5), 899 – 903.

Gray, P.P., Dunnill, P. and Lilly, M.D. (1972), The continuous-flow isolation of enzymes, In Fermentation Technology Today, (ed. G. Terui), 347 – 351, Society for Fermentation Technology, Japan.

Hackl, R.P., Wright, F.R., Gormely, L.S. (1989), Bioleaching of refractory gold ores – out of the lab and into the plant, *Process International Symposium on Biohydrometallurgy*, Wyoming, USA, 533 – 549.

Harrison, S.T.L. (1991), Bacterial cell disruption: A key unit operation in the recovery of intracellular products, *Biotechnology Advances*, 9, 217 – 240.

Harrison, S.T.L., Scholtz-Brown, N.J. and Pearce, S.A. (2002), The effect of inert particulate parameters on microbial cell disruption in a slurry bioreactor, Journal of Chemistry Technology and Biotechnology (In press).

Heslot, H., Gaillardin, C. (1991), Molecular Biology and Genetic Engineering of Yeasts, CRC Press, Boca Raton, FL. In: C.-H. Shu and S.-T. Yang (1996), Effect of particle loading on GM-CSF production by *Saccharomyces cerevisiae* in a three-phase fluidised bed reactor, *Biotechnology and Bioengineering*, **51**, 142 – 148.

Hohmann, S. (1997), Shaping Up: The Response of Yeast to Osmotic Stress, In Yeast Stress Responses, Hohmann, S. and Mager, W.H. (eds), Springer, 101 – 134.

Hohmann, S. and Mager, W.H. (1997), Yeast Stress Responses, R.G Landes Company, New York.

Hooker, B.S., Lee, J.M. and An, G. (1989), Response of plant tissue culture to a high shear environment, *Enzyme Microbial Technology*, **11**, 484 – 490.

Illing, S. (1996), An investigation of the effect of hydrodynamic stress on the growth, morphology and metabolism of microorganisms, PhD, University of Cape Town.

Illing, S., and Harrison, S.T.L. (1999), The kinetics and mechanism of *Corynebacterium glutamicum* aggregate breakup in bioreactors, *Chemical Engineering Science*, **54**, 441 – 454.

Iwahashi, H., Obuchi, K., Fujii, S. and Komatsu, Y. (1995), The correlative evidence suggesting that trehalose stabilizes membrane structure in the yeast *Saccharomyces cerevisiae*, *Cellular and Molecular Biology*, **41** (6), 763 – 769.

Jayatissa, M., and Rose, A.H. (1976), Role of wall phosphomannan in flocculation of *Saccharomyces cerevisiae*, *Journal of General Microbiology*, **96**, 165 – 174.

Joshi, J.B, Elias, C.B. and Patole, M.S. (1996), Role of hydrodynamic shear in the cultivation of animal, plant and microbial cells, *The Chemical Engineering Journal*, **62**, 121 – 141.

Kanayama, H., Sode, K., Karube, I. (1988), Continuous hydrogen evolution by immobilised recombinant *E. coli* using a bioreactor, *Biotechnology and Bioengineering*, **32**, 396 – 399.

Kapteyn, J.C., Van Den Ende, H., Klis, M. (1999), The contribution of cell wall proteins to the organization of yeast cell wall, *Biochimica et Biophysica Acta*, **1426**, 373 – 383.

Kelemen, M.V., and Sharpe, J.E.E. (1979), Controlled cell disruption: a comparison of the forces required to disrupt different micro-organisms, *Journal of Cell Science*, **35**, 431 – 441.

Kioukia, N. (1996), Influence of agitation and sparging on the growth rate and infection of insect cells in bioreactors and a comparison with hybridoma culture, *Biotechnology Progress*, **12**, 779 – 785.

Kleijntjens, R.H., van der Lans R.G.J.M. and Luyben K.C.A.M. (1992), Design of a three phase slurry reactor for soil processing, *Transitions of the Institution of Chemical Engineering*, 70 (B), 84 – 92.

Klis, F.M., Mol, P., Hellingwerf, K., Brul., S. (2002), Dynamics of cell wall structure in *Saccharomyces cerevisiae*, *FEMS Microbiology Reviews*, **738**, 1 – 8 (Article in press).

Krzystek, L., and Ledakowicz, S. (1998), Yield and maintenance coefficients in *S.cerevisae* cultures, *Journal of Chemical Technology and Biotechnology*, **71**, 197 – 208.

Kolmogorov, A.N. (1941), The local structure of turbulence in incompressible viscous fluid for very very large Reynolds numbers, *C. R. Ac. Sc.*, URSS, **30**, 301.

Kula, M.R. and Schutte, H. (1987), Purification of proteins and disruption of microbial cells, *Biotechnology Progress*, **3**, 31 – 42.

Lakhotia, S. and Papoutsakis, E.T (1992), Agitation induced cell injury in microcarrier cultures. Protective effect of viscosity is agitation intensity dependent: Experiments and modelling, *Biotechnology and Bioengineering*, **39**, 95 – 107.

Lange, H., Taillandier, P., Riba, J.P. (2001), Effect of high shear stress on microbial viability, *Journal of Chemical Technolology and Biotechnology*, **76**, 501 – 505.

Lee, M. (2000), Yeast genetic stress responses – Relevance to brewing, In *EBC Monograph: Symposium on Yeast Physiology*, **28**, 115 – 126.

Logan, B.E. and Dettmer, J.W. (1990), Increased mass transfer to microorganisms with fluid motion, *Biotechnology and Bioengineering*, **35**, 1135 – 1144.

Lowry, O.H., Roseborough, N.J., Farr, A.L. and Randall, R.J. (1951), Protein measurement with the Folin reagent, *Journal of Biology and Chemistry*, **193**, 265 – 275.

Maiorella, B., Wilke, C.R. and Blanch, H.W. (1981), Alcohol production and recovery, *Advances in Biochemistry and Engineering*, **20**, 43 – 92.

Manners, D.J., Masson, A.J. and Patterson, J.C. (1973), The structure of a β(1-3)-D-glucan from yeast cell walls, *Biochemical Journal*, **135**, 19 - 30.

Mersmann, A., Schneider, G., Voit, H., and Wenzig, E. (1990), Selection and Design of Aerobic Bioreactors, *Chemical Engineering Technology*, **13**, 357 – 370.

Michaels, J.M., Mallik, A.K., Papoutsakis, E.T. (1996), Sparging and agitation-induced injury of cultured animal cells: Do cell-to-bubble interactions in the bulk liquid injure cells?, *Biotechnology and Bioengineering*, **51**, 399 – 409.

Miller, W.M., Blanch, H.W. and Wilke, C.R. (1988), A kinetic analysis of hybridoma growth and metabolism in batch and continuous suspension culture: Effect of nutrient concentration, dilution rate and pH, *Biotechnology and Bioengineering*, **32**, 947 – 965.

Mogren, H., Lindblom, M. and Hedenskog, G. (1974), Mechanical disintegration of microorganisms in an industrial homogenizer, *Biotechnology and Bioengineering*, 16, 261 – 274.

Murray, C.R., Barich, T. and Taylor, D. (1984), The Effect of Yeast Storage Conditions on Subsequent Fermentations, *MBAA Technical Quarterly*, **21**, 189 – 194.

Napier-Munn, T.J. (1994-2001), An Introduction to Comparative Statistics and Experimental Design for Minerals Engineers, Courses Notes 2nd Edition, Version 4.12, University of Queensland.

Nemati, M. and Harrison, S.T.L. (1999), Effects of solid particles on thermophilic bioleaching of sulphide minerals, *International Biohydrometallurgy Symposium*, Spain, June 1999, 473 – 482.

Nemati, M., Lowenadler, J., and Harrison, S.T.L. (2000), Particle size effects in bioleaching of pyrite by acidophilic thermophile *Sulfolobus metallicus* (BC), *Applied Microbiology and Biotechnology*, **53**, 173 – 179.

Nemati, M. and Harrison, S.T.L. (2000), Effects of solid loading on thermophyllic bioleaching of sulphide minerals, *Journal of Chemical Technology and Biotechnology*, **75**, 526 – 532.

Nkosi, J.C. (2001), The effect of cooling on brewers' yeast quality, MSc thesis, University of Cape Town.

Norris, P.R., Burr, D.W. (1988), Bacterial oxidation of pyrite in high temperature reactors, *Biohydrometallurgy*, **87**, 532 – 536.

O'Connor, K.C. and Papoutsakis, E.T. (1992), Agitation effects on microcarrier and suspension CHO cells, *Biotechnology Techniques*, **6**, No.4, 323 – 328.

Oliver, S.G. (1991), Yeast Biotechnology, In Biotechnology Handbooks: Volume 4: *Saccharomyces*. Plenum Press, London.

Osumi, M. (1998), The ultrastructure of Yeast: Cell Wall Structure and Formation, *Micron*, **29**, No. 2/3, 207 – 233.

Pearce, S.J.A. (1993), Disruption of microorganisms due to agitation in slurries of fine particles, MSc dissertation, University of Cape Town.

Piper, P. (1997), The Yeast Heat Shock Response, In Yeast Stress Responses, Hohmann, S. and Mager, W.H. (eds), Springer, pp 75 – 93.

Plourde-Owobi, L., Durner, S., Goma, G. and François, J. (2000), Trehalose reserve in *Saccharomyces cerevisiae* : phenomenon of transport, accumaulation and role in cell viability, *International Journal of Food Microbiology*, **55**, 30 – 40.

Potgieter, T.I. (2002), Retention of fermentation biomass for extended lysine fermentations, PhD thesis, University of Cape Town.

Prokop, A., Bajpai, R.K. (1992), The sensitivity of biocatalysts to hydrodynamic shear stress, *Advances in Applied Microbiology*, **37**, 165 – 232.

Quain, D.E. (1981), The Determination of Glycogen in Yeasts, *Journal of the Institute of Brewing*, **87**, 289 – 291.

Quain, D.E. (1991), Stress and the Yeast Cell, *Fermentation*, 4 (3), 155 – 156.

Quain, D.E. and Tubb, S.R. (1982), The importance of glycogen in brewing yeast, *MBAA Technical Quarterly*, **19** (1), 29 – 33.

Rapoport, A.I., Fhrustaleva, G.M., Chammanis, G.Y. and Beker, M.E. (1995), Yeast anhydrobiosis: permeability of the plasma membrane, *Microbiology (Mikrobiologiya)*, **64**, 229 – 232.

Reed, X.B., Princz, M., Hartland, S. (1977), Second European Conference on Mixing, BHRA-Cranfield, B 1.1

Reuss, M. (1988), Influence of mechanical stress on the growth of *Rhizopus nigricans* in stirred bioreactors, *Chemical Engineering Technology.*, **11**, 176 – 187.

Rhymes, M.R., and Smart, K.A. (1996), Effect of starvation on the flocculation of ale and lager brewing yeasts, *Journal of the American Society of Brewing Chemists*, **54**, 50 – 56.

Robinson, A. (2001), Mechanical Handling Effects on Brewers' Yeast, PhD thesis, University of Cape Town.

Robinson, A., and Harrison, S.T.L. (2001), Effect of aeration in propagation on surface properties of brewers' yeast, *Applied Microbiology*, **2**, 89 – 99.

Roswear, A., Kennedy, J.F., Cabral, J.M.S. (1987), *Immobilised enzymes and cells*, Adam Hilge.

Ruis, H. (1997), Yeast Stress Response: Achievements, Goals and a Look Beyond Yeast, In Yeast Stress Responses, Hohmann, S. and Mager, W.H. (eds), Springer, pp 233 – 247.

Ryan, J.R., Loehr, R.C, Rucker, E. (1991), Bioremediation of organic contaminated soils, *Journal of Hazardous Material*, **28**, 159 - 169

Sales, K, Brandt, W.F., Rumbak, E. and Lindsey, G.C. (2000), The LEA – like Protein HSP 12 in *Saccharomyces cerevisiae* has a Plasma Membrane Location and protects Membranes Against Desiccation and Ethanol Induced Stress, *Biochimica et Biophysica Acta*, **1463**, 347 – 369.

Save, S.S., Pandit, A.B. and Joshi, J.B. (1994), Microbial cell disruption: role of cavitation, *The Chemical Engineering Journal*, **55**, B67 – B72.

Save, S.S., Pandit, A.B. and Joshi, J.B. (1997), Use of hydrodynamic cavitation for large scale microbial cell disruption, *Transactions of the Institution of Chemical Engineers*, **75C**, 41 - 49.

Saunter, N., and Thieve, D.L. (1997), in Yeast Stress Responses, Hohmann, S. and Mager, W.H. (eds), Springer, pp 171 – 175.

Scholtz-Brown, N.J. (1998), The effects of Non-biological Particulates on Microbial Cell Disruption in a Slurry Bioreactor, PhD thesis, University of Cape Town.

Scholtz-Brown, Harrison, S.T.L. (2002a), Quantifying Solids Suspension and its Effect on Microbial Cell Disruption in a Slurry Bioreactor. 1. Experimental Results, *Biotechnology and Bioengineering* (Submitted).

Scholtz-Brown, N.J., Pandit, A.B., Harrison, S.T.L. (2002), Quantifying Solids Suspension and its Effect on Microbial Cell Disruption in a Slurry Bioreactor. 2. Mathematical Models, *Biotechnology and Bioengineering* (Submitted).

Schutte, H., Kroner, K.H., Hustedt, H. and Kula, M-R. (1983), Experiences with a 20 litre industrial bead mill for the disruption of microorgansims, *Enzyme Microbiology Technology*, **5**, 143 – 148.

Schutte, H. and Kula, M-R. (1988), Analytical disruption of microorganisms in a mixer mill, *Enzyme Microbiology Technology*, **10**, 361 – 367.

Sharma, S.C. (1997), A possible role of trehalose in osmotolerance and ethanol tolerance in *Saccharomyces cerevisiae*, *FEMS Microbiology Letters*, **152**, 11 – 15.

Shu, C. and Yang, S. (1996), Effect of particle loading on GM-CSF production by *Saccharomyces cerevisiae* in a three-phase fluidized bed bioreactor, *Biotechnology and Bioengineering*, **51**, 229 – 236.

Shuler, M.L. and Kargi, F. (1992), How cells grow, In Bioprocess Engineering Basic Concepts, Prentice Hall, New Jersey.

Siderius, M. and Mager, W.H. (1997), General Stress Response: In Search of a Common Denominator, In Yeast Stress Responses, Hohmann, S. and Mager, W.H. (eds), Springer, 171 – 175.

Sissing, A. (2002), An Investigation into the effect of solid particulate phase on the bioleaching performance of *Sulfolobus metallicus*, MSc dissertation, University of Cape Town.

Slaughter, J.C. and Nomura, T. (1992a), Intracellular Glycogen and trehalose Contents as predictors of Yeast Viability, *Enzyme Microbiology Technology*, **14**, 64 – 67.

Slaughter, J.C. and Nomura, T. (1992b), Activity of the Vacuolar proteases of Yeast and the Significance of the Cytosolic protease Inhibitors during the Post-Fermentation Decline Phase, *Journal of the Institute of Brewing*, **98**, 335 – 338.

Smart, K.A., Boulton, C.A., Hinchliffe, E. and Molzahn, S. (1995), Effect of physiological stress on the surface properties of brewing yeasts, *Journal of the American Society of Brewing Chemists*, **53**, 33 – 38.

Smart, K.A., Chambers, K.M., Lambert, I., Jenkins, C. and Smart, C.A. (1999), Use of methylene violet staining procedures to determine yeast viability and vitality, *Journal of the American Society of Brewing Chemists*, **57**, 18 – 23.

Smith, J.J., Lilly, M.D. and Fox, R.I (1990), The effect of agitation on the morphology and penicillin production of *Penicillium chrysogenum*, *Biotechnology and Bioengineering*, **35**, 1011 – 1023.

Smith, A.E., Moxham, K.E., and Middelberg, A.P.J (2000a), Wall material properties of yeast cells. Part II. Analysis, *Chemical Engineering Science*, **55**, 2043 – 2053.

Smith, A.E., Zhang, Z. and Thomas, C.R. (2000b), Wall material properties of yeast cells. Part 1. Cell measurements and compression experiments, *Chemical Engineering Science*, **55**, 2031 – 2041.

Smith, A.E., Zhang, Z., Thomas, C.R., Moxham, K.E. and Middelberg, A.P. (2000), The mechanical properties of *Saccharomyces cerevisie*, *PNAS*, **97**, 9871 –9874.

Srinorakutara, T. (1998), Determination of Yeast Cell Wall Thickness and Cell Diameter Using New Methods, *Journal of Fermentation and Bioengineering*, Vol.86, **3**, 253 – 260.

Stegmann, P., Goede, J.F., Ginster, M. (1994), Implementing bioremediation – ongoing improvements in an effective solution to coping with hydrocarbon wastes, *Chemical Technology*, March/April 1994, 22 – 27.

Tamura, K, Kishido, T. and Okada, S. (1998), *Biotechnology Letters*, 20 (12), 1167 – 1169, Cited by Lee, M. (2000), Yeast genetic stress responses – Relevance to brewing, In *EBC Monograph: Symposium on Yeast Physiology*, **28**, 115 – 126.

Toma, M.K., Ruklisha, M.P., Vanags, J.J., Zeltina, M.O., Leite, M.P, Galinina, N.I., Viesturs, U.E. and Tengerdy, R.P (1991), Inhibition of microbial growth and metabolism by excess turbulence, *Biotechnology and Bioengineering*, **38**, 552 – 556.

Thomas, C.R. (1993), Shear effects on cells in bioreactors, In Processing of solid-liquid suspensions, (P. Ayazi Shamlou Ed.), Butterworth-Heinemann Ltd, London.

Tyagi, R.D., Gupta, S.K., Chand, S. (1992), Process engineering studies on continuous ethanol production by immobilised *S. cerevisiae*, *Process Biochemistry*, **27**, 23 – 32.

Vrana, D., Votruba, J., and Placek, J. (1982), Age related changes in the physiological state of budding yeast cells, *Experimental Cell. Research*, **138**, 57 – 62.

Walker, G.M. (1998), Yeast Physiology and Biotechnology, John Wiley and Sons, 1st ed, 12 – 200.

Wase, D.A.J., and Patel, Y.R. (1985), Variations in the Volumes of Microbial Cells with Changes in the Agitation Rates of Chemostat Cultures, *Journal of General Microbiology*, **131**, 725 – 736.

Webb, C., Dervakos, G. (1996), Studies in Viable Cell Immobilisation, Academic Press.

Wiemken, A. (1990), Trehalose in Yeast, Stress Protectant Rather than Reserve Carbohydrate, *Antonie van Leeuwenhoek*, **58**, 209 – 217.

Yang, J.D. and Wang, N.S. (1992), Cell inactivation in the presence of sparging and mechanical agitation, *Biotechnology and Bioengineering*, **40**, 806 – 816.

Zhang, Z., *et al.* (1995), Preliminary modelling of animal cell disruption in a closed stirred tank, *The 1995 Icheme research event / First european conference*, 1088 – 1090.

Zlotnick, H., Fernandez, M.P., Bowers, B., and Cabib, E. (1984), *Saccharomyces cerevisiae* mannoproteins form in external cell wall layer that determines wall porosity, *Journal of Bacteriology*, **159**, 1018 – 1026.

APPENDIX A : Composition of the media

Composition of agar slopes

Yeast were kept on agar slopes at 4°C for up to six months after which they were transferred to new slopes to avoid loss of viability. These slopes were used to inoculate the pre-inoculum for all experiments.

Table A.1 Composition of agar slopes

Components	Concentration (g/L)
Glucose	10 g/L
Peptone biological	5g/L
Agar	15 g/L
Malt extract	3g/L
Yeast extract	3g/L

Pre-inoculum Growth Medium

The pre-inoculum growth medium was prepared in a 100 mL shake flask, autoclaved and stored for use. The pre-inoculum growth medium consisted of a YM growth medium.

The pre-inoculum consisted of 15 mL of the solution mentioned below in table , in which a scraping from the stock yeast culture was grown at 30 °C for 24 hours in a shaker oven.

Table A.2 Composition of the pre-inoculum growth medium

Components	Concentration (g/100 ml) (made up with distilled water)
Glucose (Dextrose)	1 (10 g/L)
Biological Peptone	0.5
Yeast extract powder	0.3
Malt extract powder	0.3

Inoculum and Reactor Growth Media

The inoculum and reaction media were prepared in three parts. As the presence of salts in the medium might have led to caramelisation of the glucose, these components had to be autoclaved separately. Then the two solutions were mixed under aseptic conditions in a laminar air flow cabinet. Because of their heat labile properties, the vitamins could not be autoclaved. Therefore they were added to the autoclaved solutions by filter-sterilisation in the laminar air flow cabinet.

The inoculum consisted of :

- 60 mL of the glucose solution
- 60 mL of the salt solution
- 15 mL of the vitamin solution
- + pre-inoculum (15 mL)

The inoculum was grown at 30°C in a shaken oven for 14 hours.

The reaction medium consisted of :

- 800 mL of the glucose solution
- 500 mL of the salt solution
- 50 mL of the vitamin solution
- + inoculum (150 mL)

Table A.3 Composition of the inoculum and reactor growth media

	Inoculum Medium	**Reaction Medium**
Solutions	Mass (g) (made up with distilled water)	Mass (g) (made up with distilled water)
1. Glucose Solution	In 500 mL	In 1800 mL
Glucose (Dextrose)	13.35 (26.7 g/L)	36 (20 g/L)
Antifoam 289		2 ml to each reactor before autoclaving
2. Salt Solution	In 500 mL	In 1500mL
$(NH_4)_2SO_4$	2.59	21.03 (in 1500 ml)
KH_2PO_4	0.77	6.21
$MgSO_4,7H_2O$	0.275	2.22
$CaCl_2$	0.065	0.54
H_3BO_4	0.005	0.042
$CoSO_4,7H_2O$	0.0005	0.0042
$CuSO_4,5H_2O$	0.002	0.0162
$ZnSO_4,7H_2O$	0.005	0.0405
$MnSO_4$, H_2O	0.015	0.0123
KI	0.0005	0.042
$FeSO_4,7H_2O$	0.001	0.0081
$Al_2(SO_4)_3,18H_2O$	0.0015	0.0123
Buffer NaAcetate/Acetic Acid		35 mL
3. Vitamins	In 150 mL	In 150 mL
Biotin	0.0005	0.005
Panothenate	0.0025	0.0252
Myo-Inositol	0.0507	0.5070
Thyamine	0.0020	0.0204
Pyridoxine	0.0025	0.0252
p-Aminobenzoic Acid	0.0004	0.0042
Nicotinic Acid	0.0020	0.0204

APPENDIX B : Cell-Culture Experimental Rig

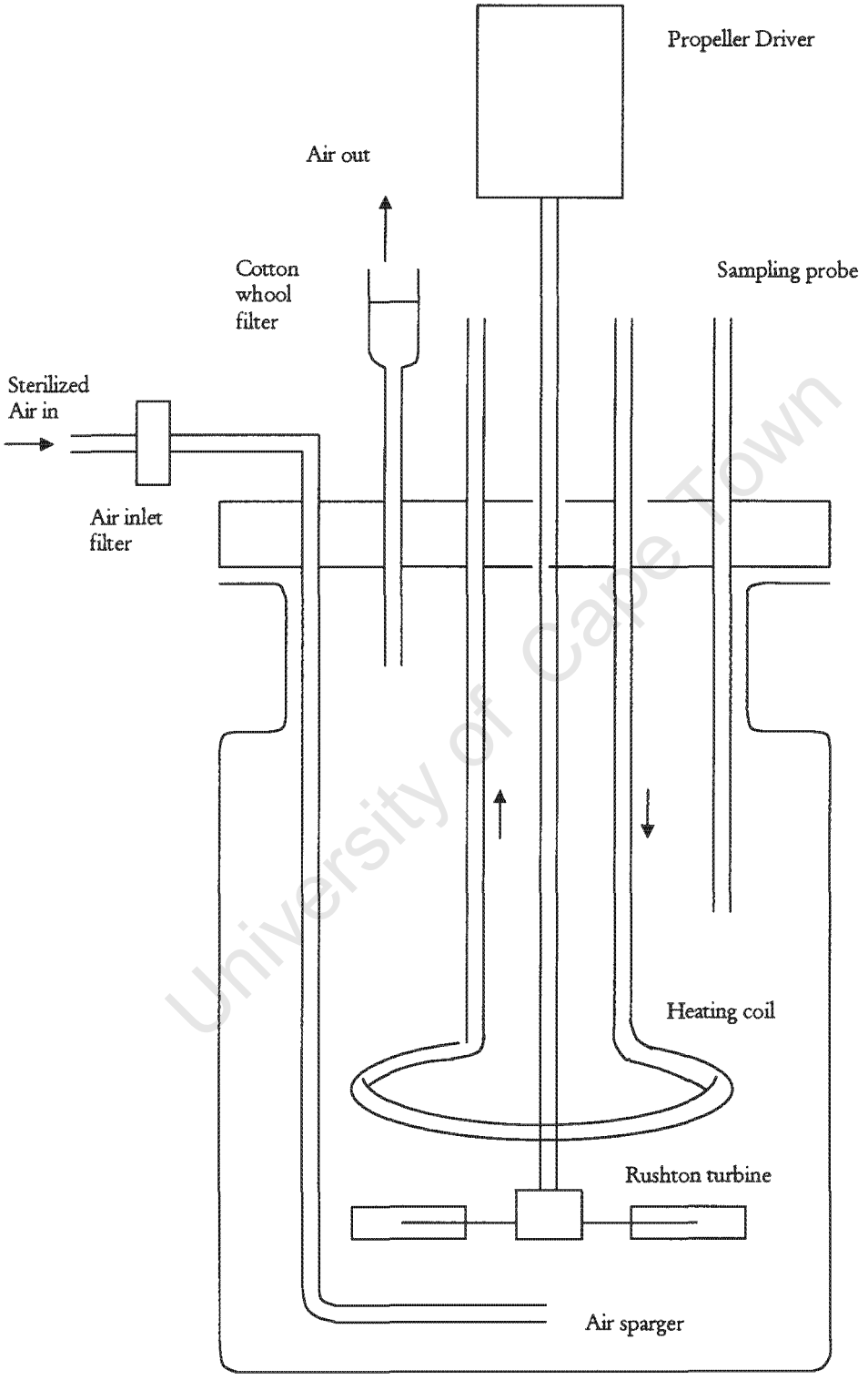

Figure B.1 : Schematic representation of the experimental rig

Geometry of cell-culture experimental rig

The symbols used on the diagram indicate the following :

Vessel
H : Liquid height in the tank (prior to agitation)
T : Tank diameter
B : Baffle width
C : Distance of impeller blade from tank bottom

Impeller
D : Impeller blade diameter
W : Impeller paddle height
L : Impeller paddle width
H_u : Impeller disk diameter

Table B.1 Dimensions of cell-culture experimental rig

Dimensions (mm)		Dimension ratio	
T	130		
H	115	H/T	0.89
B	15	B/T	0.12
C	38	C/T	0.29
D	79	D/T	0.61
L	19.5	L/D	0.25
W	15	W/D	0.19
H_u	55	H_u/D	0.70

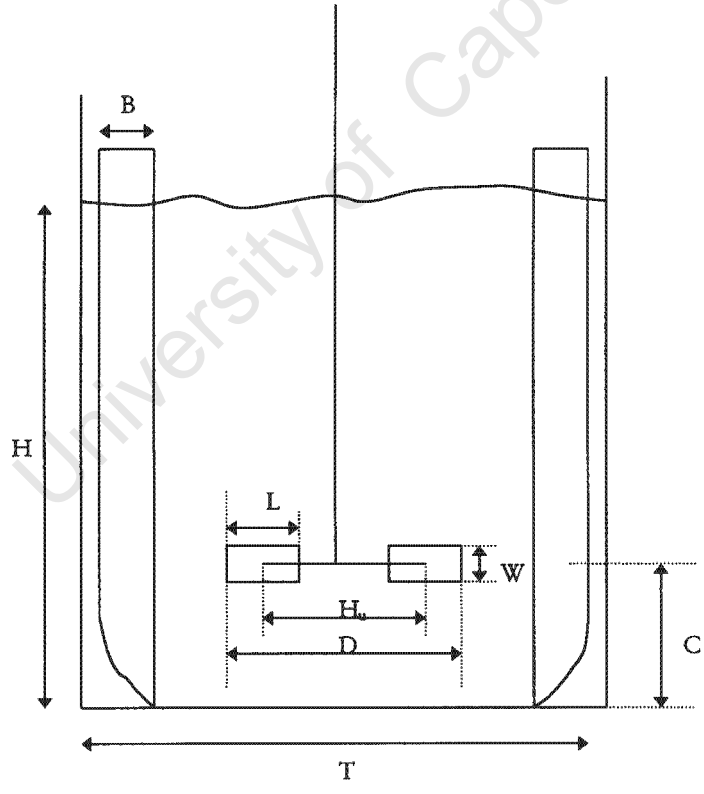

Figure B.2 Geometry of cell-culture experimental rig

APPENDIX C: Description of Analytical procedures

Cell Culture Sampling Procedure

Samples from the reactor were taken at various time intervals by means of the sampling port and a syringe under sterile conditions, to prevent contamination in the bioreactor. The sampling port was flamed before the syringe was connected.
An initial 5 mL sample first had to be removed from the reactor, as the sample line might have contained liquid from the previous sample. An actual reactor sample of 7 mL was then taken.

The bioreactor sample:

- 1 mL of the actual bioreactor sample was pipetted into a second sampling vial and taken for microscopic analysis.
- 3 mL were used for absorbance measurements. From these 3 mL of culture, 2 samples of 1 mL were taken afterwards for zeta potential analysis.
- 3 separate samples of 1 mL each were taken for cell dry mass determinations.

The waste sample:

- The waste sample initially taken was used to get an approximation of the pH in the bioreactor. This was done to check that the pH value is not critical in this investigation.

1- Absorbance

3 mL of the broth were used for absorbance measurements. Absorbance was read at 660 nm with a UV-Vis spectrophotometer, using a cuvette filled with distilled water as a blank.

2- pH measurement

Apparatus

- pH meter
- distilled water
- 5 mL sample bottle

Method

The dead volume taken from the reactor was placed in the 5 mL sample bottle. The ph meter was calibrated for a pH range of 4-7 before use.

3- Microscope Cell Counting

In order to determine the population size of the yeast culture in the reactor, a 1 mL sample was taken at various times during the fermentation. This sample was used to determine the approximate number of yeast cells present in the reactor. The number of cells was then used to determine the growth phase of the culture in the reactor.

Apparatus:

- Sample vials (for sample and for dilution, if necessary)
- Microscope (40 x magnification setting)
- Counting Chamber (0.01 mm x 0.0025 mm^2)
- 1 mL pipette (Gilson pipetman P1000)
- 0.1 mL pipette (Gilson pipetman P100)

Chemicals:

- Modified Ringer Salt solution containing methylblue

[0.25 g/L methylblue; 9.00 g/L NaCl; 0.42 g/L KCl; 0.24 g/L $CaCl_2$; 0.02 g/L $NaHCO_3$; 10.00 g/L glucose in distilled water]

Method

1- 1 mL of the bioreactor sample was extracted using a pipette and inserted into a sample vial.
2- Depending on the cell concentration, appropriate dilution of the sample was done using distilled water. (For initial counts, dilution was not required, while a 13 times dilution was required when the cell growth reached the steady state).
3- Methylblue was added to the diluted sample with a ratio 1/1.
4- A sample of the mixture was inserted into the counting chamber slide and examined under a microscope (employing a 40 times magnification).
5- As many grids as necessary were counted so as no fewer than 100 cells were counted in the entire counting chamber, and no more than 30 cells were counted per block.

The living cells show up as clear oblong structures, the dead cells as deep blue oblong structures and lysed cells as blue coloured cells with a release of a blue coloured substance from one or more positions from the cell membrane.

Budding cells are visible as living cells with a small bud extruding from the cell membrane. The cell is considered to be budding if the bud is less than half the size of the mother cell.

The number of cells per mL is calculated as:

$$Cells/mL = \frac{Total \cdot cells \cdot counted \times dilution \cdot factor \times grid \cdot factor}{Number \cdot of \cdot grids \cdot counted}$$

Where Total cells counted: actual cell count (including living, dead and lysed cells)
Number of grids counted: accrual grids used to count cells
Grid factor: 250000
Dilution factor: ranging from 2 to 13

4- Viability

Apparatus and Chemicals
Same as Microscope Cell Counting

Method
Same as Microscope Cell Counting

Dead cells (appearing in stained dark blue) are counted
Viability is defined as:

$$Viability = \frac{Total \cdot cells - Dead \cdot cells}{Total \cdot cells}$$

5- Budding Index

Apparatus and Chemicals
Same as Microscope Cell Counting

Method
Same as Microscope Cell Counting

Budding cells are counted as cells with protrusion.
The budding Index is defined as:

$$Budding \cdot Index = \frac{Budding \cdot cells}{Total \cdot cells \cdot counted}$$

6- Dry Weight Determination

Apparatus:

- Three dry weight Eppendorf tubes
- *Mikro* Centrifuge
- *Vortex Genie* mixer
- Three Eppendorf tubes
- 1 mL pipetman
- 4 decimal place balance

Method

1- Centrifuge the 3 dry weight tubes for 5 minutes at 100% power (15000 rpm).
2- Decant the supernatant liquor into the 3 Eppendorf tubes and freeze (these samples will be used for glucose and ethanol determinations as described later).
3- Add 1 mL of distilled water to each dry weight tube and re-suspend the centrifuged yeast using the *Vortex Genie* mixer.
4- Re-centrifuge the tubes and discard the supernatant. Repeat 3 times.
5- Dry the centrifuged tubes for 48 hours in an oven at 80°C for 48 hours.
6- Weigh the tubes. The dry cell mass is the difference between the tubes plus the dry yeast cell contents and the tubes alone.

7- Zeta Potential determination

Apparatus

- Eppendorf tubes
- *Mikro* Centrifuge
- *Vortex Genie* mixer
- Sample bottles
- 5 mL syringe
- 1 mL pipetman
- *Malvern Zetasizer* apparatus for zeta potential determination

Chemicals

- Glacial acetic acid/sodium acetate buffer solution (pH 4)

Method

1- Wash the yeast sample by centrifuging and re-suspending in de-ionised water as for Dry mass determination. Repeat the process 3 times, discarding the supernatant each time.
2- Add 4 mL of buffer to 2 sample bottles.
3- Add a small quantity of washed yeast (re-suspended in the buffer) to each buffer solution, and agitate.
4- "Blank" the *Zetasizer* by running the sodium acetate/acetic acid buffer before the samples are analysed.
5- Use the *Malvern Zetasizer* to read the zeta potential of the yeast. The samples are analysed twice.

6- Specify 5 measurements for each sample for greater accuracy.

8- Glucose determination

The glucose concentration was determined using the supernatants obtained during the procedure for obtaining dry mass and zeta potential. The *Glucose/GOD-Perid* kit (Boehringer Mannheim GmbH Diagnostica, catalogue No. 124.036) method was used.

Apparatus

- 0.1, 0.2, and 5 mL pipetmen
- Test tubes
- *Vortex Genie* mixer
- Disposable plastic cuvettes
- UV-VIS spectrophotometer

Chemicals

- *Glucose/GOD-Perid* kit Bottle 2: Buffer, enzymes and chromogen. Dissolve contents in 1L of distilled water.

Standard calibration curve

- The 0.1 g of glucose was dissolved in 100 mL distilled water.
- The 1 mL pipetman was used to measure out 0 – 0.7 mL of glucose solution into 8 test tubes. Each of these was done in triplicate.
- The total volumes of the tubes were made up to 1 mL using distilled water.
- Prepare the standard by pipetting 0.12 mL of each solution of glucose and 3 mL bottle 2 solution into a test tube.
- Absorbance was measured at 620 nm.
- A calibration curve was obtained between absorbance and glucose concentration.

Method

1- Dilute cell supernatants 100 times by adding 0.05 mL supernatant to 4.95 mL distilled water.
2- Prepare the sample by pipetting 0.12 mL diluted supernatant and 3 mL bottle 2 solution into a test tube.
3- Mix all samples using the Vortex genie. Cover with aluminium foil and incubate in a dark place at room temperature for 25 minutes.
4- Measure the absorbance of the samples at 620 nm. A cuvette filled with distilled water was used as a blank.
   All experiments were performed in triplicate.

9- Ethanol determination

Ethanol was measured by gas chromatography. Ethanol concentration was determined using a Perkin Elmer Autosystem fitted with a flame ionisation detector. A stainless still column (25m x 0.25mm) packed with 100% methyl silicone was used. Column temperature was from 40 to 120°C at a rate of 30°C per minute using helium as carrier gas at 20 mL/min. The detector and injector temperatures were set at 250°C. Butanol was used as the internal standard.

10- TEM Analysis

TEM Analysis was performed in order to determine if any noticeable changes occur in the cell wall structure/thickness during the course of the experimental run.

10- 1 Fixation

1- Yeast cells were pelleted by centrifugation and resuspended in fixative. They were left in fixative overnight at 4 °C.

Fixative: 2% formaldehyde + 2% glutaraldehyde in PBS (Phosphate buffered saline).

2- Cells were washed with PBS.

3- They were embedded in 1% agarose. This was achieved by mixing an equal volume of suspended yeast cells in PBS with 2% agarose at 37°C. The mixture was cooled immediately thus causing the agarose to set (harden).

4- The agarose blocks containing the yeast cells were cut into small cubes – 1 mm x 1 mm x 1 mm and infiltrated with cryoprotectant (2.3 M sucrose in PBS).

10-2 Freeze substitution fixation

5- The small cubes were placed on the surface of a copper grid and rapidly frozen at –170°C in liquid ethane using the Reichert KF80.

6- The specimens were transferred to absolute acetone at -80°C in the Automatic Freeze-substitution machine (LEICA EM AFS) for 6 hours.

7- The acetone was replaced with 4% osmium tetroxide (dissolved in acetone). The samples were left in the machine for 3 days.

8- The specimens were then warmed gradually by 1°C per hour.

9- At 4°C, the specimens were washed several times with acetone. Thereafter the specimen were warmed to 20°C and removed from the freeze–substitution chamber.

10- Once they were warmed to room temperature, samples were removed from disks and washed with acetone.

11- Cells were progressively embedded in resin: 1:2 Spurrs resin:acetone (overnight), 2:1 (overnight), 100% Spurrs resin (6 hours) and 100% resin (overnight).

12- Samples embedded in resin and baked in an oven at 60°C for 24 hours.

10-3 Sectioning

13- After polymerisation, the resin surrounding the yeast was cut off with a razor blade.

14- The embedded specimen were sectioned using ultramicrotome.

15- Thin sections (100 nm) were collected on copper grids.

16- The sections were stained and protected with uranyl acetate and lead citrate.

10-4 Electron microscopy

17- The specimens were viewed on a JEOL 200CX transmission electron microscope and photographed.

Reproducibility 0%: comparison between Run 3, Run 4 and Run 13

Agitation rate : 565 rpm
No solid.

	Cells (million/mL)				Viable cells				Budding index				Viability				Absorbance			
Time (hrs)	Run 3	Run 4	Run13	Mean	Run 3	Run 4	Run13	Mean	Run 3	Run 4	Run13	Mean	Run 3	Run 4	Run13	Mean	Run 3	Run 4	Run13	Mean
0	7.7	6.1	5.5	6.5	7.7	5.4	5.3	6.1	0.130	0.150	0.222	0.167	1.000	0.980	0.965	0.982	0.3408	0.4575	0.5508	0.4497
3	12.9	8.0	13.9	11.6	12.9	7.5	13.7	11.4	0.223	0.188	0.272	0.228	1.000	0.971	0.984	0.985	0.473	0.649	0.7249	0.6156
6.5	19.6	24.4	32.8	25.6	19.6	24.0	32.6	25.4	0.194	0.235	0.229	0.219	1.000	0.989	0.993	0.994	0.972	1.287	1.2903	1.1831
10	36.5	49.5	52.4	46.1	35.9	48.9	51.6	45.5	0.159	0.151	0.138	0.149	0.996	0.995	0.986	0.993	1.7225	1.899	1.9897	1.8704
14	48.7	59.4	56.7	54.9	47.9	59.1	55.6	54.2	0.147	0.131	0.115	0.131	0.996	1.000	0.981	0.992	1.9805	1.9835	2.0999	2.0213
19	54.3	63.0	56.0	57.7	50.7	62.7	54.9	56.1	0.146	0.090	0.110	0.115	0.985	1.000	0.981	0.989	2.1804	2.1952	2.0999	2.1585
24	60.8	61.7	57.4	60.0	58.6	60.3	56.7	58.6	0.094	0.097	0.113	0.102	0.996	0.995	0.987	0.993	2.2217	2.2452	2.2999	2.2556
27.5	59.7	64.7	58.1	60.8	57.8	63.7	57.8	59.8	0.091	0.088	0.081	0.087	0.982	0.995	0.994	0.990	2.2189	2.1967	2.1043	2.1733

	Dry mass (g/L)				Zeta potential (mV)				Glucose (g/L)			
Time (hrs)	Run 3	Run 4	Run13	Mean	Run 3	Run 4	Run13	Mean	Run 3	Run 4	Run13	Mean
0	0.1	0	0.0	0.0	-5.8	-6.3		-6.05	6.90	8.7227	9.07	8.23
3	0.4	0	0.6	0.3	-7.2	-7.8		-7.50	6.72	7.64	7.69	7.35
6.5	0.7	0.1	1.7	0.8	-7	-7.85		-7.43	4.15	4.00	2.86	3.67
10	1	0.6	1.8	1.1	-6.75	-6.15		-6.45	2.21	0.29	0.48	0.99
14	1.7	1.1	2.0	1.6	-7.2	-5.95		-6.58	0.49	0.12	0.48	0.37
19	1.9	1.5	2.0	1.8	-7.4	-6.8		-7.10	0.25	0.18	0.42	0.28
24	2.5	1.6	2.0	2.0	-7.85	-7.15		-7.50	0.29	0.18	0.38	0.28
27.5	2.4	1.9	1.8	2.0	-7.95	-6.8		-7.38	0.17	0.17	0.44	0.26

	Ethanol (g/L)			
Time (hr)	Run 3	Run 4	Run13	Mean
0	0.42	0.51		0.46
6.5	1.45	1.06		1.26
14	2.98	2.90		2.94
28	2.83	2.70		2.76
48	2.17	2.39		2.28

Reproducibility 1%: comparison between Run 5, Run 5' and Run 13'

Agitation rate : 565 rpm
1% solid

	Cells (million/mL)				Viable cells				Budding index				Viability				Absorbance			
Time (hrs)	Run 5	Run 5'	Run 13'	Mean	Run 5	Run 5'	Run 13'	Mean	Run 5	Run 5'	Run 13'	Mean	Run 5	Run 5'	Run 13'	Mean	Run 5	Run 5'	Run 13'	Mean
0	4.7	4.9	5.7	5.1	4.7	4.9	5.6	5.1	0.146	0.150	0.156	0.151	1.000	1.000	0.986	0.995	0.5198	0.6229	0.5108	0.5512
3	6.5	6.8	11.3	8.2	6.5	6.8	10.8	8.0	0.173	0.188	0.211	0.190	1.000	1.000	0.973	0.991	0.6783	0.8112	0.9786	0.8227
6.5	32.7	34.2	45.3	37.4	32.5	33.8	43.6	36.6	0.204	0.200	0.219	0.208	1.000	1.000	0.974	0.991	1.095	1.5459	1.6873	1.4427
10	52.0	47.3	55.9	51.7	46.3	46.3	51.4	48.0	0.132	0.175	0.169	0.158	0.979	0.984	0.936	0.966	1.7656	2.1917	2.0816	2.0130
14	53.3	53.8	58.9	55.3	49.7	49.8	49.5	49.7	0.112	0.056	0.117	0.095	0.968	0.961	0.865	0.931	2.1904	2.3501	2.3703	2.3036
19	57.8	56.6	57.4	57.2	51.3	51.0	47.3	49.9	0.093	0.075	0.082	0.083	0.967	0.960	0.843	0.923	2.2991	2.4278	2.4206	2.3825
24	53.4	55.6	56.0	55.0	49.8	51.4	46.6	49.3	0.088	0.076	0.052	0.072	0.966	0.965	0.845	0.925	2.3867	2.523	2.4554	2.4550
28	56.0	58.2	53.8	56.0	50.9	53.6	44.1	49.5	0.065	0.056	0.034	0.051	0.955	0.966	0.839	0.920	2.4489	2.5509	2.4649	2.4882

	Dry mass (g/L)				Zeta potential (mV)				Glucose (g/L)				Ethanol (g/L)			
Time (hrs)	Run 5	Run 5'	Run 13'	Mean	Run 5	Run 5'	Run 13'	Mean	Run 5	Run 5'	Run 13'	Mean	Run 5	Run 5'	Run 13'	Mean
0	0.03	0.47	0.23	0.24	-10.15	-8.4		-9.28	8.91	8.06	8.98	8.65	0.67	0.53		0.60
3	0.17	1.03	0.43	0.54	-9.6	-9.3		-9.45	9.03	8.26	8.46	8.59	0.80	0.68		0.74
6.5	0.40	1.03	1.47	0.97	-9.45	-9.1		-9.28	8.30	7.23	6.17	7.23	1.11	1.23		1.17
10	0.80	1.60	1.63	1.34	-8.85	-8.6		-8.73	3.93	2.84	2.88	3.22	1.82	2.10		1.96
14	1.73	2.20	1.77	1.90	-8.2	-7.9		-8.05	1.22	0.95	0.58	0.91	2.65	2.53		2.59
19	1.97	2.57	1.73	2.09	-6.75	-7.1		-6.93	1.09	0.85	0.58	0.84	2.49	2.29		2.39
24	2.17	2.23	1.90	2.10	-6.8	-6.35		-6.58	0.95	1.03	0.61	0.86	2.38	2.21		2.30
28	2.33	2.03	1.97	2.11	-5.65	-6.2		-5.93	1.08	0.96	0.43	0.82	2.19	2.03		2.11

Sample	Time	0 %	1 %
1	**14**	48.7	53.3
2		59.4	53.8
3		56.7	58.9
1	**19**	54.3	57.8
2		63.0	56.6
3		56.0	57.4
1	**24**	60.8	53.4
2		61.7	55.6
3		57.4	56.0
1	**28**	59.7	56.0
2		64.7	58.2
3		58.1	53.8

ANOVA

Source of Variation	*SS*	*df*	*MS*	*F*	*P-value*	*F crit*
Sample	35.6144	3	11.87147	1.10966	0.374246	3.238867
Columns	37.0091	1	37.0091	3.459346	0.08136	4.493998
Interaction	36.08139	3	12.02713	1.12421	0.368769	3.238867
Within	171.1727	16	10.69829			
Total	279.8776	23				

Standard error 3.270824

Difference

Cells (million/mL)						
Time (h)	0%	0.5%	1%	1.5%	2%	5%
0.0	6.5	5.9	5.1	5.3	4.7	5.4
3.0	11.6	11.3	8.2	7.0	6.9	4.8
6.5	25.6	30.8	37.4	18.7	15.3	6.3
10.0	46.1	44.3	51.7	44.7	30.2	3.9
14.0	54.9	53.3	55.3	45.5	44.3	3.7
19.0	57.7	48.9	57.2	47.9	43.5	3.8
24.0	60.0	53.3	55.0	48.4	44.5	4.0
28.0	60.8	51.0	56.0	51.7	44.8	4.3

Viable Cells (million/mL)						
Time (h)	0%	0.5%	1%	1.5%	2%	5%
0.0	6.1	5.4	5.1	5.3	4.7	5.3
3.0	11.4	10.6	8.0	7.0	6.9	3.4
6.5	25.4	30.3	36.6	18.6	15.0	1.5
10.0	45.5	43.4	48.0	44.4	28.4	1.4
14.0	54.2	51.5	49.7	44.0	40.0	1.2
19.0	56.1	47.3	49.9	46.3	38.8	1.0
24.0	58.6	49.2	49.3	44.1	38.8	0.9
28.0	59.8	48.2	49.5	48.1	38.3	0.1

Budding index						
Time (h)	0%	0.5%	1%	1.5%	2%	5%
0.0	0.167	0.085	0.151	0.094	0.065	0.102
3.0	0.228	0.108	0.190	0.099	0.092	0.126
6.5	0.219	0.162	0.208	0.136	0.130	0.091
10.0	0.149	0.103	0.158	0.104	0.088	0.054
14.0	0.131	0.103	0.095	0.056	0.083	0.068
19.0	0.115	0.052	0.083	0.056	0.063	0.030
24.0	0.102	0.048	0.072	0.052	0.017	0.027
28.0	0.087	0.050	0.051	0.027	0.022	0.019

Viability						
Time (h)	0%	0.5%	1%	1.5%	2%	5%
0.0	0.982	0.979	1.000	0.995	1.000	0.993
3.0	0.985	0.980	1.000	0.991	1.000	0.698
6.5	0.994	0.995	1.000	0.991	0.978	0.244
10.0	0.993	0.985	0.982	0.966	0.941	0.471
14.0	0.992	0.991	0.965	0.931	0.903	0.365
19.0	0.989	0.976	0.963	0.923	0.891	0.306
24.0	0.993	0.952	0.966	0.925	0.871	0.260
28.0	0.990	0.977	0.961	0.920	0.855	0.115

Dry mass (g/L)						
Time (h)	0%	0.5%	1%	1.5%	2%	5%
0.0	0.04	0.20	0.24	0.13	0.03	0.03
3.0	0.32	0.50	0.54	0.57	0.10	0.03
6.5	0.84	0.90	0.97	0.63	0.20	0.00
10.0	1.14	0.90	1.34	0.97	0.63	0.10
14.0	1.59	1.30	1.90	1.70	0.70	0.07
19.0	1.79	1.40	2.09	1.87	1.37	0.07
24.0	2.03	1.50	2.10	1.87	1.40	0.10
28.0	2.02	1.80	2.11	1.67	1.50	0.10

Absorbance						
Time (h)	0%	0.5%	1%	1.5%	2%	5%
0.0	0.4497	0.5139	0.5512	0.6168	0.6544	0.6613
3.0	0.6156	0.7238	0.8227	0.8582	0.8814	0.6767
6.5	1.1831	1.3897	1.4427	1.1931	1.5522	1.0174
10.0	1.8704	1.9250	2.0130	1.9906	1.9869	1.0690
14.0	2.0213	1.9767	2.3036	2.3922	2.3922	1.0127
19.0	2.1585	2.0536	2.3825	2.4949	2.5242	1.0265
24.0	2.2556	2.1312	2.4550	2.4604	2.5058	1.0333
28.0	2.1733	2.1568	2.4882	2.4649	2.5251	0.8318

	Zeta potential (mV)					
Time (h)	0%	0.5%	1%	1.5%	2%	5%
0.0	-6.05	-6.75	-9.28	-4.55	-3.75	-7.85
3.0	-7.50	-6.50	-9.45	-5.45	-4.25	-7.35
6.5	-7.43	-7.15	-9.28	-6.10	-4.20	-7.30
10.0	-6.45	-8.00	-8.73	-4.40	-4.10	-8.25
14.0	-6.58	-6.70	-8.05	-4.20	-3.10	-7.40
19.0	-7.10	-5.75	-6.93	-3.55	-2.20	-7.75
24.0	-7.50	-5.15	-6.58	-1.95	-2.05	-8.35
28.0	-7.38	-4.30	-5.93	-1.95	-2.90	-7.40

	Glucose (g/L)					
Time (h)	0%	0.5%	1%	1.5%	2%	5%
0.0	8.23	8.26	8.65	8.71	8.81	8.66
3.0	7.35	7.66	8.59	8.14	7.94	8.19
6.5	3.67	5.01	7.23	7.03	7.18	8.44
10.0	0.99	0.42	3.22	1.84	4.18	8.47
14.0	0.37	0.32	0.91	0.69	0.80	8.12
19.0	0.28	0.25	0.84	0.67	0.63	8.24
24.0	0.28	0.21	0.86	0.49	0.53	8.02
28.0	0.26	0.18	0.82	0.50	0.68	8.25

	Ethanol (g/L)					
Time (h)	0%	0.5%	1%	1.5%	2%	5%
0.0	0.46		0.60	0.35	0.35	0.37
6.5	1.26		1.17	0.63	0.70	0.35
15.0	2.94		2.59	2.05	1.77	0.33
24.0	2.76		2.30	1.65	1.41	0.26
28.0	2.28		2.11	1.29	1.37	0.24

Agitation rate : 565 rpm
1% solid

	Cells (million/mL)			Viable cells (million/mL)			Budding Index			Viability			Absorbance		
Time (h)	465-600	600-850	850-1130	465-600	600-850	850-1130	465-600	600-850	850-1130	465-600	600-850	850-1130	465-600	600-850	850-1130
0	5.7	5.1	4.2	5.6	5.1	4.2	0.156	0.151	0.139	0.993	0.995	1.000	0.8064	0.551167	0.7326
3	15.2	8.2	7.3	14.0	8.0	7.2	0.193	0.190	0.142	0.929	0.991	0.976	1.1018	0.8227	0.9802
6.5	24.4	37.4	27.3	22.2	36.6	25.0	0.218	0.208	0.189	0.911	0.991	0.921	1.8634	1.442733	1.6215
10	50.3	51.7	41.4	43.3	48.0	36.1	0.138	0.158	0.101	0.862	0.966	0.893	2.2124	2.012967	2.1038
14	55.6	55.3	48.0	44.1	49.7	32.1	0.084	0.095	0.090	0.792	0.931	0.722	2.3138	2.3036	2.1963
19	55.3	57.2	47.7	41.5	49.9	31.8	0.059	0.083	0.053	0.771	0.923	0.712	2.2857	2.3825	2.2145
24	54.2	55.0	45.8	40.1	49.3	31.3	0.040	0.072	0.055	0.760	0.925	0.694	2.2697	2.455033	2.2854
28	53.1	56.0	38.8	38.6	49.5	21.8	0.034	0.051	0.032	0.762	0.920	0.587	2.3919	2.488233	2.3356

	Dry mass (g/L)			Zeta potential (mV)			Glucose (g/L)		
Time (h)	465-600	600-850	850-1130	465-600	600-850	850-1130	465-600	600-850	850-1130
0	0.17	0.24	0.03	-9.8	-9.28	-7.95	8.17	8.65	8.39
3	0.20	0.54	0.07	-10.2	-9.45	-7.75	7.63	8.59	8.37
6.5	0.73	0.97	0.83	-9.6	-9.28	-7.45	4.85	7.23	6.78
10	1.17	1.34	1.33	-9.4	-8.73	-7.1	0.58	3.22	0.82
14	1.97	1.90	1.20	-8.6	-8.05	-7.15	0.48	0.91	0.71
19	2.43	2.09	1.13	-8.5	-6.93	-6.95	0.44	0.84	0.71
24	2.47	2.10	1.17	-7.8	-6.58	-6.85	0.45	0.86	0.81
28	2.60	2.11	1.27	-6.7	-5.93	-6.55	0.43	0.82	0.78

	Ethanol (g/L)		
Time (h)	465-600	600-850	850-1130
0	0.60		
6.5	1.17		
15	2.59		
24	2.30		
28	2.11		

Agitation rate : 565 rpm
1% solid

	Cells (million/mL)				Viable cells (million/mL)				Budding index				Viability				Absorbance			
Time (h)	10%	2.5%	2%	1%	10%	2.5%	2%	1%	10%	2.5%	2%	1%	10%	2.5%	2%	1%	10%	2.5%	2%	1%
0	5.1	4.0	3.9	2.5	5.1	4.0	3.9	2.5	0.151	0.133	0.198	0.169	0.995	1.000	1.000	1.000	0.551	0.695	0.631	0.391
3	8.2	8.0	10.0	4.4	8.0	7.9	10.0	4.3	0.190	0.163	0.208	0.211	0.991	1.000	1.000	0.982	0.823	0.986	1.080	0.762
6.5	37.4	18.8	25.8	18.4	36.6	18.7	24.7	18.1	0.208	0.172	0.253	0.253	0.991	0.994	0.969	0.982	1.443	1.617	1.677	1.512
10	51.7	43.5	43.1	29.8	48.0	41.8	40.6	29.4	0.158	0.142	0.219	0.227	0.966	0.969	0.955	0.990	2.013	2.165	2.147	2.017
14	55.3	48.4	49.8	33.2	49.7	45.6	44.8	31.7	0.095	0.156	0.101	0.146	0.931	0.945	0.928	0.975	2.304	2.305	2.268	2.038
19	57.2	55.0	49.8	42.0	49.9	45.2	45.1	40.3	0.083	0.089	0.065	0.125	0.923	0.833	0.928	0.964	2.383	2.344	2.321	2.119
24	55.0	54.5	50.9	37.3	49.3	46.9	46.6	35.8	0.072	0.086	0.078	0.101	0.925	0.887	0.936	0.973	2.455	2.413	2.389	2.154
28	56.0	56.0	53.1	37.8	49.5	47.7	49.1	36.8	0.051	0.077	0.068	0.046	0.920	0.871	0.952	0.980	2.488	2.396	2.411	2.188

	Dry mass (g/L)				Zeta potential (mV)				Glucose (g/L)			
Time (h)	10%	2.5%	2%	1%	10%	2.5%	2%	1%	10%	2.5%	2%	1%
0	0.24	0.03	0.03	0.09	-9.275	-9.75	-7.75	-6.4	8.65	8.05	8.54	7.96
3	0.54	0.10	0.13	0.10	-9.45	-8.85	-6.1	-5.55	8.59	7.88	8.58	7.68
6.5	0.97	0.20	0.53	0.27	-9.275	-9.45	-6.7	-5.3	7.23	5.81	7.55	3.21
10	1.34	0.80	1.17	0.57	-8.725	-7.5	-6.95	-4.95	3.22	2.51	4.19	0.46
14	1.90	0.90	1.10	1.03	-8.05	-6.7	-5.75	-3.8	0.91	0.37	0.90	0.31
19	2.09	1.10	1.23	1.67	-6.925	-5.75	-5.7	-3.4	0.84	0.05	0.63	0.37
24	2.10	1.07	1.20	1.63	-6.575	-5.6	-5.3	-3.9	0.86	0.07	0.15	0.30
28	2.11	1.43	1.23	1.63	-5.925	-5.05	-5.4	-3.05	0.82	0.05	0.45	0.41

	Ethanol (g/L)		
Time (h)	10%	2.5%	1%
0	0.60	0.32	0.36
6.5	1.17	0.84	1.77
15	2.59	2.31	2.31
24	2.30	1.83	1.95
28	2.11	1.48	1.75

Agitation rate : 565 rpm
1% solid

	Cells (million/mL)		Viable cells (million/mL)		Budding index		Viability		Absorbance		Dry mass (g/L)	
Time (h)	14 h	24h	14 h	24h	14 h	24h	14 h	24h	14 h	24h	14 h	24h
0	5.1	4.6	5.1	4.5	0.151	0.400	0.995	0.983	0.5512	0.7781	0.24	0.07
3	8.2	11.6	8.0	11.4	0.190	0.139	0.991	0.980	0.8227	1.204	0.54	0.10
6.5	37.4	37.3	36.6	34.5	0.208	0.063	0.991	0.942	1.4427	2.2081	0.97	0.87
10	51.7	54.2	48.0	45.0	0.158	0.062	0.966	0.862	2.0130	2.4258	1.34	1.50
14	55.3	54.0	49.7	44.2	0.095	0.054	0.931	0.855	2.3036	2.5037	1.90	1.83
19	57.2	54.9	49.9	41.3	0.083	0.059	0.923	0.822	2.3825	2.5512	2.09	1.93
24	55.0	56.2	49.3	40.0	0.072	0.092	0.925	0.780	2.4550	2.6808	2.10	2.23
28	56.0	54.9	49.5	37.6	0.051	0.020	0.920	0.750	2.4882	2.7486	2.11	2.53

	Zeta potential (mV)		Glucose (g/L)	
Time (h)	14 h	24h	14 h	24h
0	-10.15	-8.05	8.65	8.00
3	-9.6	-8.05	8.59	7.65
6.5	-9.45	-7.6	7.23	1.69
10	-8.85	-6.4	3.22	0.22
14	-8.2	-5.8	0.91	0.32
19	-6.75	-5.5	0.84	0.40
24	-6.8	-5.45	0.86	0.50
28	-5.65	-5.9	0.82	0.33

	Ethanol (g/L)	
Time (hr)	14 h	24h
0	0.60	0.32
6.5	1.17	1.19
15	2.59	1.40
24	2.30	0.90
28	2.11	0.58

RT: Rushton turbine
PBT: Pitched-blade turbine

	Cells (million/mL)				Viable cells (million/mL)				Budding Index				Viability				Absorbance				Dry mass (g/L)			
	RT		PBT		RT		PBT		RT		PBT		RT		PBT		RT		PBT		RT		PBT	
Time (h)	0% RT	1% RT	0% PBT	1% PBT	0% RT	1% RT	0% PBT	1% PBT	0% RT	1% RT	0% PBT	1% PBT	0% RT	1% RT	0% PBT	1% PBT	0% RT	1% RT	0% PBT	1% PBT	0% RT	1% RT	0% PBT	1% PBT
0	6.5	5.1	4.8	5.3	6.1	5.1	4.7	5.3	0.167	0.151	0.169	0.158	0.982	0.995	0.984	1.000	0.4497	0.5512	0.7686	0.7700	0.04	0.24	0.03	0.07
3	11.6	8.2	15.5	18.2	11.4	8.0	15.4	17.8	0.228	0.190	0.193	0.173	0.985	0.991	0.994	0.979	0.6156	0.8227	1.3054	1.2008	0.32	0.54	0.13	0.60
6.5	25.6	37.4	36.8	38.2	25.4	36.6	34.7	37.0	0.219	0.208	0.167	0.188	0.994	0.991	0.946	0.969	1.1831	1.4427	2.1550	1.9256	0.84	0.97	1.23	1.40
10	46.1	51.7	48.1	48.6	45.5	48.0	45.0	39.4	0.149	0.158	0.081	0.097	0.993	0.966	0.942	0.829	1.8704	2.0130	2.2211	2.1775	1.14	1.34	1.47	1.53
14	54.9	55.3	50.5	53.4	54.2	49.7	47.3	42.6	0.131	0.095	0.059	0.081	0.992	0.931	0.941	0.831	2.0213	2.3036	2.2505	2.2052	1.59	1.90	1.60	1.63
19	57.7	57.2	50.4	50.8	56.1	49.9	47.9	39.9	0.115	0.083	0.059	0.058	0.989	0.923	0.952	0.820	2.1585	2.3825	2.2954	2.2358	1.79	2.09	1.63	2.03
24	60.0	55.0	48.4	47.5	58.6	49.3	44.1	39.0	0.102	0.072	0.067	0.042	0.993	0.925	0.918	0.858	2.2556	2.4550	2.3707	2.2689	2.03	2.10	1.80	2.17
28	60.8	56.0	50.9	51.0	59.8	49.5	43.0	40.8	0.087	0.051	0.043	0.034	0.990	0.920	0.851	0.838	2.1733	2.4882	2.4559	2.2993	2.02	2.11	2.13	2.33

	Zeta potential (mV)				Glucose (g/L)			
	RT		PBT		RT		PBT	
Time (h)	0% RT	1% RT	0% PBT	1% PBT	0% RT	1% RT	0% PBT	1% PBT
0	-6.05	-9.275	-8	-8.2	8.23	8.65	8.78	8.34
3	-7.50	-9.45	-8.15	-8.65	7.35	8.59	7.40	6.68
6.5	-7.43	-9.275	-7.9	-8.4	3.67	7.23	0.51	1.20
10	-6.45	-8.725	-7.9	-8.4	0.99	3.22	0.57	0.45
14	-6.58	-8.05	-7.05	-7.55	0.37	0.91	0.60	0.45
19	-7.10	-6.925	-6.65	-7.55	0.28	0.84	0.59	0.46
24	-7.50	-6.575	-5.85	-6.7	0.28	0.86	0.63	0.58
28	-7.38	-5.925	-6.55	-6.55	0.26	0.82	0.52	0.70

	Ethanol (g/L)			
	RT		PBT	
Time (h)	0% RT	1% RT	0% PBT	1% PBT
0	0.46	0.60	0.28	
6.5	1.26	1.17	1.71	
15	2.94	2.59	1.25	
24	2.76	2.30	0.77	
28	2.28	2.11	0.67	

1% solid

	Cells (million/mL)				Viable cells (million/mL)				Budding Index				Viability				Absorbance			
Time (h)	460	565	600	850	460	565	600	850	460	565	600	850	460	565	600	850	460	565	600	850
0	4.7	5.1	5.3	4.9	4.7	5.1	5.1	4.9	0.21	0.15	0.23	0.21	1.000	0.986	0.986	1.000	0.6212	0.5512	0.7350	0.8483
3	10.0	8.2	12.8	10.1	9.8	8.0	12.6	10.0	0.20	0.19	0.27	0.24	0.988	0.973	0.982	0.992	0.8587	0.8227	0.9414	1.1188
6.5	24.4	37.4	29.8	32.7	23.8	36.6	29.2	29.9	0.19	0.21	0.25	0.21	0.982	0.974	0.983	0.917	1.2202	1.4427	1.3316	1.9265
10	33.6	51.7	40.0	41.2	32.2	48.0	38.1	35.3	0.17	0.16	0.18	0.06	0.987	0.936	0.962	0.891	1.8345	2.0130	2.0389	2.2509
14	36.8	55.3	49.0	43.5	35.3	49.7	43.3	33.8	0.17	0.09	0.09	0.04	0.971	0.865	0.898	0.816	2.1502	2.3036	2.2925	2.3574
19	38.5	57.2	49.8	43.2	35.8	49.9	43.0	32.7	0.09	0.08	0.07	0.03	0.955	0.843	0.879	0.790	2.3071	2.3825	2.4632	2.3859
24	36.0	55.0	52.0	44.0	34.8	49.3	44.8	33.6	0.10	0.07	0.03	0.03	0.979	0.845	0.875	0.806	2.2843	2.4550	2.5164	2.4794
28	37.8	56.0	49.0	43.7	35.0	49.5	41.0	28.9	0.11	0.05	0.04	0.01	0.947	0.839	0.862	0.774	2.3048	2.4882	2.5180	2.5239

	Dry mass (g/L)				Zeta potential (mV)				Glucose (g/L)			
Time (h)	460	565	600	850	460	565	600	850	460	565	600	850
0	0.87	0.24	1.10	0.03	-5.9	-9.275	-6.9	-7.55	7.43	8.65	8.33	8.98
3	1.57	0.54	1.33	0.17	-6.8	-9.45	-5.85	-7.9	6.26	8.59	7.84	8.93
6.5	2.67	0.97	2.70	0.83	-6.95	-9.275	-4.7	-6.95	0.63	7.23	4.30	7.32
10	2.70	1.34	2.80	1.17	-6.6	-8.725	-3.7	-6.65	0.36	3.22	0.43	4.27
14	2.53	1.90	2.77	1.33	-5.05	-8.05	-3.75	-5.6	0.37	0.91	0.43	0.86
19	2.60	2.09	2.70	1.53	-5.25	-6.925	-3.5	-5.7	0.09	0.84	0.26	0.43
24	2.57	2.10	2.67	1.50	-5.1	-6.575	-3.5	-5.65	0.09	0.86	0.32	0.26
28	2.67	2.11	3.00	1.43	-5.25	-5.925	-3.25	-5.5	0.09	0.82	0.28	0.11

	Ethanol (g/L)			
Time (hr)	460	565	600	850
0	0.39	0.60	0.30	0.29
6.5	1.96	1.17	1.75	1.74
15	2.95	2.59	1.27	2.19
24	2.23	2.30	0.78	1.58
28	1.91	2.11	0.64	0.97

Appendix G: Determination of the growth parameters

Different growth parameters were calculated using experimental data.

G.1 Biomass yield on consumed substrate:

$Y_{X/S}$ was calculated as follow:

$$Y_{X/S} = \frac{Final \cdot cells.concentration}{Consumed \cdot substrate}$$

The consumed substrate was calculated as the initial glucose concentration minus the final one.
The final cell concentration was the total number of cells at the end of the run.
$Y_{X/S}$ unit is million cells.mL^{-1}.g^{-1}.L.

G.2 Product yield on consumed substrate:

$Y_{P/S}$ was calculated as follow:

$$Y_{P/S} = \frac{Produced \cdot Ethanol}{Consumed \cdot substrate}$$

The consumed substrate was calculated as previously.
The ethanol produced was defined as the difference in ethanol concentration between the beginning and the end of the run.
$Y_{P/S}$ unit is $g_{ethanol} \cdot g_{glucose}^{-1}$.

G.3 Product yield on produced biomass:

$Y_{P/X}$ was calculated as follow:

$$Y_{P/X} = \frac{Produced \cdot Ethanol}{Produced \cdot biomass}$$

The ethanol produced was defined as the difference in ethanol concentration between the beginning and the end of the run.
The produced biomass was defined in terms of total cell number at the end of the run.
$Y_{P/S}$ unit is $g.L^{-1}$ million $cells^{-1}$.mL.

G.4 Lag phase using total cell number graph:

The lag phase of the growth, defined as the time necessary for the cells to acclimatise to the medium, was evaluating graphically, using the plot of the total number of cells versus time. It was determined as the time between the beginning of the run (time 0) and the time when the exponential phase starts (exponential curve on the graph).
Due to the small number of experimental points, the lag phase duration could not be measured precisely and data must be used only qualitatively.

G.5 Lag phase for glucose consumption:

The lag phase occurring before the consumption of glucose was determined in the same way as previously. The plot of the glucose concentration versus time was used for calculation.

G.6 Maximum specific growth rate:

The specific growth rate is defined as follow:

$$\mu = \frac{1}{X}\frac{dX}{dt} \quad \text{where X = biomass}$$

μ_{max} was determined for each experiment using the plot of total number of cells versus time.

The exponential part of the curve was approximated using a polynomial regression of degree 4. The derivative over t of this expression was taken and μ calculated at different times. μ_{max} corresponds to the maximum of μ.

Figure G.1 shows an example of the performed calculations.

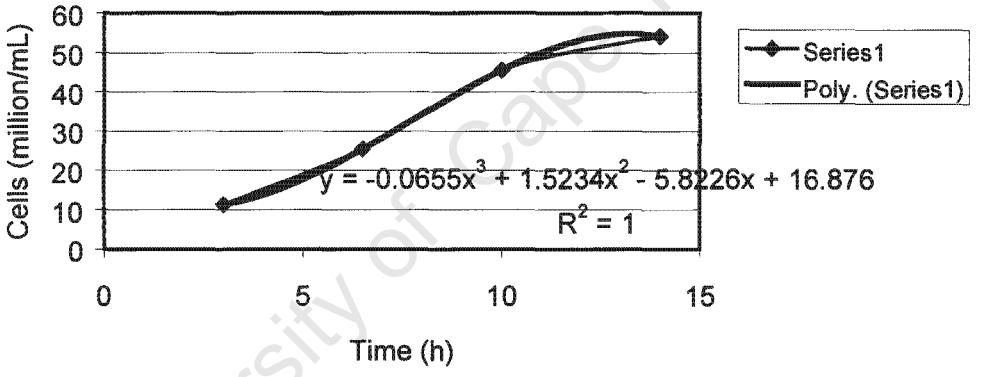

Figure G.1 Approximation of the exponential part of the curve by a polynomial expression.

The growth was approximated by:

$X = -0.0655\ t^3 + 1.5234\ t^2 - 5.8226\ t + 1F.876$

$$\frac{dX}{dt} = -0.0655 \times 3 \times t^2 + 1.5234 \times 2 \times t - 5.8226$$

$\mu = \frac{1}{X}\frac{dX}{dt}$ was calculated and plotted versus t. The maximum is μ_{max}.

From Figure G.2, μ_{max} was calculated to 0.25 h^{-1}.

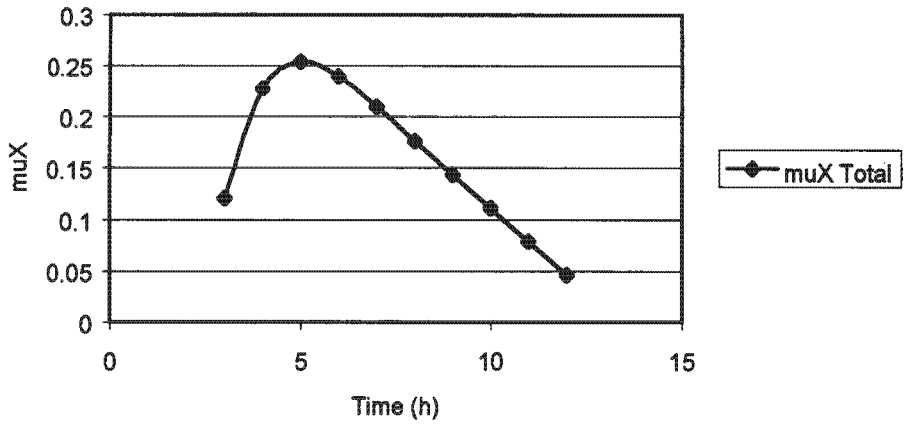

Figure G.2 Determination of μ_{max}.

$\mu_{maxViable}$ was also calculated in the same way, but using the plot of the viable cells versus time.

G.7 Specific glucose uptake rate:

Glucose uptake rate was defined as:

$$q_S = \frac{1}{X}\frac{d[S]}{dt}$$

where [S] is glucose concentration (in g/L)
X is the total cell concentration (in million/mL).
q_S unit is $g.L^{-1}.h^{-1}.million\ cells^{-1}.mL$.

The specific glucose uptake rate was calculated in the same way as the specific growth rate. The experimental curve for glucose consumption was approximated by a polynomial of degree 4. The derivative was taken and q_S calculated.

G.8 Specific ethanol production rate:

Ethanol production rate was defined as:

$$q_P = \frac{1}{X}\frac{d[P]}{dt}$$

where [P] is ethanol concentration (in g/L).
X is the total cell concentration (in million/mL).
q_P unit is $g.L^{-1}.h^{-1}.million\ cells^{-1}.mL$.

The specific ethanol production rate was calculated in the same way as the specific growth rate. The experimental curve for ethanol production was approximated by a polynomial of degree 4. The derivative was taken and q_P calculated.
Only the first part of the curve was considered as, when all the glucose is consumed, there is a shift in the substrate and ethanol is used as a substrate by the cells.

G.9 Determination of exponential phase duration:

Exponential phase duration was determined from the plot of total cell number versus time. It was evaluated graphically, as the length of the exponential part of the curve.

Appendix H: Cell wall thickness as a function of solids loading and agitation rate

Experimental conditions	Time of fermentation		
	3h	14h	28h
0% (v/v) solids loading, 565 rpm	68 nm	65 nm	68 nm
1% (v/v) solids loading, 565 rpm	118 nm	104 nm	111 nm
0% (v/v) solids loading, 850 rpm	180 nm	99 nm	100 nm

Appendix I: Experimental and modelled death constant values

Solids loading (% v/v)	k_d experimental	k_d modelled
0	0	0
0.5	0.096	0.078
1	0.119	0.110
1.5	0.120	0.135
2	0.142	0.155